POLITECNICO
MILANO 1863

SCUOLA DI INGEGNERIA INDUSTRIALE
E DELL'INFORMAZIONE

Executive Summary of the Thesis

Identification of Linear Periodically Time-Varying (LPTV) Systems using a Frequency-Domain Subspace Method

Laurea Magistrale in Aeronautical Engineering - Ingegneria Aeronautica

Author: Antonio Ramón Martín Morilla

Advisor: Prof. Marco Lovera

Academic year: 2021-2022

Abstract **- A new approach for a frequency-domain subspace-identification for linear periodic time-varying (LPTV) systems is presented in this thesis, based on the most recent publications about this field of study. Hence, it will be evaluated using a real physical-based example, considering different levels of added noise, with the aim to prove its suitability for this kind of identification. Then, the pros and cons after using it can be evaluated in order to determine if it would be possible to use this method to perform real-life LPTV systems identification.**

I. Introduction

Many systems in engineering and also in biology require, at least, a LPTV model to cover the entire problem without risk of losing any dynamics. Problems such as wind turbines, rotor bearing systems, aircraft models or power distribution network are examples of fields where LPTV models apply. In the mid-1990s, a considerable development about this kind of systems was performed. However, the computational cost of working with these systems lead to a reduced applicability. Nowadays, with the raise of new willings for current prototypes and systems, and the improvement of the computation capabilities, the interest on LPTV model subspace-identification is raising, mainly to contrast them to physical-based models [1].

The key of this project is to develop an algorithm in which, from a periodic input-output data, a frequency-domain identification of a LPTV system can be performed. This is done through a specific parametric structure of Fourier series coefficients associated with the original system. As these coefficients (that are the harmonics of the periodic functions that compose the state-space matrices) are preserved when the transformation to the harmonic space state (HSS) representation is computed, the results of the identification process are the coefficients of the harmonic expansion of each function of the state-space matrices. In general, this process may not provide the original state-space matrix coefficients, but what is always guaranteed is that the identified system can be associated to the original one through a similarity transformation. In the final part, some numerical examples will be presented including noise to the output signal before performing the identification to assess the performance of the algorithm in presence of a

realistic signal-to-noise ratio (SNR).

The rest of the document is organized as follows. Section II describes the basic LPTV system model. Section III provides the identification method. Hence, Section IV provides the results of the performed numerical simulation. Finally, Section V brings up the main conclusions of the project.

II. LPTV system model

First of all, some assumptions should be made:

- The algorithm is developed for SISO systems in time-domain.
- The period of the system, T_m, or, equivalently, its main frequency, ω_m, is known.
- To design the identification experiement, a T_i-periodic signal is chosen for the input, being T_i proportional to T_m.
- The number of states desired for the identified system are set to n_p.
- The truncation number N of the Toeplitz matrices and the number of harmonics desired in the identified model, N_{mh}, are design parameters.
- The output signal is assumed to be at steady-state.

Take an input, which is a sum of cosines, defined as follows:

$$u(t) = \sum_{k=1}^{N_i} 2\,K_k \cos(\omega_k\, t + \varphi_k) \tag{1a}$$

$$\omega_k = k\,\frac{2\,\pi}{T_i}, \quad k = 1, ..., N_i \tag{1b}$$

$$\varphi_k = \begin{cases} 0, & k = 1 \\ \varphi_{k-1} - \dfrac{\pi\,k^2}{N_i}, & k = 2, ..., N_i, \end{cases} \tag{1c}$$

holding $\omega_m \neq 0.5\,q\,\omega_k$, $q \in \mathbb{Z}$ to avoid any coincidence in harmonic responses of the single-cosine input. The phasing was introduced to avoid a lumped impulse at the beggining of the period with a residual oscillation in the rest of it.

Consider now the continuous-time state-space LPTV system, defined as follows:

$$\begin{aligned} \dot{x}(t) &= A_c(t)\,x(t) + B_c(t)\,u(t) \\ y(t) &= C_c(t)\,x(t) + D_c(t)\,u(t), \end{aligned} \tag{2}$$

Then, the objective is to have a constant system matrix $A \neq A(t)$, to simplify the identification part and to transform this system into a discrete-time one. To avoid the risk of ending up with a non-reversible system, it is recommendable to use first the Floquet-Lyapunov theory to obtain a constant A_c matrix. This will lead to find a transformation matrix $S(t)$ such that $\bar{x}(t) = S(t)\,x(t)$, leading to the following system:

$$\begin{aligned} \dot{\bar{x}}(t) &= \bar{A}_c\ \bar{x}(t) + \bar{B}_c(t)\,u(t) \\ y(t) &= \bar{C}_c(t)\,\bar{x}(t) + \bar{D}_c(t)\,u(t). \end{aligned} \tag{3}$$

Finally, using the time-varying bilinear (Tustin) transformation to discretise the system with a T_s sampling time, the final system will be the desired one:

$$\begin{aligned} x(k+1) &= A_d\ x(k) + B_d(k)\,u_d(k) \\ y(k) &= C_d(k)\,x(k) + D_d(k)\,u_d(k). \end{aligned} \tag{4}$$

Now, in order to lift the matrices and vectors that compose the system, an exponentially modulated periodic (EMP) transformation, is used. In discrete-time, the system frequency is defined as $\omega_m = 2\,\pi\,T_s/T_m$. Now, if $N_f = T_m/T_s$, consider it even for the sake of simplicity, the expansion cannot be infinitely long, but it is constrained to the Nyquist frequency [2]. Consider also N, even as N_f, the truncation number for the harmonic expansion. Take into account that N can be chosen in the range $[2, N_f] \in \mathbb{Z}$. Once chosen N, the interval $\boldsymbol{I_n} = [-N/2,\ N/2-1]$ is defined to set the considered harmonics. Then, the expansion is defined as follows:

$$Q(t) = z^t \sum_{n=-N/2}^{N/2-1} Q_n\, e^{j n \omega_m\, t}. \tag{5}$$

Consider lifting, using the EMP transformation, setting $z = 1$, the output signal, $y(t)$, and the input signal, $u(t)$, leading to $\mathcal{Y}$ and $\mathcal{U}$ respectively, looking as follows:

$$\mathcal{V} = \left[V_{-N/2}, \ldots, V_{-1}, V_0, V_1, \ldots V_{N/2-1}\right]^{\mathrm{T}}. \tag{6}$$

In the same manner, using the EMP transformation, each matrix of the state-space system can be lifted using Toeplitz matrices, leading to:

$$\mathcal{Q} = \begin{bmatrix} Q_0 & Q_{-1} & \cdots & Q_{-N/2} & Q_{N/2-1} & \cdots & Q_1 \\ Q_1 & Q_0 & \cdots & Q_{-N/2+1} & Q_{-N/2} & \cdots & Q_2 \\ \vdots & \vdots & & \vdots & \vdots & & \vdots \\ Q_{-1} & Q_{-2} & \cdots & Q_{N/2-1} & Q_{N/2-2} & \cdots & Q_0 \end{bmatrix}. \tag{7}$$

This now defines the following equivalent LTI system:

$$\begin{aligned} z\,\mathcal{N}_d\,\mathcal{X} &= \mathcal{A}\,\mathcal{X} + \mathcal{B}\,\mathcal{U} \\ \mathcal{Y} &= \mathcal{C}\,\mathcal{X} + \mathcal{D}\,\mathcal{U} \end{aligned} \tag{8}$$

where $\mathcal{N}_d = \text{blkdiag}\{e^{j\,n\,\omega_m} I_{n\times n} \mid n \in \boldsymbol{I_n}\}$, being $I_{n\times n}$ the squared identity matrix of n dimension. From this structure, the harmonic transfer function (HTF) can be defined just by relating the input harmonics and the output harmonics vectors:

$$\mathcal{G}\,(z) = \mathcal{C}\,(z\,\mathcal{N}_d - \mathcal{A})^{-1}\,\mathcal{B} + \mathcal{D} \tag{9}$$

Finally, with the objective to obtain a measurement of the uncertainty of the identified parameters, a number N_{mont} of added-noise output signals can be computed, to perform a Monte Carlo analysis in order to compute the mean and variance values of each identified parameter.

III. Identification method

The algorithm presented in this thesis is based on the approach of Uyanik et al. [2], to transform a LPTV discrete-time state-space system (with the system matrix constant) into an equivalent LTI one, which is the identified system. With some different approaches, this method intends to avoid the counterparts of the referenced method.

The first step is focused on obtaining a time-domain output signal to perform the identification. To ensure the obtained signal is in steady state, output signal will be computed by computing the HTF from the reference system and also lifting the input signal. Then, $\mathcal{Y} = \mathcal{G}(z=1)\mathcal{U}$. Once the lifted output vector is computed, it is returned to the time domain using the EMP definition, provided in equation (5), by setting also $z = 1$. Finally, to consider the added Gaussian noise of the output signal in discrete-time, $y(k) = \bar{y}(k) + w(k)$, where $w \sim G(0, \sigma^2)$ and $\sigma^2 = y_{\text{pow}}/\,\text{SNR}$, being y_{pow} the power of the noise-free signal, which will be the degree of freedom to select the desired amount of added noise.

Then, take the output signal, $y(k)$, and the input signal, $u(k)$, and lift them, using the EMP transformation, setting $z = 1$, obtaining the $\mathcal{Y}^*$ and $\mathcal{U}$ vectors.

Consider now the state-space matrices but A_d, which is constant. Then, each of the components of each matrix can be expanded in a trigonometric Fourier series, denoted as follows:

$$\begin{aligned} Q_i(k) = Q_{i0} + \sum_{n=1}^{N_{\text{harm}}} &\left(Q_{\text{c}_{in}} \cos\left(n\,\omega_m\,T_s\,k\right)\right. \\ &\left. + Q_{\text{s}_{in}} \sin\left(n\,\omega_m\,T_s\,k\right)\right), \\ &i = 1, ..., n_p \end{aligned} \tag{10}$$

where $Q(k)$ stands for $B_d(k)$, $C_d(k)$ and $D_d(k)$, while N_{harm} the number of harmonics desired for the expansion. Using the EMP transformation definition, each matrix of the state-space system can be lifted using Toeplitz matrices, which will contain each of the harmonics of the trigonometric expansion, as shown in equation (7), leading to the equivalent LTI system in equation (8), and finally, to the HTF in equation (9).

The next step is to set now the number of inputs, n_i, outputs, n_o, and states, n_p that the identified system will have, as well as the number of harmonics, N_{harm}, for the $B_d(k)$, $C_d(k)$ and $D_d(k)$ functions. Hence, all the harmonic values are collected into a vector, Θ, including also the coefficients of A_d. This vector is defined as follows:

$$\begin{aligned} \Theta &= \left[\Theta_A^{\text{T}}, \Theta_B^{\text{T}}, \Theta_C^{\text{T}}, \Theta_D^{\text{T}}\right]^{\text{T}} \\ \Theta_A &= \left[A_{11}, A_{21}, ..., A_{n_p\,1}, ..., A_{n_p\,n_p}\right]^{\text{T}} \\ \Theta_Q &= \left[Q_{10}, Q_{\text{c}_{11}}, ..., Q_{\text{s}_{11}}, ..., Q_{\text{s}_{n_p N_{\text{harm}}}}\right]^{\text{T}}, \\ &\qquad Q = B,\, C,\, D. \end{aligned} \tag{11}$$

Now, for each added-noise output realisation that was computed and lifted, $\mathcal{Y}^*$ an optimization process will be performed to obtain the desired parameters. The procedure for each iteration would be the following:

* Select Θ and compute A_d, $B_d(k)$, $C_d(k)$ and $D_d(k)$.
* Lift the time-domain matrices to compute the Toepliz matrices $\mathcal{A}_\mathcal{F}$, $\mathcal{B}_\mathcal{F}$, $\mathcal{C}_\mathcal{F}$ and $\mathcal{D}_\mathcal{F}$ as shown in (7).
* Compute the $\mathcal{N}_d$ matrix.
* Compute the HTF matrix, $\mathcal{G}(z)$ as it was defined in equation (9). Set $z = 1$.
* Compute $\mathcal{Y}_\mathcal{F}(\Theta) = \mathcal{G}(z=1)\mathcal{U}$.

As a consequence of the uncertainty computations, this procedure will be repeated N_{mont}

times for each case. Hence, the problem to optimize is the following:

$$\hat{\Theta} = \underset{\Theta}{\operatorname{argmin}} \quad \|\mathcal{Y}_{\mathcal{F}}(\Theta) - \mathcal{Y}^*\|_2 \qquad (12)$$

To solve the optimization problem, the chosen method is the one implemented in MATLAB's `fmincon` with a custom configuration. Once the optimizer provides a result, called $\hat{\Theta}$, the state-space model matrices, $\hat{A}_d$, $\hat{B}_d(k)$, $\hat{C}_d(k)$, $\hat{D}_d(k)$, can be reconstructed. To compute the uncertainty of each identified parameter, the mean, μ, variance, σ^2 and coefficient of variation, σ/μ, are computed from the obtained dataset. This will be helpful to decide the influence of each parameter on the actual system.

If desired, the original system can be recovered by returning first to the continuous-time domain, by using the inverse bilinear (Tustin) transformation. As the data was computed in discrete-time, the intersample data will be missing. This can be obtained via linear interpolation. Finally, applying back the Floquet transformation, $x(t) = S(t)^{-1}\,\bar{x}(t)$, the original state-space system can be recovered.

Finally, notice that, if instead of imposing the Fourier trigonometric expansion in equation (10), each term is free to have a different number of harmonics, this will lead to a black-box identification. Using this method will simplify the steps, but it will not probably return the desired system (or at least, one with physical meaning), but an equivalent one.

IV. Numerical example

In this section, a numerical case study is related to illustrate the performance of the presented algorithm, as well as to verify its robustness and accuracy in different situations. The considered example is a model for the out-of-plane bending of a helicopter rotor blade developed by Bittanti and Lovera [3], that takes the commanded pitch angle, and once defined the rotor characteristics and the flight condition, it provides a time-periodic SISO space-state model that returns the vertical shear force as the output.

This model has two degrees of freedom, which are the rotor advance ratio, μ, which is a non-dimensional number that defines the forward velocity of the rotor with respect to the hover velocity of the blade tip, and the number of bending modes considered for the blade, called n_{modes}. Due to the model derivation, the system size will be $2 \times n_{\text{modes}}$. As the hover flight condition ($\mu = 0$) is time-invariant, it has been chosen the maximum value of the advance ratio, with physical meaning according to the literature, to exploit the perodically-time varying characterisation of the model. Hence, $\mu = 0.35$ for all the performed examples. Some other parameters that have been set for all the examples are $N_{\text{harm}} = 3$, $N = 120$, $T_s = 0.01$ s, $N_{\text{mont}} = 20$. The input has been designed to be a sum of cosines of 56 different frequencies, with $K_k = 0.05 \forall k \in [0, 56]$, leading to an input period of $T_i = 4.68$ s.

The carried out examples were $n_{\text{modes}} = 1$ and $n_{\text{modes}} = 2$. Then, as a real flexible system has an infinite number of modes, it was desired to select a different number of modes for the reference output signal and for the identified model, setting $n_{\text{modes sys}} = 1$ with $n_{\text{modes ref}} = 2$ for the third case and $n_{\text{modes sys}} = 1$ with $n_{\text{modes ref}} = 5$ for the last performed case. Once set this, the only degree of freedom for each case is the SNR for the added Gaussian noise.

Focusing now in the two first cases, the output signal was sucessfully recovered, as well as the majority of the terms that compose the state-space system. An example of the algorithm performance is provided in Figure 1.

As it can be noticed, the estimated output captures the behaviour of the reference one. However, the presence of noise may affect the results, but the output is captured anyways. Then, in order to quantify the sensitivity with respect to the added noise, some errors can be defined:

$$\varepsilon_A = \|A_{\text{ref}} - \hat{A}_{\text{ident}}\|_2 \qquad (13a)$$

$$\varepsilon_{Q\,i} = \int_0^{f_{\max\ \text{inp}}} \left| |Q_i|_{\text{ref}}(f) - |\hat{Q}_i|_{\text{id}}(f) \right| \mathrm{d}f \qquad (13b)$$

$$\varepsilon_{\text{Tot}} = \|\sum \varepsilon_{Q\,i}\|_2, \qquad \begin{matrix} i = 1, ..., n_p \\ Q = B, C, D, \end{matrix} \qquad (13c)$$

and a trend of the errors with respect to the SNR value is provided in Figure 2 in order to

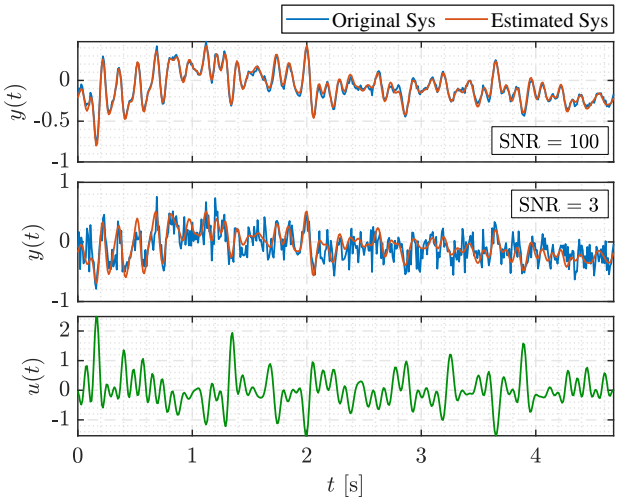

Figure 1: Example of the method performance in the bending model numerical example. $n_{\text{modes}} = 2$. SNR $= 100$ & 3

understand the range of noise values in which the method provides reasonable results.

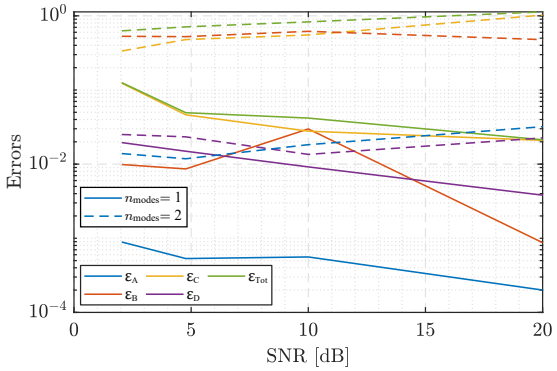

Figure 2: Errors in the bending model numerical example. $n_{\text{modes}} = 1$ & 2

As it can be seen, the error grows with the number of modes, since the number of parameters to identify increases exponentially. These errors are mostly in $\hat{B}_d$ and $\hat{C}_d$ matrices, where the amplitude of the harmonics is not perfectly captured. However, despite of these errors, the identified matrices are still similar to the reference ones, in the sense of maintaining the same order of magnitude, and the estimated output is still close to the reference one, even in the worst-noise case.

With respect to the third and the fourth cases, considering the application of this example to real life, the blade will have a infinite number of modes. Therefore, the next step is to test the behaviour of the method identifying a system which is not exactly the same as the reference output source. The results of this analysis prove that the method recovers the output signal when the SNR value is higher than 3. However, as the reference system is now different from the identified one, the comparison must be performed using another method. Regarding the HTF definition, it can be understood as follows:

$$\mathcal{G}(z) = \begin{bmatrix} \ddots & \vdots & \vdots & \vdots & \\ \cdots & G_0(z \cdot z_m^{-1}) & G_{-1}(z) & G_{-2}(z \cdot z_m) & \cdots \\ \cdots & G_1(z \cdot z_m^{-1}) & G_0(z) & G_{-1}(z \cdot z_m) & \cdots \\ \cdots & G_2(z \cdot z_m^{-1}) & G_1(z) & G_0(z \cdot z_m) & \cdots \\ & \vdots & \vdots & \vdots & \ddots \end{bmatrix}, \quad (14)$$

where $z_m = e^{j\,\omega_m}$. Hence, as a direct comparison between the reference and the estimated HTF would add some numerical errors that are meaningless, a better analysis can be performed regarding the functions the main modes of the system. These system main modes can be computed from the ratio between the output and the system period,

$$H_n = n\,\frac{T_{\text{output}}}{T_{\text{system}}} = 30\,n, \quad n \in \mathbb{Z}. \quad (15)$$

Notice that, as the magnitude of the mode decreases as n increases, the most relevant modes are H_0 and H_1. Then, Figure 3 shows the comparison between the first two system main modes of the reference system and the estimated one.

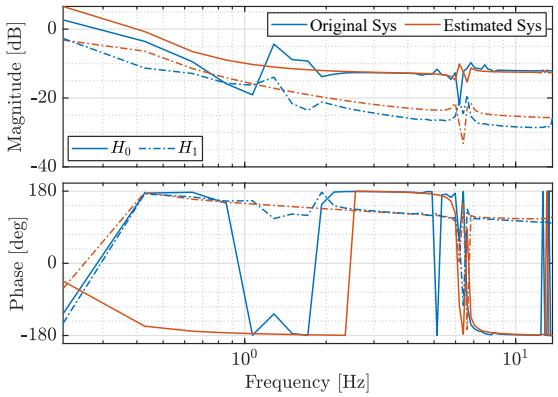

Figure 3: H_0 and H_1 bode-like charts. $n_{\text{modes signal}} = 5$, $n_{\text{modes system}} = 1$. SNR $= 10$

To provide a comparison between all the computed cases, an error definition can be per-

formed:

$$\varepsilon_m = \sum_{i=0}^{1} \int_{f_{\text{min inp}}}^{f_{\text{max inp}}} |H_{i,\,\text{ref}}(f) - H_{i,\,\text{id}}(f)|\,\mathrm{d}f. \quad (16)$$

This definition leads to Figure 4, which shows at a glance what has been commented before. With respect to the behaviour in noise presence, the algorithm performs worse as the SNR value decreases, which means that the added noise increases. However, it can be noticed that this behaviour is not logaritmic, but there is a point in which the error cannot be lower even if the reference output signal is affected by a low amount of noise. On the other part, with respect to the number of modes considered in the reference output signal, increasing it without making the size of the identified model bigger, will mean that the errors will grow.

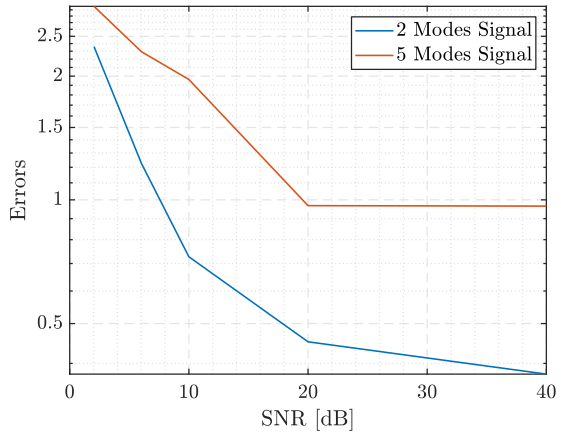

Figure 4: Errors comparsion between $n_{\text{modes signal}} = 2$ and $n_{\text{modes signal}} = 5$

V. Conclusions

In this Thesis, a new method for a frequency-domain subspace-identification method for LPTV systems was developed. It starts taking a LPTV continuous-time system in state-space form, to transform it into an equivalent discrete-time LTI system. This procedure required the use of a bilinear (Tustin) transformation and, later, a frequency-domain lifting. Then, the LTI system was estimated in the output-error framework. Finally, the algorithm was tested using a physical-based rotorcraft model, with several cases to exploit a range of possibilities to prove its effectiveness and robustness in several cases of application. With respect to the results, it has been proved that the method provides good results in the sense of recovering the original system in several modes and noise conditions. Also, even if it has not been fully tested in this thesis, this method also works well if a black-box identification is desired, providing also good results, but possibly, without any phyisical meaning.

References

[1] U. Saetti and M. Lovera, "Time-periodic and high-order time-invariant linearized models of rotorcraft: A survey," *Journal of the American Helicopter Society*, vol. 67, pp. 1–19, 01 2022.

[2] I. Uyanık, U. Saranl, M. M. Ankaral, N. J. Cowan, and O. Morgül, "Frequency-domain subspace identification of linear time-periodic (ltp) systems," *IEEE Transactions on Automatic Control*, vol. 64, no. 6, pp. 2529–2536, 2019.

[3] S. Bittanti and M. Lovera, "On the zero dynamics of helicopter rotor loads," *European Journal of Control*, vol. 2, no. 1, pp. 57–68, 1996. [Online]. Available: https://www.sciencedirect.com/science/article/pii/S0947358096700298

Politecnico di Milano
Scuola di Ingegneria Industriale e dell'Informazione
Corso di Laurea Magistrale in Ingegneria Aeronautica

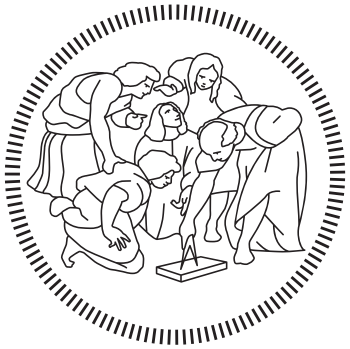

Identification of Linear Periodically Time-Varying (LPTV) Systems using a Frequency-Domain Subspace Method

Advisor: Prof. Marco LOVERA

Thesis by:
Antonio Ramón MARTÍN MORILLA Matr. 963842

Academic Year 2021–2022

Acknowledgments

It has been a long trajectory since I started my MSc in Seville, and many friends that I left when I moved into Milan, and there were many others that I have met in these two years in Italy.

Como primera mención, me gustaría agradecer de todo corazón a mis padres y a mi familia, que siempre me ha mostrado todo su apoyo y su ánimo, incluso en los momentos más complicados. Dicen que las familias biológicas no se pueden escoger, pero si pudiera hacerlo, no dudaría en hacerlo una y mil veces.

Sin olvidar a la familia que se escoge, desde los amigos de la más tierna infancia, como Antonio o Juan Carlos, hasta los Aerochachos, que son como hermanos para mí, y que me han demostrado en todos estos años que han estado, están y estarán para siempre. A Ana, Antonio, Isa, Jose, Juanma, Lina, Manu, Marta, Rafa y Sara, muchísimas gracias por todo. Y la verdad es que no sería justo si no mencionara a Fran González, Fran Garrocho, Diego, Anais, y un largo etcétera de personas que han estado siempre para lo que he necesitado. He de reconocer que sois increíbles.

También me gustaría agradecer a todas esas personas conocidas durante mi estancia en Milán, con las que podría escribir un libro solo de anécdotas. Si bien es cierto que me gustaría mencionar en especial a Tasio, Sabrina, Jose, Sergio, Carlos, Diego, Nacho y Ana. Sin ellos, esta estancia no habría sido la misma. Anche se non tutti sono spagnoli. Con l'aiuto di belle persone come Carmen, Riccardo e Tere mi sono trovato benissimo in Italia. Spero continueremo a rimanere in contatto, perché siete davvero speciali per me.

E anche se Umberto Eco, nel suo manuale di *Come si fa una tesi di laurea*, diceva: *È di cattivo gusto ringraziare il relatore. Se vi ha aiutato ha fatto solo il suo dovere*, mi piacerebbe ringraziare il mio relatore, Marco Lovera, perché ci sono molti modi per fare un lavoro, però non tutti sono corretti. La ringrazio veramente per il suo aiuto e i suoi consigli che mi hanno aiutato tanto a fare e scrivere questa tesi.

And last but not least, I would like to thank you, reader, for spending your time trying to understand the black magic developed in this Master Thesis.

Abstract

The purpose of this thesis is to present a new approach for a linear periodic time-varying (LPTV) identification methodology, based on the most recent publications about this field of study. Nowadays, the development of more complex systems that cannot be modeled as linear time-invariant (LTI) has lead to the study of the identification of LPTV systems. Then, with the emergence of those complex systems and the improvement of the processors computing power, the development of LPTV identification methods is raising, mostly to contrast real data acquired from real systems with physical-based models. This procedure is focused on the frequency-domain subspace-identification method, with the objective of recovering the original LPTV system from input-output data. At the same time, this method will be evaluated in a real physical-based example, proving its suitability for this kind of identification. Accordingly, the final ambitions of this project is to propose a method for LPTV systems identification, to test it and to capture its pros and cons after using it and, eventually, to determine if it would be possible to use this method to perform real-life LPTV systems identification. This has been achieved by developing a procedure that has been implemented in MATLAB so as the procedure and the optimizer could be configured there. After testing the algorithm with noise-free data with sucessful results, as a physical-based system was used to test the model, some added white noise was considered so as the robustness of the method could be also guaranteed. The results show that with a reasonable amount of added noise (comparable to the requirements of certain signal processing procedures), in terms of signal-to-noise ratio, the identification is not compromised. On the other hand, the method shows also robustness when a deformable model (in a modal expansion) is considered, approximating the real system to a less complex identified one. In this case, the method is more noise sensitive than in the previous cases. Finally, the results raise up the fact that the algorithm is implementable and useful for this kind of applications.

Sommario

Lo scopo di questa tesi è quello di presentare un nuovo approccio per una metodologia di identificazione sui sistemi lineari che variano periodicamente nel tempo (LPTV), basato sulle più recenti pubblicazioni relative a questo campo di studio. Al giorno d'oggi, lo sviluppo di sistemi più complessi che non possono essere modellati come sistemi lineari invarianti nel tempo (LTI) ha portato allo studio dell'identificazione di sistemi LPTV. In seguito, con l'emergere di questi sistemi complessi e il miglioramento della potenza di calcolo dei processori, lo sviluppo di metodi di identificazione LPTV sta aumentando, soprattutto per mettere a confronto i dati reali acquisiti da sistemi reali con modelli basati sulla fisica. Questa procedura si concentra sul metodo di identificazione nel dominio della frequenza, con l'obiettivo di recuperare il sistema LPTV originale dai dati di *input-output*. Allo stesso tempo, questo metodo sarà valutato in un esempio basato su un modello fisico reale, dimostrando la sua idoneità per questo tipo di identificazione. Di conseguenza, l'obiettivo finale di questo progetto è quello di proporre un metodo per l'identificazione di sistemi LPTV, di testarlo e di coglierne i pro e i contro dopo averlo utilizzato e, infine, di determinare se sia possibile utilizzare questo metodo per eseguire l'identificazione di sistemi LPTV nella vita reale.
L'obiettivo è stato raggiunto mediante lo sviluppo di una procedura che è stata implementata in MATLAB in modo che la procedura e l'ottimizzatore potessero essere configurati lì. Dopo aver testato l'algoritmo con dati privi di rumore con risultati positivi, poiché per testare il modello è stato utilizzato uno basato su un sistema fisico, è stata considerata la possibilità di aggiungere rumore bianco in modo da garantire la robustezza del metodo. I risultati mostrano che con una quantità ragionevole di rumore aggiunto (paragonabile ai requisiti di alcune procedure di elaborazione dei segnali), in termini di rapporto segnale/rumore (SNR), l'identificazione non viene compromessa. D'altra parte, il metodo mostra robustezza anche quando si considera un modello deformabile (in un'espansione modale), che approssima il sistema reale a un sistema identificato meno complesso. In questo caso, il metodo è più sensibile al rumore rispetto ai casi precedenti. Infine, i risultati dimostrano che l'algoritmo è implementabile e utile per questo tipo di applicazioni.

Contents

List of Figures

Abbreviations

Notation	Description
ACS	Attitude Control Systems.
AFCS	Aircraft Flight Control System.
CV	Coefficient of Variation.
DFT	Discrete Fourier Transform.
EMP	Exponentially Modulated Periodic.
FIR	Finite Impulse Response.
FRF	Frequency Response Function.
FVL	Future Vertical Lift.
HHC	High Harmonic Control.
HSS	Harmonic State-Space.
HTF	Harmonic Transfer Function.
ITF	Instantaneous Transfer Function.
LAC	Load Alleviation Control.
LEO	Low Earth Orbit.
LMS	Least Mean Squares.
LPTV	Linear Periodically Time-Varying.
LPV	Linear Parameter-Varying.
LSTV	Linear Switched Time-Varying.
LTI	Linear Time-Invariant.
LTP	Linear Time-Periodic.
LTV	Linear Time-Varying.
MAV	Micro Air-Vehicle.

Notation	Description
NLTI	NonLinear Time-Invariant.
NLTP	NonLinear Time-Periodic Systems.
NPLTV	NonLinear Periodically Time-Varying.
PTV	Periodic Time-Varying.
SIMO	Single-Input Multiple-Output.
SISO	Single-Input Single-Output.
SNR	Signal-to-Noise Ratio.
SVD	Singular Value Decomposition.

Introduction

In this Master Thesis, a subspace-identification method for linear periodic time-varying (LPTV) systems based on frequency-domain is introduced. Many systems in engineering and also in biology require, at least, a LPTV model to cover the entire problem without risk of losing any dynamics. Systems such as wind turbines, rotor bearing systems, aircraft models or power distribution network are examples of fields where LPTV models apply. Therefore, in Section 1.1, several examples will be provided to raise conciousness of the importance of LPTV systems for periodic systems dynamics modelling. In the mid-1990s, a considerable development about this kind of systems was performed. However, the computational cost of working with these systems lead to a reduced applicability. Nowadays, with the raise of new willings for current prototypes and systems, and the improvement of the computation capabilities, the interest on LPTV model subspace identification is raising, mainly to contrast them to physical-based models.

The PhD Thesis of Wereley [8] sets the basis for a frequency-domain analysis method for LPTV systems. The concept was to expand the periodic system matrices in time-domain expressed in a LPTV space-state formulation into their Fourier series coefficients. Using the principle of harmonic balance, the harmonic transfer function (HTF) could be obtained. This conception, as it will be detailed in Chapter 2, led to doubly infinite HTF in continuous-time. This was, at first, problematic for a numerical implementation. However, this was finally adapted to discrete-time systems, which leads to finite-dimensional matrices.

To the date of publication of this thesis, the literature is more focused on using this input-output methodology through HTF than utilizing the harmonic space-state representation (HSS). This does not mean there are no previous contributions to identification methods that use the HSS representation. These contributions are equivalent to identification methods often used for linear time-invariant (LTI) systems. In fact, in Chapter 3 a review with different examples is provided to context the choice and the development of this project.

The key of this project is to develop an algorithm in which, from a periodic input and output, a frequency-domain identification of a LPTV system can be

performed. This is done through a specific parametric structure of Fourier series coefficients associated with the original LPTV system. As these coefficients (that are the harmonics of the periodic functions that compose the state-space matrices) are preserved when the transformation to the HSS representation is computed, the results of the identification process are the coefficients of the harmonic expansion of each function of the state-space matrices. In general, this process may not provide the original state-space matrix coefficients, but what is always guaranteed is that the identified system can be associated with the original one through a similarity transformation. In Chapter 5, some numerical examples will be presented including noise to the output signal before performing the identification to assess the performance of the algorithm in presence of a realistic signal-to-noise ratio (SNR).

The aim of this thesis is to apply a novel approach for a LPTV idenfication methodology, based on [6], which is oriented to exploit the subspace identification method, so as the original LPTV system can be recovered. Then, the algorithm will be tested on a physical-based example of rotorcraft field, demonstrating that it is suitable for this kind of identification. As a consequence, the final goal of this project is to propose a method for the LPTV systems identification, test it on some examples and extract the pros and cous of its use and to determine if it would be useful for the identification of real-life LPTV systems.

The thesis is organized as follows:

- In Chapter 1, a general overview is provided about different examples of time-varying systems, periodic or not, linear or not, and latest published identification methods for LPTV systems.
- In Chapter 2, some mathematical preliminaries are provided to help the reader with the understanding of the methods that can be mentioned and also with the developed one.
- In Chapter 3, a review of the state of the art of the novel approaches published regarding the LPTV systems identification is presented.
- In Chapter 4, a detailed description of the developed LPTV system idenfication algorithm is carried out.
- In Chapter 5, a physical-based LPTV model based on rotorcraft is explained and used to test the method developed in the previous chapter.
- In Chapter 6, some final conclusions are provided and future developments that could be interesting to research related to the presented project.

Chapter 1

General overview

This chapter aims to be an introductory part for the reader who is not used to work with LPTV systems to get some real-life examples and also latest published identification methods for this kind of systems.

1.1 Time-variant examples

The purpose of this section is to cover some of the different types of time-variant systems that model some physical effects that can be found in nature. From generic time-variant systems to linear periodically time-varying (LPTV) systems, some examples will be provided, so the reader can understand the importance of these systems and also can apply all the theory developed in this thesis to actual systems.

1.1.1 Time-variant systems

Over the years, rotor systems have widely spread in several fields, as manufacturing, aerospace or energy industry. For example, the vibration performance and the operational reliability of the machinery with rotor systems may be considerably influenced by their internal bearings behaviour [9]. In fact, the existing imperfections due to manufacturing process or a rough operation environment may cause several defects on the bearings, whether localizated or distributed ones. The negative point is that it is not possible to detect these imperfections within reasonable time to apply the corrective actions on it. The consequence of this is that the rotor can exhibit some malfunctions that can finally lead to catastrophic disasters. This is why modelling them can be helpful to develop a better understanding of the vibration effect.

In [1], the main goal is to analyze the effects of the bearing defects on the dynamic behaviour of a rotor system, by modelling it as a rotor with rolling

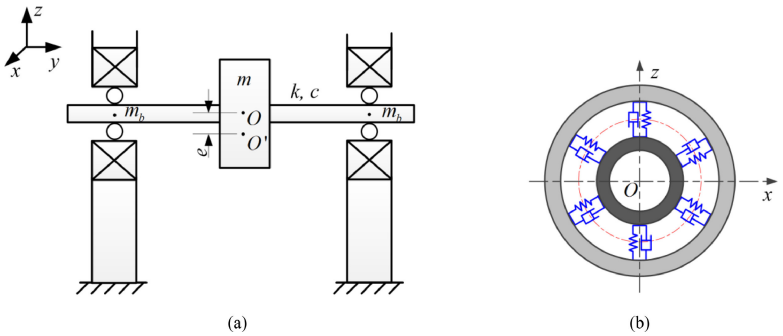

Figure 1.1: Dynamic model of a rotor system considering manufacturing defects [1]

element bearing supported with an eccentricity representing the manufacturing defects (see Figure 1.1). The resulting model shows the impact of the diverse effects that can be taken into account (the impact and the response of distributed and/or localized defects), arriving at a non-linear time-variant system that must be solved with an integrator. This was one of the many examples that can be found in multiple disciplines of engineering.

1.1.2 Time-periodically varying systems

Systems with periodic dynamics also exist across several engineering fields, such as spacecraft, rotorcraft, wind turbines or jet engines. A line of investigation that has been developed in the last years is the flight dynamics of flapping-wing micro air-vehicles (MAVs). These cover the flapping kinematics, the aerodynamic modelling and the dynamic equations of motion [10]. The multi-disciplinary nature of these vehicles leads to a multiobjective kinematics optimization that includes control authority, maneuverability, and aerodynamic performance.

This results on a nonlinear time-periodic system (NLTP), that needs to be preprocessed either for its stability or identification analysis [12]. Two main approaches are considered for the stability analysis of NLTP systems [2], one based on Floquet theory and the other one based on averaging methods. The first one is based on solving the dynamic equations to find the periodic orbit and linearizing the system along this periodic orbit to end up with a linear periodically time-varying system (LPTV). The mathematical transformation of the LPTV into a linear time-invariant (LTI) one will be discussed in the next chapter. The second one uses the averaging techniques to transform the NLTP systems into equivalent nonlinear linear time-invariant (NLTI) systems in a way that the original periodic orbit collapses to a single point in the state-space. Figure 1.3 presents a more visual explanation of this.

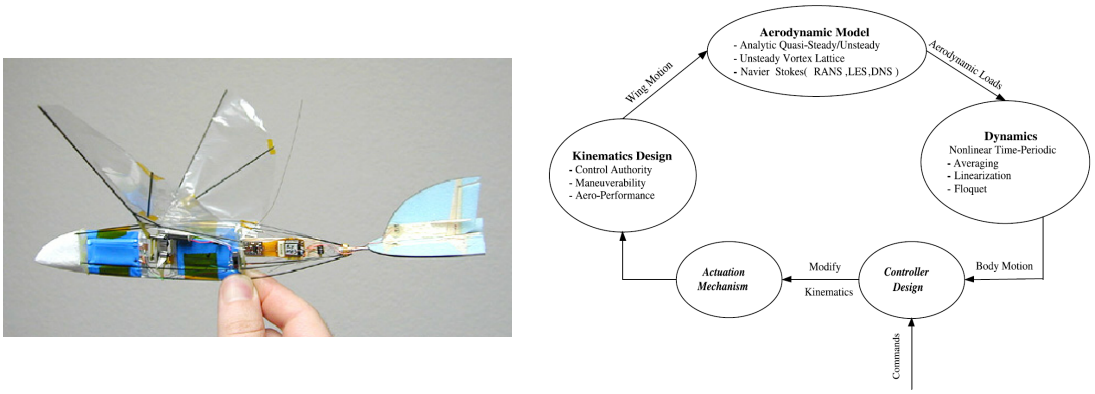

(a) An example of a MAV [11] (b) MAV dynamics and control scheme [10]

Figure 1.2: Example of a MAV and its dynamics modelling

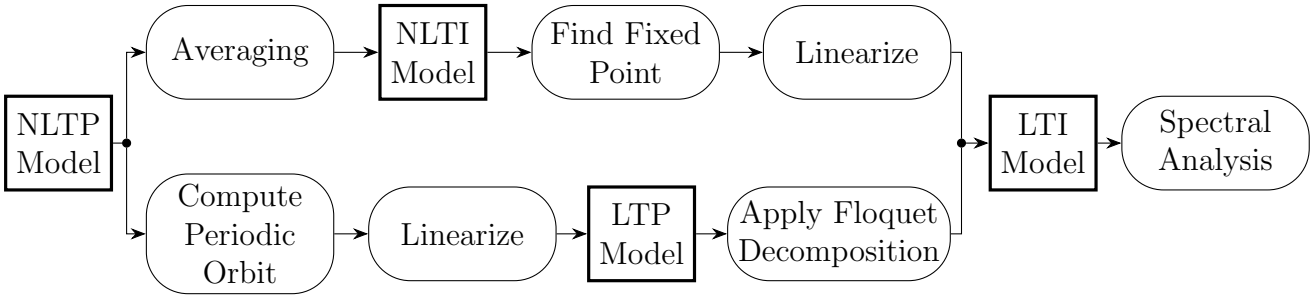

Figure 1.3: Two main approaches used to analyze NLTP systems [2]

Although the averaging approach is commonly used in vibrational analysis [13], because it avoids direct calculation of the periodic orbit, the Floquet-based approach is more used in applications for the dynamic analysis, identification and control of rotorcraft [14].

With respect to the spacecraft field, attitude control systems (ACS) are fundamental in the operation of spacecraft, constituing a necessary component for the successful satellite operation. In practice, there exist a number of possible solutions for attitude control. However, a particularly effective and reliable one has been developed, based on the use of electromagnetic actuators, being specially effective for low Earth orbit (LEO) satellites. Despite the use of magnetic coils for satellite control has been considered since the 1960s, the feasibility of periodic techniques for the small satellites control using magnetic actuators started to be an active research topic from the 2000s. In this sense, Silani and Lovera, [15], collected a review of the existing approaches, up to the date of the publication, based on linear and nonlinear control theory, focusing particularly on periodic control, as well as a solution to the problem in terms of model-based predictive

control.

Some examples can also be found in the wind turbines area, in which the preventive analysis is one of the main tasks for guaranteeing the structural integrity of wind turbines. In the last years, with the development of large offshore wind turbines, this task has become increasingly complex and very demanding. Then, the fact of developing new techniques that allow reducing their operative and maintenance cost is, at the very least, one of the most challenging goals of wind engineering for the next years [16]. Actually, wind turbines have a highly nonlinear periodically time-varying behaviour. Hence, their response to wind and control inputs may vary dramatically over their operational domain. Therefore, for controlling them, nonlinear model-based control can be used, but it usually requires a simple but accurate model [3]. Improved control allows optimal use of the existing generating machinery, as well as better utilization of the local wind resource. In addition, control may extend the service-life of turbines by reducing undesired motion [17].

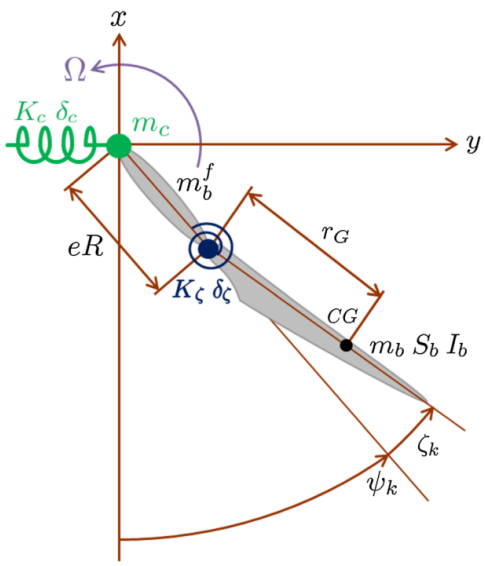

Figure 1.4: Schematic view of the wind-turbine rotor & tower model system [3]

1.1.3 Linear time-periodically varying systems

Finally, LPTV systems, that have been widely used in the many fields, are being proposed in academia for future research lines, either for new ones or to improve existing ones. In this cases, one can find proposals as:

- Using LPTV systems for flight envelope limit detection and protection in rotorcraft, since they are a viable and numerically effective manner to predict envelope limits. In the past, some other methods had been proposed, like

Figure 1.5: Bell V-280, FVL prototipe, in hover configuration [4]

stochastic ones or neural networks [18] [19]. However, LPTV systems are deterministic and may be identified across the entire flight envelope. In [20], LPTV systems derived from a high-fidelity FLIGHTLAB© simulation model of a UH-60, was used to predict and limit rotor loads.

- The development on active control systems for the attenuation of vibrations in helicopters has increased through years [21] [22], to improve the comfort of the crew and passengers and to reduce the fatigue that the rotor and the structure of the aircraft may suffer, as well as to protect the on-board equipment from damage. The analysis of this problem is performed in publications as [23] or [24], where the LPTV model developed in [25] is used for the analysis. This model will be relevant in Chapter 5 to test the algorithm developed in this thesis.

- Flight control design based on LPTV models identified from flight-test data can be useful for the U.S. Army plan to develop a new generation of military helicopters with increased capabilities and reduced maintenance and operational cost. This is the so-called Future Vertical Lift (FVL) project [26]. The new generation of helicopters will operate at significantly higher speeds than current helicopters. This would request the study of the higher harmonic rotor loads to alleviate them and reduce the maintenance cost. Then, LPTV physics-based and identified models will be necessary for the future implementation of higher harmonic control (HHC) and load alleviation control (LAC) on their design and production.

- Subspace Model Identification has been used in many cases, whether in academic research or in industry, with successful results. However, the LPTV model identification may become a complex task. The motivation behind

using existing subspace methods, that can be extended to LPTV models, is that using them would allow to keep ease of use and implementation, numerical robustness and non-iterative nature. These facts represent such great advantages, that is why they can be really considered as a solution for LPTV modelling and identification problems. Another fact to be taken into account is that early developments in this field took place in the at mid-1990s [27], where the computational capacity was not quite large, and could be a real problem. Nowadays, the development of the technology has arrived to a point in which that is not a problem anymore and any personal computer can process a vast amount of data without taking such a long time.

- The aeroacoustics of the main and the tail rotor can be also considered in an NLTP system that represents the rotorcraft flight dynamics. Then, as it was explained above, the NLTP model can be approximated to an LPTV one by linearizing about a period with a certain flight condition. Then, the LPTV system can be harmonically decomposed into an LTI system (see Chapter 2), which can be used to achieve an active noise-reduction flight control laws that can be derived by means of time-invariant control theory.
  Then, two main approaches have been developed regarding this. The first one uses primary flight controls to reduce the generated noise in maneuvering flight [28]. The second one is based on the use of a high-order LTI model to design combined HHC-AFCS control laws that reduce the noise in trimmed flight [29].

- Orbit control of satellites, in the case of Zeng et al. [30], aims at an accurate regulation of the error between the desired trajectory and the actual one. If the reference orbit is circular, then the control problem can be formulated with reference to the Euler-Hill linearised model for relative motion, which is time-invariant. However, when the reference orbit is elliptical, the equations of the relative motion becomes LPTV [31].

1.2 Literature review

In [14], Saetti and Lovera carried out a review about the LPTV systems and the different models for time-periodic models for rotorcraft and their expansion to high-order time-invariant systems. This survey also includes a list of novel approaches that have been developed in the last years, both in time and in frequency domain. This thesis studies these new approaches and chooses one of them for its development, test and the analysis of its pros and cons of its implementation into a real-life model. The following publications have been collected and are presented to the reader as a review. Later, on Chapter 3, a more technical presentation of them will be provided.

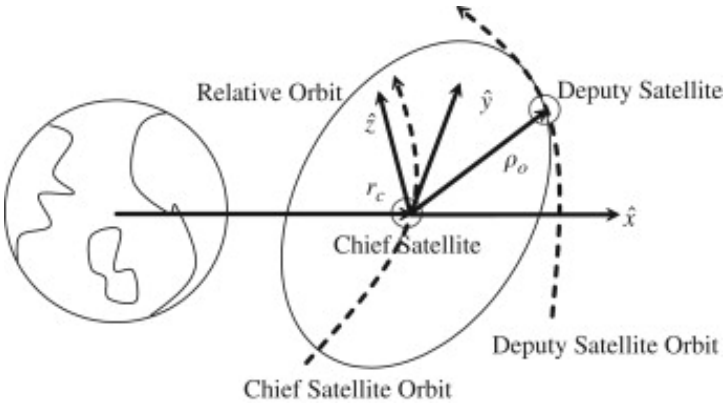

Figure 1.6: Formation keeping reference systems scheme [5]

- In [32], Wutao and Mehr developed a frequency-domain identification method for finite impulse response (FIR) LPTV systems in discrete-time by using the discrete Fourier transform (DFT). By choosing an input the period of which is a multiple of the period of the system, the period of the output can be computed, as it is equal to the largest one. Then, the identification is reduced to a least-squares solution of a set of linear equations.

- In [33], Louarroudi, Pintelon and Lataire presented a non-parametric estimation so as the evolution of the dynamics of a periodic time-varying (PTV) system (both for continuous and discrete time and for linear and non-linear systems) can be tracked by applying a multisine input, in an output-error framework. From the non-parametric estimates, the evolution of the dynamics is described by the instantaneous transfer function (ITF). Finally, an application of this methodology is applied to a NPLTV electronic example circuit.

- In [34], Goos and Pintelon described a frequency-domain identification technique to estimate multivariate linear parameter-varying (LPV) continuous-time state-space models, where a periodic variation of the parameters is imposed. The proposed identification method designs a periodic input signal, taking the periodicity of the parameter variation into account. It is shown that, when an integer number of periods is observed for both the input and the scheduling, the state-space model representation has a specific, sparse structure in the frequency domain. Then, a weighted non-linear least-squares algorithm minimizes the output error. Finally, two initialization methods are explored to generate starting values, one based on a LTI approximation and another one focused on LTV input–output differential equations, from which a corresponding state-space realization is computed.

- In [35], Wood performed a dissertation about model-based identification and control of kites for wind power generation. The deviation of a kite

from a periodic cycle can be modelled as a LPTV system. Therefore, a subspace identification method is derived from input and output data to obtain periodic state-space models. This identification method approach is called *Energy (cumulative spectrum) bound noise fitting*. Finally, the black-box modelling method is illustrated on a simulation case study.

- In [6], Uyanik, Ankarali, Cowan and Morgul proposed a new methodology for subspace-based state-space identification for LPTV systems. As LPTV systems can be lifted to equivalent LTI systems, firstly the input–output data from an unknown LPTV system is lifted as if they were collected from an equivalent LTI system. Then, a frequency-domain subspace identification method is used to find the LTI system estimate. Subsequently, the proposal for a novel method to obtain a time-periodic realization for the estimated lifted LTI system is provided by exploiting the specific parametric structure of Fourier series coefficients of the frequency-domain lifting method. This method can be used to obtain state-space estimates for unknown LPTV systems as well as to obtain Floquet transforms for known LPTV systems.

- In [36], Yin, Iannelli, Khosravi, Parsi and Smith proposed a new methodology in LPTV system identification. In contrast to other methods that totally separate dynamics at different tag times for identification, this method is focused on imposing appropriate structural constraints on the LTI reformulation of LPTV systems. This method adopts a periodically-switched truncated infinite impulse response model for LPTV systems, where the structural constraints are interpreted as the requirement to place the poles of the non-truncated models at the same locations for all sub-models. This constraint is imposed by combining the atomic norm regularization framework for LTI systems with the *group lasso* technique in regression. As a result, the estimated system is both uniform and low-order, which is hard to achieve with other existing estimators. Then, Monte Carlo simulations used to show that the grouped atomic norm method not only shows better results compared to other regularized methods, but also outperforms the subspace identification method under high noise levels in terms of model fitting.

Chapter 2

Mathematical preliminaries

In this chapter, an overview of the mathematical properties and definitions around the LPTV systems will be provided to help the reader with the understanding of the following chapters.

2.1 Linear time-varying system

Following the formulation that can be found in [37] and [38], and starting from scratch, let $\mathcal{T}$ be the time domain of t, so as $\mathcal{T} = \{t \in \mathbb{R} : 0 \leq \tau \leq t\}$ in continuous time, while $\mathcal{T} = \{t \in \mathbb{Z} : 0 \leq \tau \leq t\}$ in discrete time. Notice that τ stands for the initial time. Now let $x \in \mathbb{R}^n$ be the state vector. The simplest definition of a LTV system is the following:

$$\begin{aligned} \dot{x}(t) &= A(t)\,x(t) && \text{in continuous-time} \\ x(t+1) &= A(t)\,x(t) && \text{in discrete-time} \\ x(\tau) &= x_\tau \end{aligned} \tag{2.1}$$

where $A : \mathcal{T} \to \mathbb{R}^{n\times n}$ is the system matrix (by definition, a square matrix) which computes the derivative of the state, for continuous-time, or the state at $t+1$, for discrete-time, for a given t and a given $x(t)$, and $x(\tau) \in \mathbb{R}^n$, also noted as x_τ, is the initial state. Notice that $A(t)$ does not depend on the state.

The solution of the state equation can be represented as follows:

$$x(t) = \Phi_A(t,\tau)\,x_\tau \tag{2.2}$$

where $\Phi_A : \mathcal{T} \times \mathcal{T} \to \mathbb{R}^{n\times n}$ is the *transition matrix* of $A(t)$, that maps the initial state to the current one. This matrix has the following properties:

$$\begin{aligned} \dot{\Phi}_A(t,\tau) &= A(t)\,\Phi_A(t,\tau) && && \text{in continuous-time} \\ \Phi_A(t,\tau) &= A(t-1)\,A(t-2)\cdots A(\tau), && t > \tau && \text{in discrete-time} \\ \Phi_A(\tau,\tau) &= I_{n\times n}, && \forall \tau \in \mathcal{T} \end{aligned} \tag{2.3}$$

where $I_{n\times n}$ is the square identity matrix of dimension n. The transition matrix also holds the following properties:

$$\Phi_A(t,\tau) = \Phi_A(t,\tau_1)\,\Phi_A(\tau_1,\tau), \tag{2.4}$$

both in continuous-time and in discrete-time, and

$$\begin{aligned} \Phi_A(t,\tau)^{-1} &= \Phi_A(\tau,t) \\ \frac{\mathrm{d}}{\mathrm{d}\tau}\left(\Phi_A(t,\tau)\right) &= -\Phi_A(t,\tau)\,A(\tau), \end{aligned} \tag{2.5}$$

only in continuous-time.

Considering Abel's identity [39], the following can be stated:

$$\det(\Phi_A(t,\tau)) = \exp\left(\int_\tau^t \operatorname{tr}(A(s))\,\mathrm{d}s\right). \tag{2.6}$$

This means that, in continuous time, the transition matrix is never singular (its determinant is always positive, as the exponential function, for a real argument, is always positive), which means it is always invertible. However, for a general case it is not possible to obtain an explicit expression for the transition matrix, because the exponential solution is not valid in every case $\left(\Phi_A(t,\tau) \neq \exp\left(\int_\tau^t A(s)\,\mathrm{d}s\right)\right)$. In fact, according to Rugh [40], the previous solution will only hold when:

$$A(t)\int_\tau^t A(s)\,\mathrm{d}s = \int_\tau^t A(s)\,\mathrm{d}s\,A(t), \quad \forall\, t,\tau. \tag{2.7}$$

2.2 Linear periodically time-varying (LPTV) systems

A particular case of a LTV system is the LPTV system, that can be represented by a coefficient matrix of T-periodic functions. This can be represented by adding to the system described in equation (2.1) the following condition:

$$A(t) = A(t+T), \quad T = 2\pi/\omega > 0. \tag{2.8}$$

In this case, the transition matrix is *bi-periodic*:

$$\Phi_A(t+T,\tau+T) = \Phi_A(t,\tau). \tag{2.9}$$

A special case of the transition matrix can be defined exploiting the property of periodicity of the transition matrix:

$$\Psi_A(\tau) = \Phi_A(\tau+T,\tau) \tag{2.10}$$

which is called *monodromy matrix* at time τ. The eigenvalues of the monodromy matrix (λ) do not depend on time (or τ), being called *characteristic multipliers* of A. Whatsmore, and according to equation (2.6), all the characteristic multipliers in a continuous-time system must be not null, but not necessary in a discrete-time system.

The characteristic multipliers describe the stability of the system. That is to say, the system will be asymptotically stable if and only if its characteristic multipliers belong to the open unit disc.

It should be taken into account that the stability conditions can be formulated according to the Lyapunov equations:

$$\begin{aligned} -\dot{P}(t) &= A(t)^{\mathrm{T}}\, P(t) + P(t)\, A(t) + Q(t) && \text{in continuous-time} \\ P(t) &= A(t)^{\mathrm{T}}\, P(t+1)\, A(t) + Q(t) && \text{in discrete-time} \\ Q(t) &= Q(t+T),\ \ x^{\mathrm{T}}\, Q(t)\, x > 0 && \forall t,\ \ \forall\, x \neq 0. \end{aligned} \tag{2.11}$$

The steady-state solution $\bar{P}(t)$ of this equation will describe an asymptotically stable periodic system if and only if it is unique, periodic and positive definite.

So far, the treatment and definitions were made considering a free response system, but this can be extended to a forced-response linear state-space model [14]. Therefore, a general LPTV state-space model can be written, in continuous-time, as:

$$\begin{aligned} \dot{x}(t) &= A_c(t)\, x(t) + B_c(t)\, u(t) \\ y(t) &= C_c(t)\, x(t) + D_c(t)\, u(t) \end{aligned} \tag{2.12}$$

or in discrete-time as:

$$\begin{aligned} x(t+1) &= A_d(t)\, x(t) + B_d(t)\, u(t) \\ y(t) &= C_d(t)\, x(t) + D_d(t)\, u(t) \end{aligned} \tag{2.13}$$

where:

- $u : \mathcal{T} \to \mathbb{R}^{n_i \times 1}$ is the input vector
- $y : \mathcal{T} \to \mathbb{R}^{n_o \times 1}$ is the output vector
- $B : \mathcal{T} \to \mathbb{R}^{n \times n_i}$ is the input matrix
- $C : \mathcal{T} \to \mathbb{R}^{n_o \times n}$ is the output matrix
- $D : \mathcal{T} \to \mathbb{R}^{n_o \times n_i}$ is the feedthrough matrix

being n_i and n_o the number of inputs and outputs, respectively. These matrices also hold the T-periodic property shown in equation (2.8). The smallest T for which these periodicity conditions hold is defined as the period of the system. Notice that $T \in \mathbb{R}$ in continuous-time while $T \in \mathbb{Z}$ in discrete-time.

2.3 Floquet-Lyapunov theory

Let $x(t) \in \mathbb{R}^n$ be a solution of a LPTV system defined in equation (2.12) or equation (2.13), depending on the considered time domain. Then, as stated in [41], it is possible to find a T-periodic invertible state-space transformation, $\bar{x}(t) = S(t)\,x(t)$, such that in the new coordinates, the system matrix is time-invariant ($\bar{A}(t) = \bar{A}$). This will lead to the following:

$$\begin{aligned}
\dot{\bar{x}}(t) &= \dot{S}(t)\,x(t) + S(t)\,\dot{x}(t) \\
&= \left(S(t)\,A(t)\,S(t)^{-1} + \dot{S}(t)\,S^{-1}\right)\,\bar{x}(t) && \text{in continuous-time} \\
\bar{x}(t+1) &= S(t+1)\,x(t+1) \\
&= \left(S(t+1)\,A(t)\,S(t)^{-1}\right)\,\bar{x}(t) && \text{in discrete-time}
\end{aligned} \tag{2.14}$$

Then:

$$\bar{A} = \begin{cases} S(t)\,A(t)\,S(t)^{-1} + \dot{S}(t)\,S^{-1} & \text{in continuous-time} \\ S(t+1)\,A(t)\,S(t)^{-1} & \text{in discrete-time} \end{cases} \tag{2.15}$$

The quest now is to find a pair $S(t)$ and $\bar{A}$ that satisfies the following differential equation (in the continuous-time case):

$$\dot{S}(t) = \bar{A}\,S(t) - S(t)\,A(t), \quad S(\tau) = I_{n\times n}. \tag{2.16}$$

The solution can be found by solving $e^{\bar{A}\,T} = \Psi_A(\tau)$, where τ is any given time point. Then, the appropriate (T-periodic) transformation matrix is the following:

$$S(t) = e^{(t-\tau)\bar{A}}\,\Phi_A(\tau, t). \tag{2.17}$$

The discrete-time case is not that straightforward because it can lead to a non-reversible system. However, in the reversible case (that is, $A(t)$ is non-singular $\forall t$), the Floquet representation always exists and the matrix $\bar{A}$ can be computed by solving $\bar{A}^T = \Psi_A(\tau)$ [†] and the transformation matrix is defined by:

$$S(t) = \bar{A}^{t-\tau}\,\Phi_A(\tau, t). \tag{2.18}$$

So far, a relationship between the monodromy matrix and the time-invariant system matrix has been provided, among others. Therefore, the eigenvalues of $\bar{A}$ are named *characteristic exponents*. According to this relationship, the associated characteristic exponents (ρ) can be defined as follows:

$$\Psi_A(\tau) = \begin{cases} e^{\bar{A}T} \\ \bar{A}^T \end{cases} \quad \rightarrow \quad \lambda = \begin{cases} e^{\rho T} & \text{in continuous-time} \\ \rho^T & \text{in discrete-time.} \end{cases} \tag{2.19}$$

[†]Notice that T stands for the system period and not the transpose operator T

Notice that the characteristic exponents are not uniquely defined due to the polydromy of the complex exponential functions. In continuous-time:

$$e^{(a+i\,b)\,T+i\,2\,k\,\pi} = e^{a\,T}\left(\cos\left(b\,T+2\,k\,\pi\right)+i\,\sin\left(b\,T+2\,k\,\pi\right)\right),\quad k\in\mathbb{Z}, \tag{2.20}$$

whatever the value of k, the same number is computed. It also happens in discrete-time, where

$$\begin{aligned}(a+i\,b)^T = r^T\,e^{(\theta+2\,k\,\pi)\,T} &= r^T\,e^{\psi(k)\,T}\\ &= r^T\,\left(\cos\left(\psi(k)\,T\right)+i\,\sin\left(\psi(k)\,T\right)\right),\quad k\in\mathbb{Z},\end{aligned} \tag{2.21}$$

being $r=\sqrt{a^2+b^2}$ and $\theta=\operatorname{atan2}(a,b)$, in which, as in the previous case, the same number can be computed whatever the value of k.

2.4 Frequency-domain reformulation

In 1990, a frequency response formulation analogous to the classical LTI Bode gain and phase response was developed for continuous-time LPTV systems at MIT. Thanks to Wereley and Hall contributions [42], [43] and [44], the development of a comprehensive open-loop analysis theory for LPTV systems, characterising poles, zeros and their directional properties, a generalised Nyquist criterion or a complete frequency domain interpretation arose.

On one hand, it is possible to recall the fundamental Bode notion in LTI systems: a sinusoidal input with a given frequency will be mapped by the LTI frequency response function operator into sinusoidal output of the same frequency but where the amplitude and/or the phase may change. On the other hand, if a sinusoidal input is applied to a LPTV system, the steady-state output will be the sum of infinite sinusoids that will appear in the output at the input frequency plus or minus the multiples of the LPTV fundamental frequency, each one with a different amplitude and/or phase (see Figure 2.1).

In LTI theory, this fact suggested the existence of a transfer function that mapped the input to the output. For LPTV systems, this concept of transfer function was developed, being commonly called *harmonic transfer function* (HTF). This harmonic transfer function maps periodic input signals to steady-state periodic output signals. The following subsections will explain all the formulation up to the HTF construction.

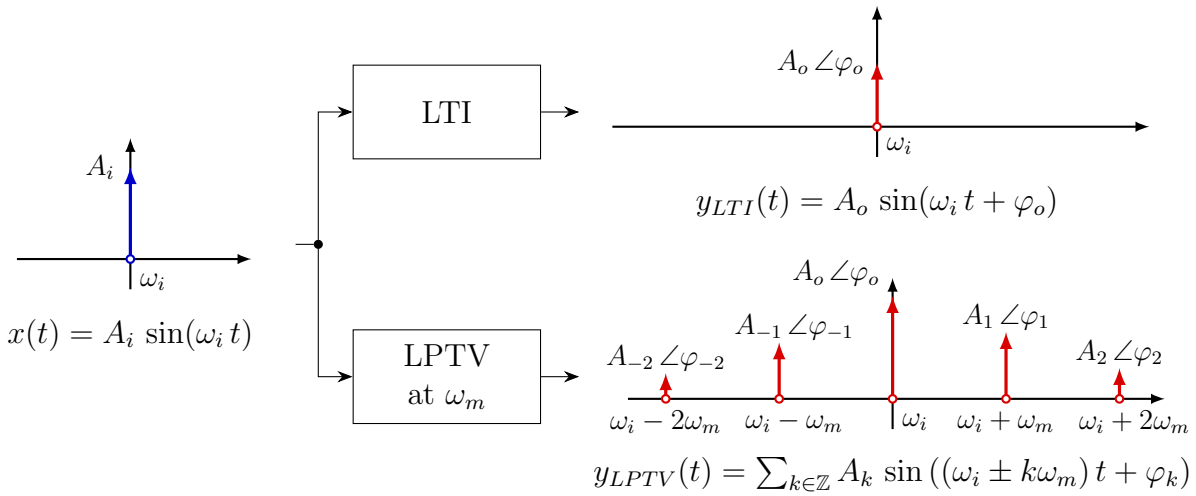

Figure 2.1: LTI vs LPTV sinusoidal input-output comparison

2.4.1 Fourier expansion series

Considering the system of equation (2.12), let us consider now a complex Fourier series expansion of each matrix at the fundamental system frequency:

$$Q(t) = \sum_{n=-\infty}^{\infty} Q_n \, e^{jn\omega_m t} \tag{2.22}$$

where $Q(t)$ can be any of the space-state matrices of the system.
Notice that in the discrete-time form, the system frequency would be $\omega_m = 2\pi T_s/T$, being T_s the sampling time and T the period of the system, to be consistent with the developed formulation. Now, if $N_f = T/T_s$, consider it even for the sake of simplicity, the expansion cannot be infinitely long, but it is constrained to the Nyquist frequency [6]. Consider also N, even as N_f. At the end of this section, its meaning will be detailed. Then, the expansion is defined as follows:

$$Q(t) = \sum_{n=-N/2}^{N/2-1} Q_n \, e^{jn\omega_m t}. \tag{2.23}$$

2.4.2 Exponentially Modulated Periodic Signals

The class of *exponentially modulated periodic* (EMP) signals is an extension of the class of periodic signals, in which an exponential modulation, with a frequency, which is a complex scalar, that can be freely chosen according to what is desired,

is added. Then the modulated expansion would be as follows:

$$Q(t) = \begin{cases} e^{s\,t} \sum_{n=-\infty}^{\infty} Q_n\, e^{jn\,\omega_m\,t} & \text{in continuous-time} \\ z^t \sum_{n=-\infty}^{\infty} Q_n\, e^{jn\,\omega_m\,t} & \text{in discrete-time.} \end{cases} \tag{2.24}$$

This class of signals is a generalization of the class of T-periodic signals. Actually, if $s = 0/z = 1$, an ordinary time-periodic signal expansion is recovered. The use of EMP signals is well-extended in the treatment of T-periodic signals, mostly, to derive an EMP steady-state form of a T-periodic system in the frequency domain.

Expanding equation (2.12) or equation (2.13) using the EMP expansion in equation (2.24) [42]:

$$\begin{cases} 0 = \sum_{n\in\mathbb{Z}} \left(s_n\, X_n - \sum_{m\in\mathbb{Z}} A_{n-m}\, X_m - \sum_{m\in\mathbb{Z}} B_{n-m}\, U_m \right) e^{s\,t}\, e^{jn\,\omega_m\,t} \\ 0 = \sum_{n\in\mathbb{Z}} \left(Y_n - \sum_{m\in\mathbb{Z}} C_{n-m}\, X_m - \sum_{m\in\mathbb{Z}} D_{n-m}\, U_m \right) e^{s\,t}\, e^{jn\,\omega_m\,t}. \end{cases} \tag{2.25}$$

The discrete-time form would be similar, as it was developed before. Let $\boldsymbol{I_n}$ the interval $[-N/2,\, N/2-1]$:

$$\begin{cases} 0 = \sum_{n\in\boldsymbol{I_n}} \left(z e^{jn\,\omega_m} X_n - \sum_{m\in\boldsymbol{I_n}} A_{n-m}\, X_m - \sum_{m\in\boldsymbol{I_n}} B_{n-m} U_m \right) z^t\, e^{jn\,\omega_m\,t} \\ 0 = \sum_{n\in\boldsymbol{I_n}} \left(Y_n - \sum_{m\in\boldsymbol{I_n}} C_{n-m} X_m - \sum_{m\in\boldsymbol{I_n}} D_{n-m}\, U_m \right) z^t\, e^{jn\,\omega_m\,t}. \end{cases} \tag{2.26}$$

Therefore, the set of exponentials $\{e^{jn\,\omega_m\,t} | n \in \mathbb{Z}\}$ constitutes an orthonormal basis in the range $[0, T]$. This leads, by the principle of harmonic balance, to the result that each term enclosed in the parentheses must be zero to ensure that the overall sum is null. Hence, the systems (2.25) and (2.26) hold the following:

$$\begin{cases} s_n\, X_n = \sum_{m\in\mathbb{Z}} A_{n-m}\, X_m + \sum_{m\in\mathbb{Z}} B_{n-m}\, U_m \\ Y_n = \sum_{m\in\mathbb{Z}} C_{n-m}\, X_m + \sum_{m\in\mathbb{Z}} D_{n-m}\, U_m \end{cases} \tag{2.27}$$

in continuous-time, and

$$\begin{cases} z\, e^{jn\,\omega_m} X_n = \sum_{m\in\boldsymbol{I_n}} A_{n-m}\, X_m + \sum_{m\in\boldsymbol{I_n}} B_{n-m}\, U_m \\ Y_n = \sum_{m\in\boldsymbol{I_n}} C_{n-m}\, X_m + \sum_{m\in\boldsymbol{I_n}} D_{n-m}\, U_m \end{cases} \tag{2.28}$$

in discrete-time version.

2.4.3 Harmonic State-Space Model

However, for a better manipulation, these summations can be expressed in a matrix form, using Toeplitz matrices. Actually, a T-periodic matrix can be expressed in terms of its harmonics (Fourier coefficients) as a doubly infinite block-Toeplitz matrix, which is called the *Toeplitz form*:

$$\mathcal{Q} = \begin{bmatrix} \ddots & \vdots & \vdots & \vdots & \vdots & \vdots & \\ \cdots & Q_0 & Q_{-1} & Q_{-2} & Q_{-3} & Q_{-4} & \cdots \\ \cdots & Q_1 & Q_0 & Q_{-1} & Q_{-2} & Q_{-3} & \cdots \\ \cdots & Q_2 & Q_1 & Q_0 & Q_{-1} & Q_{-2} & \cdots \\ \cdots & Q_3 & Q_2 & Q_1 & Q_0 & Q_{-1} & \cdots \\ \cdots & Q_4 & Q_3 & Q_2 & Q_1 & Q_0 & \cdots \\ & \vdots & \vdots & \vdots & \vdots & \vdots & \ddots \end{bmatrix}. \tag{2.29}$$

Notice that in the discrete-time domain, these matrices will not be infinite but they will be limited by the maximum harmonic that can be computed (recalling the $\boldsymbol{I_n}$ interval). Then, the discrete-time version would be as follows:

$$\mathcal{Q} = \begin{bmatrix} Q_0 & Q_{-1} & \cdots & Q_{-N/2} & Q_{N/2-1} & Q_{N/2-2} & \cdots & Q_1 \\ Q_1 & Q_0 & \cdots & Q_{-N/2+1} & Q_{-N/2} & Q_{N/2-1} & \cdots & Q_2 \\ \vdots & \vdots & & \vdots & \vdots & \vdots & & \vdots \\ Q_{-1} & Q_{-2} & \cdots & Q_{N/2-1} & Q_{N/2-2} & Q_{N/2-3} & \cdots & Q_0 \end{bmatrix}. \tag{2.30}$$

However, the state, input and output are vectors, which can be also expressed in a doubly infinite vectors composed by the harmonics of their Fourier series expansion, as shown in equations (2.24), leading to the following structure:

$$\mathcal{V} = \begin{bmatrix} \vdots \\ V_{-1} \\ V_0 \\ V_1 \\ \vdots \end{bmatrix}. \tag{2.31}$$

In the discrete-time case, these vectors will not be infinite but they will be limited to the $\boldsymbol{I_n}$ interval.

Using the Toeplitz form of the matrices, the systems (2.27), (2.28) can be expressed as EMP steady-state response systems composed by constant coefficients. This is called the *harmonic state-space* (HSS) model, which represents a lifted LTI equivalent for a periodic class of input-output signals. These models are defined as follows:

$$\begin{aligned} s\,\mathcal{X} &= (\mathcal{A} - \mathcal{N}_c)\,\mathcal{X} + \mathcal{B}\mathcal{U} \\ \mathcal{Y} &= \quad \mathcal{C} \quad \mathcal{X} + \mathcal{D}\mathcal{U} \end{aligned} \tag{2.32}$$

for the continuous-time form, and:

$$\begin{aligned} z\,\mathcal{N}_d\,\mathcal{X} &= \mathcal{A}\,\mathcal{X} + \mathcal{B}\,\mathcal{U} \\ \mathcal{Y} &= \mathcal{C}\,\mathcal{X} + \mathcal{D}\,\mathcal{U} \end{aligned} \tag{2.33}$$

for the discrete-time form. Notice that the matrices $\mathcal{N}_c$ and $\mathcal{N}_d$ are a consequence of the delay between X_n and X_m in the systems (2.27) and (2.28). Therefore, these $\mathcal{N}$ matrices are defined as block diagonal matrices containing the delay of each equation of the system:

$$\begin{aligned} \mathcal{N}_c &= \text{blkdiag}\{j\,n\,\omega_m\,I_{n\times n}\} = \\ &= \text{blkdiag}\{n\,C\} = \\ &\begin{bmatrix} \ddots & \vdots & \vdots & \vdots & \vdots & \vdots & \\ \cdots & -2C & 0 & 0 & 0 & 0 & \cdots \\ \cdots & 0 & -C & 0 & 0 & 0 & \cdots \\ \cdots & 0 & 0 & 0 & 0 & 0 & \cdots \\ \cdots & 0 & 0 & 0 & C & 0 & \cdots \\ \cdots & 0 & 0 & 0 & 0 & 2C & \cdots \\ & \vdots & \vdots & \vdots & \vdots & \vdots & \ddots \end{bmatrix} \end{aligned} \qquad \begin{aligned} \mathcal{N}_d &= \text{blkdiag}\{e^{j\,n\,\omega_m}I_{n\times n}\} = \\ &= \text{blkdiag}\{e^{n\,D}\,I_{n\times n}\} = \\ &\begin{bmatrix} e^{-\frac{N}{2}D}\,I & \cdots & 0 & 0 & 0 & \cdots & 0 \\ \vdots & \ddots & \vdots & \vdots & \vdots & & \vdots \\ 0 & \cdots & e^{-D}\,I & 0 & 0 & \cdots & 0 \\ 0 & \cdots & 0 & I & 0 & \cdots & 0 \\ 0 & \cdots & 0 & 0 & e^{D}\,I & \cdots & 0 \\ \vdots & & \vdots & \vdots & \vdots & \ddots & \vdots \\ 0 & \cdots & 0 & 0 & 0 & \cdots & e^{\left(\frac{N}{2}-1\right)D}\,I \end{bmatrix} \end{aligned} \tag{2.34}$$

where $C = j\,\omega_m\,I_{n\times n}$, $D = j\,\omega_m$ and $I = I_{n\times n}$ defined for the sake of simplicity of notation.

2.4.4 Harmonic Transfer Function

Once the systems are defined, the harmonic transfer function can be defined just by relating the input harmonics and the output harmonics vectors:

$$\mathcal{G}\,(s/z) = \begin{cases} \mathcal{C}\,(s\,\mathcal{I} - \mathcal{A} + \mathcal{N}_c)^{-1}\,\mathcal{B} + \mathcal{D} & \text{in continuous-time} \\ \mathcal{C}\,(z\,\mathcal{N}_d - \mathcal{A})^{-1}\,\mathcal{B} + \mathcal{D} & \text{in discrete-time} \end{cases} \tag{2.35}$$

$$\mathcal{G}(s/z) = \begin{bmatrix} \ddots & \vdots & \vdots & \vdots & \\ \cdots & G_0(s - s_m/z\cdot z_m^{-1}) & G_{-1}(s/z) & G_{-2}(s + s_m/z\cdot z_m) & \cdots \\ \cdots & G_1(s - s_m/z\cdot z_m^{-1}) & G_0(s/z) & G_{-1}(s + s_m/z\cdot z_m) & \cdots \\ \cdots & G_2(s - s_m/z\cdot z_m^{-1}) & G_1(s/z) & G_0(s + s_m/z\cdot z_m) & \cdots \\ & \vdots & \vdots & \vdots & \ddots \end{bmatrix} \tag{2.36}$$

where $s_m = j\,\omega_m$ and $z_m = e^{j\,\omega_m}$. Each term of the matrix can be defined using indices, expressing them as $G_{a\,b} = G_a(s - b\,s_m/z\cdot z_m^b)$. The index b expresses the corresponding harmonic of the input, while the index a expresses the harmonic delay between the harmonic of the input and the harmonic of the output.

An example may clarify the definitions. If the considered system was a LTI one, then, the HTF would only have non-zero values on the main diagonal, this is, $G_{0\,b}$. This links with Figure 2.1, where there is no frequency delay between the input and the output in a LTI system. This explains why all the terms in which $a \neq 0$ are null.

Notice also that the variable s/z is the chosen one when the exponential modulation is performed. Then, if it is not desired to modulate the signal, $s = 0/z = 1$. Also, notice that $\mathcal{G}(s)$ is actually an infinite-dimensional operator and that it cannot be implemented exactly in a numerical code. This difficulty can be circumvented by setting a parameter N, as in the discrete-time case, that will set the number of the harmonic where the truncation will be done. In fact, this parameter was already defined in the discrete-time fomulation, at the beginning of this section. The effect of this parameter is that the truncation can be also used in case that the parameter N_f becomes so large that the computation time would become excessive. This is why, in this case, $N \in [2, N_f] \in \mathbb{Z}$. However, the study of the impact of the truncation will not be discussed further in this thesis.

Chapter 3

State of the art

In this chapter, the main objective is to provide a review of the latest research lines about reformulations for identification algorithms for LPTV systems provided in Section 1.2, focusing more now on the mathematical aspects. This will let us justify later, in Chapter 4, some decisions that were made. The order of this chapter will be the same as in Section 1.2, each section being dedicated to each publication.

3.1 Identification of linear periodically time-varying systems using periodic sequences

In the publication by Wutao and Mehr [32], the main goal is to perform an idenfication in frequency domain by converting the LPTV system into a linear switched time-varying (LSTV) blocked system. Then, applying a periodic input, the steady-state of the output will be also periodic. Considering now the DFT of the input and the output, a least-mean-square (LMS) algorithm can be used for the identification.

Consider a M-periodic LPTV system. Then, the input-output response can be expressed as the infinite sum of the product of $g(m, i)$, which is the system response at time m to an impulse applied at time i in its input, and $x(i)$, the input at time i. As an inherent property of LPTV systems, the system response operator is bi-periodic, $g(m + M, i + M) = g(m, i)$, $\forall\, m, i$. Then, a new operator can be defined as $h(m, i) = g(m, m - i)$ leading to:

$$y(m) = \sum_{i=0}^{\infty} g(m, i)\, x(i) = \sum_{i=0}^{\infty} h(m, m - i)\, x(i). \tag{3.1}$$

Now, setting the impulse response

$$H_m(z) = \sum_{i=0}^{\infty} h(m,i)\, z^{-i} = H_{m+M} = \sum_{i=0}^{\infty} h(m+M,i)\, z^{-i}, \tag{3.2}$$

a representation of the LPTV system is obtained by setting M LTI subsystems that will be switched at the output, as shown in Figure 3.1. This switch is connected to the output of the m-th LTI subsystem H_m at time m, until time $M-1$ is reached, then, the switch comes back to time 0 and restarts the period. To model the switch, the output of the m-th LTI subsystem at time n is multiplied by the factor $(1/M)\sum_{\ell=0}^{M-1} W_M^{(n-m)\,\ell} = (1/M)\sum_{\ell=0}^{M-1} e^{-j\,2\,\pi/M\,(n-m)\,\ell}$.

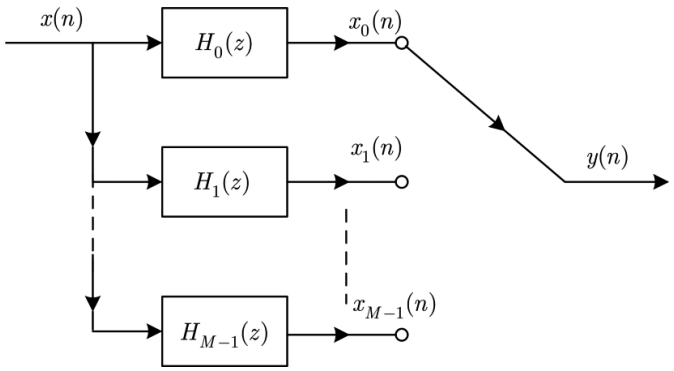

Figure 3.1: M-periodic LPTV system scheme as M LTI systems switched at output

Then, the output $Y(z)$ can be modeled as the sum of $Y_m(z)$, $m \in [0, M-1]$, where

$$Y_m(z) = \frac{1}{M}\sum_{\ell=0}^{M-1} W_M^{-m\ell} H_m\left(zW_M^{-\ell}\right) X\left(zW_M^{-\ell}\right). \tag{3.3}$$

Now, one assumption made by the authors is that the impulse response of each subsystem is of finite length. This lets us define an upper limit for the sum in equation (3.2), defining L_m as the length of the m-th branch. By substitution, $H_m(z) = e_m^{\mathrm{T}}(z)\, h_m$, where $h_m^{\mathrm{T}} = [h(m,0), h(m,1), \cdots, h\,(m, L_m-1)]$ and $e_m^{\mathrm{T}}(z) = \left[1, z^{-1}, \cdots, z^{-(L_m-1)}\right]$. This leads to the following:

$$\begin{aligned} Y_m(z) &= \frac{1}{M}\sum_{\ell=0}^{M-1} W_M^{-m\ell} X\left(zW_M^{-\ell}\right) e_m^{\mathrm{T}}\left(zW_M^{-\ell}\right) h_m \\ &= \left[c_m^{(0)}(z), c_m^{(1)}(z), \cdots, c_m^{(L_m-1)}(z)\right] h_m = c_m^{\mathrm{T}}(z)\, h_m. \end{aligned} \tag{3.4}$$

Finally, this leads to a matricial expression for the output in the frequency domain,

$$Y = c^{\mathrm{T}}(z)\, h, \tag{3.5}$$

where $h^{\mathrm{T}} = \left[h_0^{\mathrm{T}}, h_1^{\mathrm{T}}, \cdots, h_{M-1}^{\mathrm{T}}\right]$ and $c^{\mathrm{T}}(z) = \left[c_0^{\mathrm{T}}(z), c_1^{\mathrm{T}}(z), \cdots, c_{M-1}^{\mathrm{T}}(z)\right]$.

To design the identification experiment, a N-periodic signal is chosen, being $N = K\,M$, $K \in \mathbb{Z}$, obtaining also a N-periodic output. Due to the periodicity of the signals, the DFT of them can be computed. Now, evaluating (3.5) at $z = W_N^{-k}$,

$$Y\left[k\right] = Y\left(W_N^{-k}\right) = c^{\mathrm{T}}\left(W_N^{-k}\right) h = c^{\mathrm{T}}\left[k\right] h \tag{3.6}$$

defines the DFT coefficients of the output.

Consider some Gaussian noise ($w \sim G(0, \sigma^2)$) in the output signal. This can be expressed as the vector, $\mathcal{W}$, which is the N-point DFT of the noise which accounts for the measuring error and system noise. Then, the system to identify is defined as $\mathcal{Y} = \mathcal{C}h + \mathcal{W}$, where

$$\mathcal{Y} = \begin{bmatrix} Y[0] \\ Y[1] \\ \vdots \\ Y[N-1] \end{bmatrix}, \quad \mathcal{C} = \begin{bmatrix} c_0^{\mathrm{T}}[0] & c_1^{\mathrm{T}}[0] & \cdots & c_{M-1}^{\mathrm{T}}[0] \\ c_0^{\mathrm{T}}[1] & c_1^{\mathrm{T}}[1] & \cdots & c_{M-1}^{\mathrm{T}}[1] \\ \vdots & \vdots & \ddots & \vdots \\ c_0^{\mathrm{T}}[N-1] & c_1^{\mathrm{T}}[N-1] & \cdots & c_{M-1}^{\mathrm{T}}[N-1] \end{bmatrix}. \tag{3.7}$$

Finally, the identification problem is reduced to a minimization problem over h, which is:

$$\hat{h} = \underset{h}{\operatorname{argmin}} \quad \|\mathcal{Y} - \mathcal{C}h\|^2 = \mathcal{C}^{\dagger}\mathcal{Y}, \tag{3.8}$$

where $\mathcal{C}^{\dagger} = \left(\mathcal{C}^{*}\,\mathcal{C}\right)^{-1}\mathcal{C}^{*}$ stands for the Moore–Penrose inverse and $\mathcal{C}^{*}$ for the conjugate transpose.

3.2 Nonparametric tracking of the time-varying dynamics of weakly nonlinear periodically time-varying systems using periodic inputs

In this paper [33], Louarrondi, Pintelon and Lataire present a procedure for (N)LPTV systems by applying multisine excitations as input. The main idea is that a LPTV can be decomposed into infinte series of HTFs. Then, using a local polynomial approximation, the HTFs are identified in an output-error framework, using data from a single experiment. From these nonparametric estimates, the evolution of the dynamics, described by the instantaneous transfer function (ITF), can then be recovered in a simple manner.

A general input-output relation of a general LPTV system can be provided using the convolution integral of the time-varying kernel, $g(\tau, t)$, and the input.

Thus, due to the periodic property of $g(\tau, t+T_{\text{sys}}) = g(\tau, t)$, this can be expressed as a Fourier series, becoming what follows:

$$y_0(t) = \sum_{l=-\infty}^{+\infty} \left(g_l(t) * u_0(t)\right) e^{jl\omega_{\text{sys}}t} \tag{3.9}$$

being $*$ the convolution product.

Then, the ITF of a LPTV system can be described as an infinite sum of independent HTFs, $G_l(\omega)$, (see Figure 3.2a). From a practical point of view, this infinite sum needs to be truncated to a N_b order, leading to:

$$G_{N_b}(\omega, t) = \sum_{l=-N_b}^{+N_b} G_l(\omega)\, e^{jl\omega_{\text{sys}}t}, \tag{3.10}$$

and to the following truncated output:

$$y_{N_b}(t) = G_{[N_b]}\left\{u_0(t)\right\} = \frac{1}{2\pi}\int_{-\infty}^{+\infty} G_{N_b}(\omega, t)\, U_0(\omega)\, e^{j\omega t}\, d\omega. \tag{3.11}$$

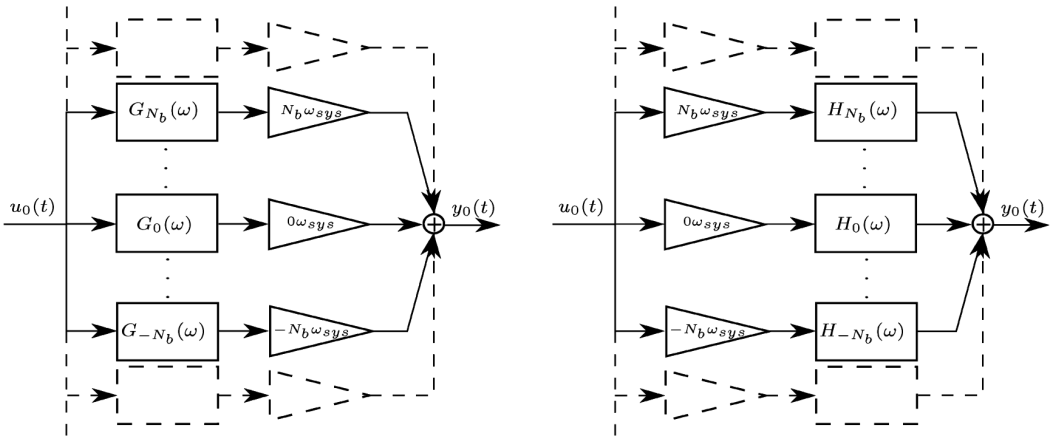

(a) The triangle blocks denote a time-domain multiplication, while the gains stand for $e^{j\, l\omega_{sys}t}$

(b) The gains are interchanged with the dynamic blocks

Figure 3.2: Block-schematic equivalent representations of a LPTV system by weigthed sum of LTI systems

On the other side, the input signal is a band-limited periodic random phase multisine defined as follows:

$$u_0(t) = \frac{1}{\sqrt{N_{\text{exc}}}} \sum_{k \in \pm\mathbb{K}_{\text{exc}}} U_k\, e^{j(k\omega_{\text{exc}}t + \phi_k)}, \tag{3.12}$$

being $\mathbb{K}_{\text{exc}}$ the set of excited frequencies. With respect to the phases, ϕ_k, they have been selected to distribute uniformly the inputs. Also, $\omega_{\text{sys}} = p/q\,\omega_{\text{exc}}$, where $p, q \in \mathbb{Z}$, are design parameters. It is also important to remark that the input u_0 and the output y_0 are observed at steady-state so they are both periodic with period $T = p\,T_{\text{sys}}$.

Since the identification will be done in the frequency domain, the model has to be converted to the frequency domain. The authors justify this fact stating that it is straightforward to select the frequency band that covers the system dynamics of interest. Now, by applying model equivalences (see Figure 3.2b), $G_l(\omega) = H_l\left(\omega + l\omega_{\text{sys}}\right)$ can be defined. Hence, the input-output relation in the frequency domain can be expressed as:

$$Y_0(k) = \sum_{l=-N_b}^{+N_b} H_l\left(\omega_k\right) U_0(k - pl). \tag{3.13}$$

The next step is to set up the noise model for the identification scheme: $Y(k) = \mathbf{H}\left(\omega_k\right)\mathbf{U}(k) + W(k)$, with $\mathbf{U}(k) = \mathbf{U}_0(k)$, being this one the input vector containing the shifted versions of the input spectrum $\mathbf{U}(k) = [U\left(k - pN_b\right) \ldots U(k) \ldots U\left(k + pN_b\right)]^T$, $\mathbf{H}\left(\omega_k\right) = [H_{N_b}\left(\omega_k\right) \ldots H_0\left(\omega_k\right) \ldots H_{-N_b}\left(\omega_k\right)]$ and $W(k)$ the term containing the errors due to the output noise and output stochastic non-linear distortions.

Therefore, the frequency response function (FRF), $\mathbf{H}\left(\omega_k\right)$, can be locally approximated by a polynomial of degree R: $\mathbf{H}\left(\omega_{k+l}\right) \simeq \mathbf{H}\left(\omega_k\right) + \sum_{r=1}^{R} \mathbf{h}_r(k) l^r$. This leads to the final structure of the model:

$$\mathbf{Y}(k) = \Theta(k)\,\mathbf{K}(k) + \mathbf{V}(k) \tag{3.14}$$

where the structure of each matrix is $\mathbf{Q}(k) = [Q(k-n), Q(k-n+1), \ldots Q(k), \ldots, Q(k+n)]$, while $\mathbf{Q}(k)$ stands for $\mathbf{Y}(k)$, $\mathbf{K}(k)$ and $\mathbf{V}(k)$. Solving this equation in the least-squares sense, the local polynomial estimate of the FRF is computed, and then, an estimate of the ITF is obtained by applying equation (3.10).

3.3 Continuous-time identification of periodically parameter-varying state-space models

In [34], Goos and Pintelon present a frequency domain identification method based on estimating multivariate LPV continuous-time state-space models, with a periodic variation of the parameters. The proposed method designs a periodic input signal, which is related to the periodicity of the parameter variation. On their publication, a sparse structure in the frequency domain is developed to speed up

the estimation computation. Finally, a weighted non linear least squares algorithm is used to minimize the output error.

A general definition for a LPV system can be given as follows:

$$\begin{cases} \dot{x}(t) = A(p(t))\,x(t) + B(p(t))\,u(t) \\ y_0(t) = C(p(t))\,x(t) + D(p(t))\,u(t), \end{cases} \tag{3.15}$$

where the matrices are defined as $Q(p(t)) = \sum_{i=1}^{N_p} Q_i \phi_i(p(t))$, while the input is defined as a multisine excitation at different frequencies and uniformly distributed phases.

This structure can be transformed into the frequency domain by the DFT. The continuous-time state-space in frequency domain is:

$$\begin{cases} s\,X(k) = A(P(k)) * X(k) + B(P(k)) * U(k) \\ Y(k) = C(P(k)) * X(k) + D(P(k)) * U(k), \end{cases} \tag{3.16}$$

where $*$ stands for the circular convolution product of the spectra and $k \in [-N/2+1, N/2]$ denotes the DFT bin number. Imposing now the parametrization defined above on this system and rewriting the circular convolution as the product of a Toeplitz matrix and a vector, a compact notation of the state-space system is provided in equation (3.17), where the definitions of each component are defined in equation (3.18).

$$\begin{cases} E\,X = \alpha\,P_x\,X + \beta\,P_u\,U \\ Y(\theta) = \gamma\,P_x\,X + \delta\,P_u\,U \end{cases} \tag{3.17}$$

$$E = I_{N_x} \otimes j\,\mathrm{diag}\left(\omega_0, \omega_1, \ldots, \omega_{\frac{N}{2}}, \omega_{-\frac{N}{2}+1}, \ldots, \omega_{-1}\right) \tag{3.18a}$$

$$\alpha = \left[\; A_1 \otimes I_N \;\middle|\; A_2 \otimes I_N \;\middle|\; \ldots \;\middle|\; A_{N_p} \otimes I_N \;\right] \tag{3.18b}$$

$$\beta = \left[\; B_1 \otimes I_N \;\middle|\; B_2 \otimes I_N \;\middle|\; \ldots \;\middle|\; B_{N_p} \otimes I_N \;\right] \tag{3.18c}$$

$$\gamma = \left[\; C_1 \otimes I_N \;\middle|\; C_2 \otimes I_N \;\middle|\; \ldots \;\middle|\; C_{N_p} \otimes I_N \;\right] \tag{3.18d}$$

$$\delta = \left[\; D_1 \otimes I_N \;\middle|\; D_2 \otimes I_N \;\middle|\; \ldots \;\middle|\; D_{N_p} \otimes I_N \;\right] \tag{3.18e}$$

$$P_x = \begin{bmatrix} \text{Toeplitz}\ \left(P_1, P_1^H\right) \otimes I_{N_x} \\ \vdots \\ \text{Toeplitz}\ \left(P_{N_p}, P_{N_p}^H\right) \otimes I_{N_x} \end{bmatrix} \tag{3.18f}$$

$$P_u = \begin{bmatrix} \text{Toeplitz}\ \left(P_1, P_1^H\right) \otimes I_{N_u} \\ \vdots \\ \text{Toeplitz}\ \left(P_{N_p}, P_{N_p}^H\right) \otimes I_{N_u} \end{bmatrix}, \tag{3.18g}$$

where A_i, B_i, C_i and D_i are the original real time-domain matrices, I_N is a $N \times N$ identity matrix and $\otimes$ stands for the Kronecker product.

From this compact notation, it can be noticed that the matrices are actually only defined by a limited number of constant real parameters that compose the model parameter vector θ to be identified. In order to perform the identification, the weighted output error has been chosen as the optimization criterion, and the Gaussian Maximum Likelihood Estimator is formulated in the frequency domain, defining the output error as $\varepsilon(\theta) = Y(\theta) - Y$. Then, the minimization problem can be formulated, under several assumptions, as follows:

$$\hat{\theta}_{\mathrm{ML}} = \underset{\theta}{\operatorname{argmin}} \quad \varepsilon(\theta)^H \, C_e^{-1} \, \varepsilon(\theta), \tag{3.19}$$

where $\varepsilon(\theta)^H$ is the complex conjugate of $\varepsilon(\theta)$ and C_e is the error covariance matrix, which can be estimated non-parametrically in the frequency domain, by simply observing multiple periods of the output signal. As only stationary output noise is considered, the noise is uncorrelated over frequency, and C_e becomes a (non-constant) block diagonal matrix (the noise can still be correlated over the different outputs).

3.4 Model-based flight control of kites for wind power generation

In this Doctoral Thesis [35], Wood developes a model-based identification and control focused on Airborne Wind Energy, which is a new methodology to capture energy stored in the wind using tethered aircraft. Focusing on the identification chapter of the thesis, its work is based on giving a formal representation of LPTV system and introducing a subspace identification method to obtain low-order state-space realisations from input and output data. This allows to obtain periodic state-space models. This identification method approach is called *Energy (cumulative spectrum) bound noise fitting.*

The first step of this algorithm is to select a set of data structure parameters (s, c) that are sufficiently large, given the system period, P, and a data length, M. Also, it is necessary to select the singular value threshold, $\bar{s}$, and weighting parameters from $\lambda_0, ..., \lambda_{P-1}$.

Then, for a series of values, $\varepsilon \in [\varepsilon_{\min}, \varepsilon_{\max}]$, the algorithm follows to solve the nuclear norm minimisation problem given in equation (3.20) with constraint set, $\mathcal{W} = \mathcal{W}_E^{(\varepsilon)}$ (or $\mathcal{W} = \mathcal{W}_C^{(\varepsilon,\eta)}$),

$$\begin{array}{ll} \min_w & \sum_{\tau=0}^{P-1} \lambda_\tau \| \mathcal{S}_\tau^{(s,c)} \, (\tilde{y} - w) \, \Pi_\tau^{\perp} \|_* \\ \text{s.t.} & w \in \mathcal{W}, \end{array} \tag{3.20}$$

where w is the optimisation variable that can be understood as the residual signal meant to emulate a noise realisation, $\tilde{y}$ is the output data affected by additive noise ($\tilde{y} = y + \sigma^y$, being σ^y the additive output noise), $\Pi_\tau^\perp$ stands for the full-rank input annihilator matrices, that hold $U_\tau^{(s,c)}\Pi_\tau^\perp = 0$, $\forall\tau = 0, ..., P-1$, and $\mathcal{S}_\tau^{(s,c)}$ is the stacking operator for a finite sequence of a discrete-time signal, $v = (v_0, v_1, \ldots, v_{M-1})$, $v_k \in \mathbb{R}^i$:

$$\mathcal{S}_\tau^{(s,c)}(v) = \begin{bmatrix} v_\tau & v_{P+\tau} & \cdots & v_{(c-1)P+\tau} \\ v_{\tau+1} & v_{P+\tau+1} & \cdots & v_{(c-1)P+\tau+1} \\ \vdots & \vdots & \cdots & \vdots \\ v_{\tau+s-1} & v_{P+\tau+s-1} & \cdots & v_{(c-1)P+\tau+s-1} \end{bmatrix} \tag{3.21}$$

with $s, c \in \mathbb{Z}_{++}$ and $M \geq (c-1)P + \tau + s$. Hence, the optimiser will be denoted as $w^{(\varepsilon)*}$.

Before going on with the algorithm, it may be necessary to define the constraints. The energy bound noise constraint (equation (3.22a)) is a bound on the energy of the emulated noise signal, w. According to its definition, $[w_k]_i$ is the i-th element of the noise candidate vector at time instant k, and ε bounds the energy of the noise for each output. However, if a more complex constraint is used to enforce *noise-like* properties of the estimated residual, the cumulative spectrum noise constraint can be imposed (equation (3.22b)). In its definition, the tolerated deviation from cumulative spectrum linearity, η is used and also the DFT of w, W.

$$\mathcal{W}_{\mathrm{E}}^{(\varepsilon)} = \left\{ w \,\middle|\, \sum_{k=0}^{M-1} |[w_k]_i|^2 \leq \varepsilon \,, i = 1, \ldots, o \right\} \tag{3.22a}$$

$$\mathcal{W}_{\mathrm{C}}^{(\varepsilon,\eta)} = \left\{ w \,\middle|\, \frac{1}{M}\sum_{k=0}^{j-1} |[W_k]_i|^2 \leq \left(\eta + \frac{j}{M}\right)\varepsilon \,, \begin{matrix} i = 1, \ldots, o \\ j = 1, \ldots, M \end{matrix} \right\} \tag{3.22b}$$

Returning to the algorithm, for each considered noise level, ε, and all tags, $\tau = 0, ..., P-1$, the projected output structure is approximated by truncating singular values below the threshold, $\bar{s}$,

$$\mathcal{S}_\tau^{(s,c)}\left(\tilde{y} - w^{(\varepsilon)*}\right)\Pi_\tau^\perp = \hat{\mathcal{U}}_{\tau,1}^*\hat{\mathcal{S}}_{\tau,1}^*\hat{\mathcal{V}}_{\tau,1}^* + \hat{\mathcal{U}}_{\tau,2}^*\hat{\mathcal{S}}_{\tau,2}^*\hat{\mathcal{V}}_{\tau,2}^* \approx \hat{\mathcal{U}}_{\tau,1}^*\hat{\mathcal{S}}_{\tau,1}^*\hat{\mathcal{V}}_{\tau,1}^*, \tag{3.23}$$

calculating also, the candidate state dimension, $\hat{n}_\tau^{(\varepsilon)} = \operatorname{rank}\left(\tilde{\mathcal{U}}_{\tau,1}^*\right)$, and the system order, $\hat{n}_{\max}^{(\varepsilon)} = \max_{\tau=0,\ldots,P-1}\hat{n}_\tau^{(\varepsilon)}$.

Thus, for each of the values of $\hat{n}_{\max}^{(\varepsilon)}$ of interest, it is necessary to find the corresponding minimum ε. And finally, for all resulting ε, an estimate periodic state-space realisation can be computed using the estimated system output,

$\hat{y} = \tilde{y} - w^{(\epsilon)*}$, instead of $\tilde{y}$.

As all the black-box algorithms, this one generates a series of models with different orders. From this set of models, the selection of one is done based on a desired trade-off between the model order and the fit to the data set. Then, the dimension of the state vector at different tags can be emphasised with the weighting parameters by setting $\lambda_\tau = 1/\left\|\mathcal{S}_\tau^{(s,c)}(\tilde{y})\Pi_\tau^\perp\right\|_*$ for $\tau = 0, ..., P-1$. This allows to discourage tags for which the sum of the singular values of the raw output data matrix is large to dominate the cost function.

An upper bound for ε can be found from intuition as the smallest value for which $\tilde{y} \in \mathcal{W}_\mathrm{E}$

$$\varepsilon_{\max} = \max_{i=1,...,0} \sum_{k=0}^{M-1} \left|[\tilde{y}_k]_i\right|^2 . \tag{3.24}$$

This corresponds to the noise level required to assign all of energy in the measured output to noise. Then, all models of order greater than zero correspond to lower values of ε and can be found by gridding or interactive searching for values for which $\hat{n}_{\max}^{(\varepsilon)}$ changes.

3.5 Frequency-domain subspace identification of linear time-periodic (LTP) systems

The proposal of Uyanik et al. in [6] is based on a new methodology for subspace-based state-space identification for LPTV systems. The approach is based on lifting a discrete-time LPTV system to an equivalent LTI one by doing so with the input-output data[†]. Then, using frequency-domain identification methods, the LTI system is identified. Finally, by exploiting the specific parametric structure of Fourier series coefficients of the frequency-domain lifting method, the time-periodic realisation for the estimated system is performed. The authors also state that this method can also be used to obtain a Floquet transformation for known LPTV systems.

Regarding to the Floquet-Lyapunov theory developed in Section 2.3, an LPTV system can always be expressed in the following form:

$$\begin{aligned} \dot{x}(t) &= \quad A \quad x(t) + B(t)\, u(t) \\ y(t) &= C(t)\, x(t) + D(t)\, u(t). \end{aligned} \tag{3.25}$$

Now, to move this continuous system into a discrete-time one, the time-varying bilinear (Tustin) transformation is used, leading to A_d, $B_d(k)$, $C_d(k)$ and $D_d(k)$,

[†]see Section 2.4.3 for a better understanding of the lifting concept.

that are the discrete-time state-space matrices of the system.

Then, the state-space is lifted using the Toeplitz forms. Notice that, as A_d is time-invariant, its Toeplitz form will be a block diagonal matrix of this one: $\mathcal{A}_d = \text{blkdiag}\{A_d\}$. This leads to the HSS model that was developed in Subsection 2.4.3. Now, if the modulation matrix is inverted, new definitions arise: $\mathcal{A}_{dN} = \mathcal{N}_d^{-1}\mathcal{A}_d$, $\mathcal{B}_{dN} = \mathcal{N}_d^{-1}\mathcal{B}_d$, and the HSS model is expressed as follows:

$$\begin{aligned} z\mathcal{X}_d &= \mathcal{A}_{dN}\,\mathcal{X}_d + \mathcal{B}_{dN}\,\mathcal{U}_d \\ \mathcal{Y}_d &= \ \mathcal{C}_d\ \ \mathcal{X}_d + \mathcal{D}_d\ \ \mathcal{U}_d. \end{aligned} \tag{3.26}$$

Remember that, since a discrete-time version of the HSS is being used, the matrices will not be infinite but the lifting will be limited to the interval $\boldsymbol{I_n} = [-N/2,\, N/2-1]$.

Regarding the chosen input, it is a sum-of-cosines ($u(t) = \sum_{m=1}^{M} 2K_m \cos(\omega_m t)$) with a chosen frequency so as $\omega_m \neq 0.5\,k\,\omega_p$, $k \in \mathbb{Z}$, where ω_p is the system frequency. Then, each term of the sum can be divided into two terms ($u_c(t) = 2K\cos(\omega_m t) = Ke^{j\omega_m t} + Ke^{-j\omega_m t} = u_c^+(t) + u_c^-(t)$). Let us consider from now onwards just the positive part of the decomposition, $u_c^+(t)$. The next step now is to modulate each $u_c^+(t)$ term as an EMP signal with a $z = e^{j\omega_m}$ as the modulation term. Since a (half-)cosine in ω_m is modulated with its same frequency, the resulting lifted vector will be equivalent to the same (half-)cosine in the zero frequency. Then, this leads to $\mathcal{U}_d = [0, ..., K, ..., 0]^{\mathrm{T}}$ being K positioned in the middle term of the vector, which is the $N/2+1$ position.

Consequently, the operations $\mathcal{B}_{dN}\,\mathcal{U}_d$ and $\mathcal{D}_d\,\mathcal{U}_d$ can be performed in an equivalent manner as $\overline{\mathcal{B}}_{dN}\,\overline{\mathcal{U}}_d$ and $\overline{\mathcal{D}}_d\,\overline{\mathcal{U}}_d$, where $\overline{\mathcal{B}}_{dN} = \mathcal{N}_d^{-1}\left[B_{-N/2}, ..., B_0, ..., B_{N/2-1}\right]^{\mathrm{T}}$ and $\overline{\mathcal{D}}_d = \left[D_{-N/2}, ..., D_0, ..., D_{N/2-1}\right]^{\mathrm{T}}$ are the column $N/2+1$ of the original Toeplitz matrices and $\overline{\mathcal{U}}_d = K$. This transformation leads to a single-input multiple-output (SIMO) equivalent LTI system.

Noting that $\overline{\mathcal{Q}}_m(k) = \overline{\mathcal{Q}}_{-m}^*(k)$ for any coefficient of a Fourier expansion and looking for a real-value identification, the state and output vectors can be transformed by $\mathcal{X}(k) = \mathcal{T}_x\,\mathcal{X}_d(k)$, $\mathcal{Y}_d(k) = \mathcal{T}_y\,\mathcal{Y}_d(k)$, where:

$$\mathcal{T}_x = 0.5\begin{bmatrix} 2I_{n_p} & 0 & 0 & 0 \\ 0 & I_{(N/2-1)n_p} & 0 & J_{(N/2-1)n_p} \\ 0 & 0 & 2I_{n_p} & 0 \\ 0 & -jJ_{(N/2-1)n_p} & 0 & jI_{(N/2-1)n_p} \end{bmatrix} \tag{3.27}$$

with a similar expression for $\mathcal{T}_y$, being I_n the $n \times n$ identity matrix and J_n the $n \times n$ antidiagonal matrix. This leads to the following real-valued state-space

system:

$$\begin{aligned} e^{j\omega_m}\mathcal{X} &= \mathcal{T}_x\,\mathcal{A}_{dN}\,\mathcal{T}_x^{-1}\,\mathcal{X} + \mathcal{T}_x\,\overline{\mathcal{B}}_{dN}\,\overline{\mathcal{U}}_d \\ \mathcal{Y} &= \mathcal{T}_y\,\mathcal{C}_d\,\mathcal{T}_x^{-1}\,\mathcal{X} + \mathcal{T}_y\,\overline{\mathcal{D}}_d\,\overline{\mathcal{U}}_d. \end{aligned} \tag{3.28}$$

Now, using black-box identification methods such as CVA [45], N4SID [46] or MOESP [47], the identification is performed. Then, to obtain an equivalent lifted LTI system, it is needed to backsubstitute the $\mathcal{T}_y$ transformations, leading to $\hat{\mathcal{C}} = \mathcal{T}_y^{-1}\,\hat{\overline{\mathcal{C}}}$, $\hat{\mathcal{D}} = \mathcal{T}_y^{-1}\,\hat{\overline{\mathcal{D}}}$.

The drawback of this process is that it requires extra processing after the idenfication part to unlift the matrices. This part is performed by a similarity transformation $\mathcal{T}_c = \text{diag}\{\gamma_1, ..., \gamma_n\}$, that can be computed by setting $\mathcal{V}\,\Gamma = 0$, where $\mathcal{V}$ includes all the constraint equations for all Fourier series coefficients, $\Gamma = \left[\gamma_1, \gamma_2, \ldots, \gamma_{(2N_h+1)}\right]^{\mathrm{T}}$ and N_h is the number of harmonics in the state. Then, as $\mathcal{V}$ is rank deficient with a nullspace dimension equal to 2, the SVD is used to find its eigenvectors. It is necessary to select two eigenvectors corresponding to the least significant singular values as the basis of the nullspace of $\mathcal{V}$. Then, defining $\Gamma = \alpha_1\,v_1 + \alpha_2\,v_2$, being α_1, α_2 free, the similarity transformation $\mathcal{T}_c$ can be constructed and the LPTV system can be recovered.

3.6 Linear time-periodic system identification with grouped atomic norm regularization

Yin et al. propose a new methodology for LPTV system identification in [36], focusing on imposing appropriate structural constraints on the LTI reformulation of LPTV systems. This constraint is imposed by combining the atomic norm regularization framework for LTI systems with the *group lasso* technique in regression. As a result, the estimated system is both uniform and low-order.

The discussion starts from a discrete-time LPTV state-space system and the assumptions that the period P is known, that the system is stable and that the state dimension is much lower than the number of periods observed. This method is based on the switched reformulation model that was explained in Section 3.1. Then, using the input-output definition provided in equation (3.1), and changing the notation $g(t,i) = g_i^t$, the following matrix can be defined:

$$\mathbf{g} = \begin{bmatrix} g_1^1 & g_1^2 & \cdots & g_1^P \\ g_2^1 & g_2^2 & \cdots & g_2^P \\ \vdots & \vdots & \ddots & \cdots \\ g_N^1 & g_N^2 & \cdots & g_N^P \end{bmatrix} \in \mathbb{R}^{N\times P}, \tag{3.29}$$

where N is the truncation term of the infinite sum.

It will be also necessary to introduce the atomic norm. The underlying idea is to replace the search for a rank-revealing system matrix with the search for an order-revealing decomposition of the system. Then, consider a set of stable first-order systems

$$\mathcal{A} = \left\{ a_w(q) = \frac{1-|w|^2}{q-w} \mid w \in \mathbb{D} \right\}, \tag{3.30}$$

where $\mathbb{D}$ is the open unit disk. Hence, assuming also that the sub-models have no repeated poles, *i.e.*, the monodromy matrix is diagonalizable, the sub-models can be decomposed as linear combinations of atoms by performing partial fraction expansions of the transfer functions:

$$G_\tau(q) \approx \sum_{k=1}^{n_p} c_k^\tau \cdot a_{w_k}(q) = \mathbf{c}_\tau^{\mathrm{T}} \mathbf{a}(q), \tag{3.31}$$

where the infinite atom set is approximated by fine gridding $\{w_k\}$ with an atom vector $\mathbf{a}(q) = \left[a_{w_1}(q), ..., a_{w_{np}}(q)\right]^{\mathrm{T}}$. The vector $\mathbf{c}_\tau = \left[c_1^\tau, ..., c_{n_p}^\tau\right]^{\mathrm{T}}$ denotes the corresponding coefficients, and n_p is the number of atoms in the grid.

Then, the algorithm for LPTV system identification with grouped atomic norm regularization is described as follows:

Given the input, u, the noise-added output, z, and the dataset for cross validation, $u_v(t)$ and $z_v(t)$, select N, $\{w_k\}$, and weighting factor vector γ_{grid}. Then, compute $\mathbf{g}^a = \left[\mathbf{g}_1^a, ..., \mathbf{g}_{n_n}^a\right]$, where $\mathbf{g}_k^a$ is the N-truncated impulse response of $a_{w_k}(q)$.

Now, it is suggested to proceed with the optimization problem for each $\gamma \in \gamma_{grid}$:

$$\begin{aligned} \min_{\mathbf{c}} \quad & V_{LS}\left(\mathbf{g}^a \mathbf{c}\right) + \gamma \cdot J_{GA}(\mathbf{c}), \\ \text{s. t.} \quad & c_k^\tau = \mathrm{conj}\left(c_l^\tau\right), \forall w_k = \mathrm{conj}\left(w_l\right), \tau = 1, 2, \cdots, P, \end{aligned} \tag{3.32}$$

where the cost functions are defined as:

$$V_{LS}(\mathbf{g} \mid u(t), z(t)) = \sum_{\tau=1}^{P} \sum_{k=0}^{n-1} \left[z(kP+\tau) - \sum_{i=1}^{N} g_i^\tau u(kP+\tau-i) \right]^2 \tag{3.33a}$$

$$J_{GA}(\mathbf{c}) = \sum_{k=1}^{n_p} \left\| \mathbf{c}^{(k)} \right\|_2, \tag{3.33b}$$

and the error can be defined as $\epsilon(\gamma) = V_{LS}(\mathbf{g}^a\, \mathbf{c}(\gamma) \mid u_v(t), z_v(t))$.

Once finished the loop, solve the optimization problem

$$\gamma^* = \arg\min_{\gamma} \quad \epsilon(\gamma), \tag{3.34}$$

and denote $\mathbf{c}^* = \mathbf{c}(\gamma^*)$, from which the LPTV system can be reconstructed.

Chapter 4

State-space LPTV model identification

In this chapter, a different approach for subspace-based state-space frequency-domain identifcation for LPTV systems is developed. It is based on the first steps of the approach of Uyanik et al. [6], but modifying several steps so as the objetive is to match the identified model with the real one. The approach is based on lifting a discrete-time LPTV system to an equivalent LTI one by doing that with the input-output data, but with a different approach for the modulation part. Then, as each of the components of the state-space matrices will be T-periodic, their expansion into trigonometric Fourier series is performed, and choosing the harmonic truncation number, the list of parameters to identify is obtained. Performing now the identification in the output-error framework, and considering white Gaussian noise in the output measurement, the parameters are identified. As the identified parameters are the trigonometric harmonics of each component, the LPTV system is inmediately recovered. Finally, to quantify the uncertainty over the identified parameters, a Monte Carlo approach is used by idenfying the system several times but changing the noise realisation, keeping its variance content.

First of all, some assumptions should be made:

- The algorithm is developed for single-input single-output (SISO) systems in the time-domain.
- The period of the system, T_m, or, equivalently, its main frequency, ω_m, is known.
- To design the identification experiment, a T_i-periodic signal is chosen for the input, being T_i an integer multiple of T_m.
- The structure of the identified state-space model is chosen beforehand, this is, the number of states desired for the identified system, n_p.

- The index for the truncation N of the Toeplitz matrices and the number of harmonics desired in the identified model, N_{mh}, are design parameters.
- The output signal is assumed to be at steady-state.

With respect to the input, it is defined as an infinite sum of cosines, phased following the Schroeder formula [48]. This phasing lets us have an uniform amplitude for the input, instead of having a lumped impulse at $t = k\,T_i$, $k \in \mathbb{Z}$. This effect is due to all the cosines being maximum in these time instants, and the input the sum of the amplitudes of the cosines (see Figure 4.1a). The input is prescribed as follows:

$$u(t) = \sum_{k=1}^{N_i} 2\,K_k \cos(\omega_k\,t + \varphi_k) \tag{4.1a}$$

$$\omega_k = k\,\frac{2\,\pi}{T_i}, \quad k = 1, ..., N_i \tag{4.1b}$$

$$\varphi_k = \begin{cases} 0, & k = 1 \\ \varphi_{k-1} - \dfrac{\pi\,k^2}{N_i}, & k = 2, ..., N_i \end{cases} \tag{4.1c}$$

where K_k is freely chosen for each input. According to what is stated in [49], the input frequencies must hold $\omega_m \neq 0.5\,q\,\omega_k$, $q \in \mathbb{Z}$. Therefore, the unsuitable frequencies from equation (4.1b) will be removed.

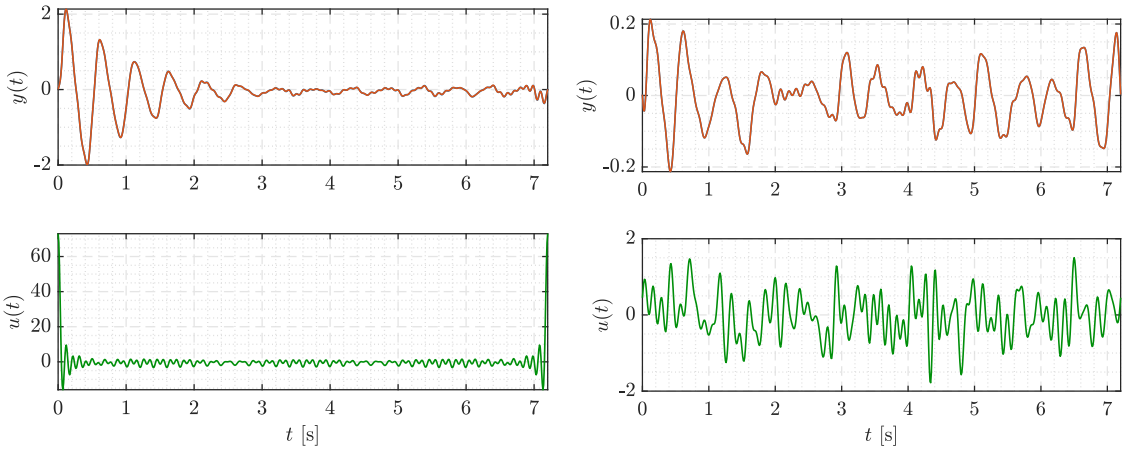

(a) Input without considering the cosine phasing (b) Input considering the Schroeder's cosine phasing

Figure 4.1: Input Schroeder's cosine phasing comparison

As Figure 4.1 shows, the fact of having a lumped impulse in the input generates a damped-oscillatory response, due to the residual input. Notice that the rest

of the input is almost null with respect to the values at $t = k\,T_i$, $k \in \mathcal{Z}$. Hence, the output is more related to the impulsive input than to the rest of it, which is not desired in this case. Therefore, to measure all the output, a sensor with a very wide accuracy range may be needed. On the other hand, the Schroeder phasing provides a more distributed amplitude in the input. The consequence of this is a more uniform response, which can be measured in a better manner, since its magnitude is always contained in the same range.

With respect to the system, given a continuous-time state-space model as the one described in equation (2.12),

$$\begin{aligned} \dot{x}(t) &= A_c(t)\,x(t) + B_c(t)\,u(t) \\ y(t) &= C_c(t)\,x(t) + D_c(t)\,u(t), \end{aligned} \tag{4.2}$$

the objective now is to apply the Floquet-Lyapunov theory (Section 2.3) to obtain an equivalent system with constant A matrix.

Focusing now on a numerical approach, consider $\tau = 0$. This will be helpful to compute, for example, the transition matrix, which will be a function of $A_c(t)$, *tau* and $\tau + T_m$. Notice that the choice of τ is arbitrary. Then, it is necessary to solve the differential equation in equation (2.3) numerically. Setting $\Phi_A(\tau, \tau) = I_{n_p \times n_p}$, the tolerances of the integrator and a vector of time from τ to $\tau + T_m$, the integration can be performed. Notice that `ode45` [50] does not solve differential equations expressed as matrices. A solution to this would be to reshape $\Phi_A(\tau)$ as a vector that contains all its columns, creating also a block diagonal matrix of $A_c(t)$ (see equation (4.3)). Once the integration is performed, an inverse reshape should be done to recover the matrix form. This manner, the resultant matrix will be $\Psi_A(\tau)$, the monodromy matrix.

$$\begin{bmatrix} \dot{\Phi}_{11} \\ \dot{\Phi}_{21} \\ \vdots \\ \dot{\Phi}_{(n_p-1)\,n_p} \\ \dot{\Phi}_{n_p\,n_p} \end{bmatrix} = \begin{bmatrix} A_c(t) & 0 & \cdots & 0 \\ 0 & A_c(t) & \cdots & 0 \\ \vdots & \vdots & \ddots & \vdots \\ 0 & 0 & \cdots & A_c(t) \end{bmatrix} \begin{bmatrix} \Phi_{11} \\ \Phi_{21} \\ \vdots \\ \Phi_{(n_p-1)\,n_p} \\ \Phi_{n_p\,n_p} \end{bmatrix} \tag{4.3}$$

Once the monodromy matrix is computed, and according to the definition provided in equation (2.19), the time-invariant matrix can be defined as

$$\bar{A}_c = \frac{1}{T_m}\,\ln\left(\Psi_A(\tau)\right). \tag{4.4}$$

The next step is to compute now the transition matrix, $S(t)$, according to equation (2.17), $S(t) = e^{(t-\tau)\bar{A}_c}\,\Phi_A(\tau, t)$. Once this matrix is computed, the new

state-space system can be defined as follows:

$$\bar{B}_c(t) = S(t)\, B_c(t), \quad \bar{C}_c(t) = C_c(t)\, S^{-1}(t), \quad \bar{D}_c(t) = D_c(t), \tag{4.5a}$$

$$\begin{aligned} \dot{\bar{x}}(t) &= \bar{A}_c\ \bar{x}(t) + \bar{B}_c(t)\, u(t) \\ y(t) &= \bar{C}_c(t)\, \bar{x}(t) + \bar{D}_c(t)\, u(t). \end{aligned} \tag{4.5b}$$

Now, it is necessary to transform this continuous-time system into a discrete-time one, using the time-varying bilinear (Tustin) transformation, which is the following:

$$\begin{aligned} \Omega &= \left(\frac{2}{T_s} I_{n_p \times n_p} - \bar{A}_c\right)^{-1}, \qquad B_d(k) = \frac{2}{\sqrt{T_s}}\, \Omega\, \bar{B}_c\left(kT_s\right), \\ A_d &= \left(\frac{2}{T_s} I_{n_p \times n_p} + \bar{A}_c\right) \Omega \qquad , C_d(k) = \frac{2}{\sqrt{T_s}}\, \bar{C}_c\left(kT_s\right)\, \Omega, \\ D_d(k) &= \bar{D}_c\left(kT_s\right) + \bar{C}_c\left(kT_s\right)\, \Omega\, \bar{B}_c\left(kT_s\right), \end{aligned} \tag{4.6}$$

where $I_{n_p \times n_p}$ is the identity matrix of $n_p \times n_p$ dimensions, and T_s stands for the sampling time. The last term to transform is the input, that can be easily discretized as $u_d(k) = u(kT_s)$. This leads to the following discrete-time state-space system:

$$\begin{aligned} x(k+1) &= A_d\ x(k) + B_d(k)\, u_d(k) \\ y(k) &= C_d(k)\, x(k) + D_d(k)\, u_d(k). \end{aligned} \tag{4.7}$$

4.1 Identification part

First of all, consider lifting the output signal, $y(k)$, denoted as $\mathcal{Y}^*$ and the lifted input signal, denoted as $\mathcal{U}$.

Considering now the state-space matrices but A_d, which is constant, each of the components of each matrix can be expanded in a trigonometric Fourier series, denoted as follows:

$$Q_i(k) = Q_{i0} + \sum_{n=1}^{N_{\text{harm}}} \left(Q_{\text{c}_{in}} \cos\left(n\, \omega_m\, T_s\, k\right) + Q_{\text{s}_{in}} \sin\left(n\, \omega_m\, T_s\, k\right)\right), \qquad i = 1, ..., n_p \tag{4.8}$$

where $Q(k)$ stands for $B_d(k)$, $C_d(k)$ and $D_d(k)$.

The next step is to set now the number of inputs, n_i, outputs, n_o, and states, n_p that the identified system will have, as well as the number of harmonics, N_{harm}, for the $B_d(k)$, $C_d(k)$ and $D_d(k)$ functions. Then, each Q_{i0}, $Q_{\text{c}_{im}}$ and $Q_{\text{s}_{im}}$ value is

collected into a Θ vector, which will be the parameters vector, including also the coefficients of A_d. This vector is defined with the following structure:

$$\begin{aligned}\Theta &= \left[\Theta_A^{\mathrm{T}},\, \Theta_B^{\mathrm{T}},\, \Theta_C^{\mathrm{T}},\, \Theta_D^{\mathrm{T}}\right]^{\mathrm{T}} \\ \Theta_A &= \left[A_{11}, A_{21}, ..., A_{n_p\,1}, A_{12}, ..., A_{n_p\,n_p}\right]^{\mathrm{T}} \\ \Theta_Q &= \left[Q_{10}, Q_{\mathrm{c}_{11}}, Q_{\mathrm{c}_{12}}, ..., Q_{\mathrm{s}_{11}}, Q_{\mathrm{s}_{12}}, ..., Q_{20}, ..., Q_{\mathrm{s}_{n_p N_{\mathrm{harm}}}}\right]^{\mathrm{T}}, \\ &\qquad\qquad\qquad\qquad\qquad\qquad Q = B,\, C,\, D.\end{aligned} \tag{4.9}$$

Therefore, the number, n_Θ, of parameters to identify can be computed as:

$$n_\Theta = \underbrace{n_p^2}_{A(t)} + \underbrace{2\,n_p\,(2\,N_{\mathrm{harm}}+1)}_{B(t)+C(t)} + \underbrace{2\,N_{\mathrm{harm}}+1}_{D(t)}. \tag{4.10}$$

This raises the importance of the Floquet transformation, as n_Θ grows quadratically with n_p, keeping N_{harm} fixed.

Then, for each added-noise output signal, $y(t)$, that was computed and lifted, an optimization process will be performed to obtain the desired parameters. The procedure for each iteration would be the following:

- Select Θ and compute A_d, $B_d(k)$, $C_d(k)$ and $D_d(k)$.
- Lift the time-domain matrices to compute the Toepliz matrices $\mathcal{A}_\mathcal{F}$, $\mathcal{B}_\mathcal{F}$, $\mathcal{C}_\mathcal{F}$ and $\mathcal{D}_\mathcal{F}$.
- Compute the $\mathcal{N}_d$ matrix according to equation (2.34) in the discrete-time domain version.
- Compute the HTF matrix, $\mathcal{G}(z)$ as defined in equation (2.35) in the discrete-time domain version. Set $z = 1$.
- Compute $\mathcal{Y}_\mathcal{F}(\Theta) = \mathcal{G}(z=1)\,\mathcal{U}$.

Hence, the optimization problem to be solved is:

$$\hat{\Theta} = \underset{\Theta}{\operatorname{argmin}} \quad \left\|\mathcal{Y}_\mathcal{F}(\Theta) - \mathcal{Y}^*\right\|_2 \tag{4.11}$$

A flow diagram of the algorithm is shown in Figure 4.2 to help the reader get on a better understanding of it.

The last thing to configure is the optimizer. In this case, the chosen one is MATLAB's `fmincon` function [52], which was configured with the following options:

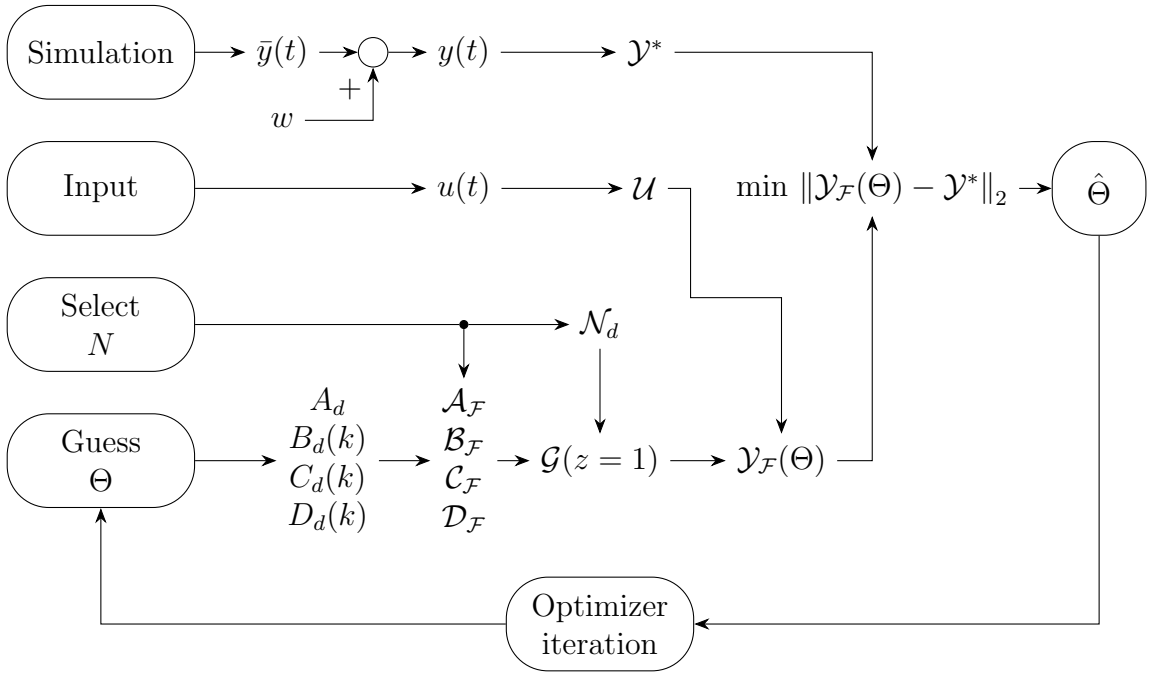

Figure 4.2: Algorithm diagram

- Algorithm: `'interior-point'` which is suggested from MATLAB's documentation. This method is a large-scale algorithm that handles large, sparse problems, as well as small dense problems. As our problem may become large, its choice is justified.
- CheckGradients: Since the gradient is not provided, the option `false` is chosen.
- MaxFunctionEvaluations: A very large number is chosen so as the optimization does not depend on this parameter.
- MaxIterations: A number larger than default is chosen. Depending on the specific problem, this value may change.
- ObjectiveLimit: set to 10^{-3}, since a better result cannot be obtained due to noise.
- UseParallel: To decrease the time of gradients computation, parallel computation is set to `true`.

Once the optimizer provides a result, called $\hat{\Theta}$, the state-space model matrices, $\hat{A}_d$, $\hat{B}_d(k)$, $\hat{C}_d(k)$, $\hat{D}_d(k)$, can be reconstructed. To compute the uncertainty of each identified parameter, the mean, μ, variance, σ^2 and coefficient of variation, σ/μ, are computed from the obtained dataset. This will be helpful to decide the

influence of each parameter on the actual system.

If desired, the original system can be recovered by returning first to the continuous-time domain, by using the inverse bilinear (Tustin) transformation:

$$\begin{aligned} \Omega_c &= \left(I_{n_p \times n_p} + \hat{A}_d\right)^{-1}, & \hat{B}_c(t) &= \frac{2}{\sqrt{T_s}}\,\Omega_c\,\hat{B}_d\,(k)\,, \\ \hat{A}_c &= \frac{2}{T_s}\,\Omega_c\,\left(\hat{A}_d - I_{n_p \times n_p}\right), & \hat{C}_c(t) &= \frac{2}{\sqrt{T_s}}\,\hat{C}_d\,(k)\;\Omega_c, \end{aligned} \tag{4.12}$$

$$\hat{D}_c(t) = \hat{D}_d\,(k) - \hat{C}_d\,(k)\;\Omega_c\,\hat{B}_d\,(k)\,,$$

while the intersample data can be obtained via linear interpolation. Finally, returning to equation (4.5a) and backmultiplying, the original state-space system can be recovered.

4.2 Black-box modelling

Imposing the Fourier expansion on equation (4.8) means to use a grey-box method, since a structure of the matrices is being imposed in some manner. However, if this expansion cannot be computed, or a black-box modelling is desired, the change would be just to add to Θ each of the possible harmonics of each component of the state-space matrices. The resulting system will not probably be the desired one, but an equivalent one, up to a transformation matrix. However, from this equivalent system the user may tell the position of the main harmonics (see Figure 4.2).

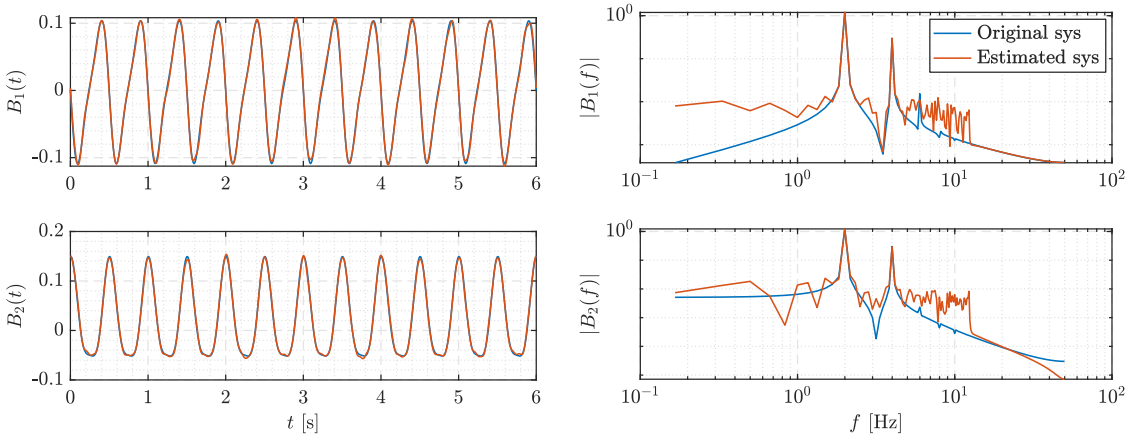

(a) B matrix in time domain

(b) B matrix in frequency domain

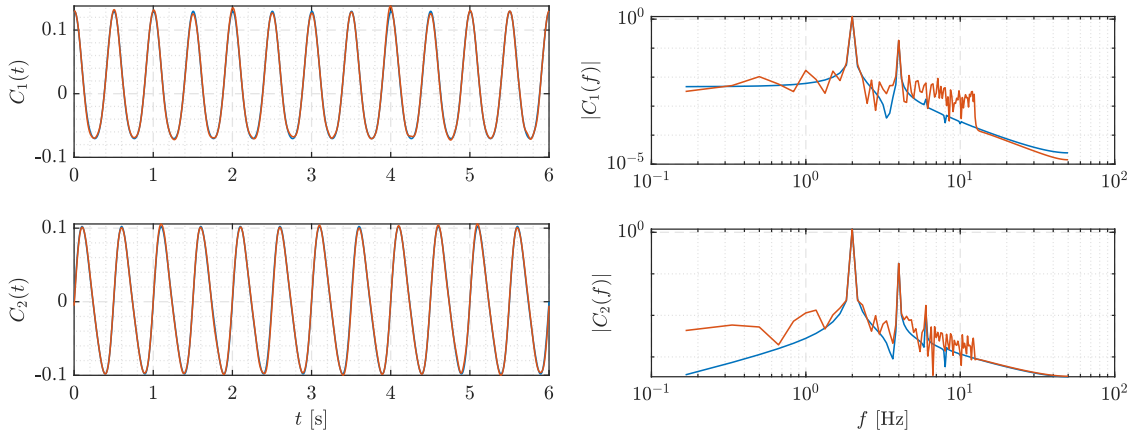

(c) C matrix in time domain

(d) C matrix in frequency domain

Figure 4.2: Simple black-box identification performed on the numerical example on [6]

Notice that, despite all the possible harmonics of the matrices (from $-N/2$ to $N/2-1$) are excited, the most relevant peaks can be associated with the main frequency of the system. Nevertheless, this procedure is very inefficient, since the number of parameters is much larger than using a grey-box approach, and leads to much higher computation time to obtain the results. Then, using this black-box approach, some relevant information can be collected to use later a grey-box approach as the one explained in Section 4.1.

Chapter 5

Numerical examples

In this chapter, a numerical case study is related to illustrate the performance of the algorithm developed in the previous chapter, as well as to verify its robustness and accuracy in different situations.

5.1 Out-of-plane bending of a rotor blade

Bittanti and Lovera developed in [25] a model for the out-of-plane bending of a helicopter rotor blade based on the physical derivation provided in [53] in order to investigate its non-minimum phase characteristics.

The formulation of the model starts from the bending equation, considering the bending moment acting on every section of the blade. This bending moment must be equilibrated by the other forces acting on the blade, that are the inertial forces and the aerodynamic loads. Integrating each section and considering the rotor angular frequency, Ω as constant (which is reasonable in normal conditions), equation (5.1) is obtained. This describes the structural response of the blade to the external distributed loading, called L_{S}.

$$\frac{d^2}{dr^2}\left[E(r)I(r)\frac{d^2z(r,t)}{dr^2}\right] - \frac{d}{dr}\left[\left(\int_r^R m(\rho)\Omega^2\rho d\rho\right)\frac{dz(r,t)}{dr}\right] + \\ +m(r)\ddot{z}(r,t) = L_{\mathrm{S}}(r,t), \tag{5.1}$$

where EI is the blade stiffness, while m stands for the distributed mass of the beam, being all of them a function of the radius from the hub of the rotor.

To solve equation (5.1), a modal expansion is performed using the separation of variables method ($z(r,t) = \sum_{k=1}^{k_{\max}} \eta_k(r)\, e^{i\nu_k t}$, where ν is the frequency associated with the free vibration of the mode shape $\eta(r)$). After the expansion, a remark suggests that the modal expansion must be finite and mostly covers ranges from

1 to 5 modes.

Considering now *blade element theory* [54] for the aerodynamic loads, the lift of each section, $\Delta L(r,t)$, and the inflow angle, $\phi(r,t)$ are defined in equations (5.2a) and (5.2b).

$$\Delta L(r,t) = \frac{1}{2}\rho\, u(r,t)^2\, c\, c_l(r,t) \tag{5.2a}$$

$$\phi(r,t) = \tan^{-1}\left(\frac{u_p(r,t)}{u_t(r,t)}\right) \tag{5.2b}$$

$$u_{\mathrm{t}}(r,t) = \Omega\, r + V\cos\alpha\sin\psi \tag{5.2c}$$

$$u_{\mathrm{p}}(r,t) = V\sin\alpha + v_i + \dot{z}(r,t) + z'(r,t)V\cos\alpha\cos\psi \tag{5.2d}$$

$$u(r,t) = \sqrt{u_p(r,t)^2 + u_t(r,t)^2}, \tag{5.2e}$$

where ρ stands for the air density, $u(r,t)$ is the velocity of each blade section, decomposed in vertical, $u_{\mathrm{p}}(r,t)$, and horizontal, $u_{\mathrm{t}}(r,t)$, components respectively, c is the chord of the section, c_l is the two-dimensional lift coefficient, α is the angle of attack of the blade section, while ψ is the angular position of the blade in the horizontal plane with respect to a reference. Finally, V stands for the forward velocity of the rotor and v_i is the induced velocity of the rotor. Then, under the small angle assumption, the vertical aerodynamic load can be determined as follows:

$$L_{\mathrm{S}}(r,t) \simeq \Delta L(r,t)\cos(\phi(r,t)) = \Delta L(r,t)\frac{u_t(r,t)}{u(r,t)}. \tag{5.3}$$

Then, the formulation of the model is complete. Nevertheless, some parameters should be defined to characterise the modeled rotor. These non-dimensional parameters are, the blade Lock number γ, and the rotor advance ratio, μ, defined as follows:

$$\gamma = \frac{\rho\, a\, c\, R^4}{I_{q1}}, \qquad\qquad \mu = \frac{V\,\cos\alpha}{\Omega\, R}, \tag{5.4}$$

where a defines the slope of the lift coefficient, R the total radius of the blade and I_{q1} the first modal moment of inertia.

The Lock number is the ratio of aerodyinamic to inertial forces, which characterises each rotor. According to [53], the value of this parameter is typically 8 to 10 for articulated rotors and 5 to 7 for hingeless rotors, while high-stiffness blades can reach 14. The rotor advance ratio is the ratio of the forward velocity to rotor tip velocity, it is a non-dimensional velocity to describe the forward flight condition (or the hovering one if $\mu = 0$). Its value may depend on the technology of the considered rotor.

Finally, the model takes the commanded pitch angle, and once defined the rotor characteristics and the flight condition, it provides a time-periodic SISO space-state model that returns the vertical shear force as the output. The model size is $n_p = 2\,n_{\text{modes}}$, where n_{modes} stands for the selected number of modes. The considered rotor in [25] was the AgustaWestland AW109, a fully articulated, four-bladed helicopter, and so was done in this example.

Figure 5.1: AW109 [7]

Number of blades	N [-]	4
Rotor angular freq.	Ω [rad/s]	40.32
Rotor radius	R [m]	5
Blade chord	c [m]	0.3
Mass per unit length	m [kg]	4.98
Stiffness	EI [Nm^2]	1.8E 3
Lift-coefficient slope	a [rad^{-1}]	5.7
Lock number	γ [-]	7.8
Rotor advance ratio	μ [-]	$0 \div 0.35$

Table 5.1: Main parameters of the AW109

According to [25], if the rotorcraft is in hover condition ($\mu = 0$), the behaviour can be modeled as a LTI system. However, as μ increases, the response can be modeled as a LPTV system. Taking this into account, $\mu = 0.35$ was selected for all the performed examples.

With respect to the application of the method, the parameters to define are $N = 120$ and $T_s = 0.01$ s. The choice of these parameters, and some others as n_{modes} or N_{mont}, are based on a trade-off between time of computation and obtained results. The examples were run using MATLAB 2021b under a Intel Core i7-9750H (@ 2.60 GHz).

Regarding the input, a realisation composed by sum of 56 cosines, with $K_k = 0.05 \forall k \in [0, 56]$ is used. This signal is characterised by $T_i = 4.68$ s. This input is made so as it can excite all the possible frequencies available with the N value choice.

5.2 Simulation part

This step is focused on obtaining a time-domain output signal to perform the identification. Focusing on simulation, there are many ways of getting the output signal. Nevertheless, to ensure the obtained signal is at steady state, the HTF will be computed by lifting the matrices of the system and the input signal, following the methodology explained in Section 2.4. Once the lifted output vector

is computed, it is returned to the time domain using the definition of Fourier expansion, provided in equation (2.23):

$$\bar{y}(k) = \sum_{n=-N/2}^{N/2-1} Y_n \, e^{j n \omega_m k}, \tag{5.5}$$

remembering that, in discrete-time, $\omega_m = 2\,\pi / T_m \, T_s$.

Considering now the noise modelling, some Gausian noise ($w \sim G(0, \sigma^2)$) is added using the MATLAB function `awgn` [51]. This function takes as inputs the zero-noise signal, $\bar{y}(t)$, the signal-to-noise ratio (SNR) in dB and the signal power, in dBW, to return the added-noise signal, $y(k) = \bar{y}(k) + w(k)$. The signal power is computed as follows:

$$y_{\text{pow}}[\text{dBW}] = 10 \, \log_{10} \left(\bar{y}^2_{\text{RMS}} \right) = 10 \, \log_{10} \left(\frac{1}{N} \sum_{n=1}^{N} |\bar{y}_n|^2 \right). \tag{5.6}$$

This definition provides a direct relationship between the SNR and the variance of the added noise, which is: $\sigma^2 = y_{\text{pow}} / \, \text{SNR}$, where both data is expressed in decimal units.

To obtain a measurement of the uncertainty of the identified parameters, a number N_{mont} of added-noise realisations can be computed, to perform the same number of identification processes and compute the mean and variance values of the parameters.

5.3 Identification with $n_{\text{modes}} = 1$

The first case that was considered is the rigid-body model, which is $n_{\text{modes}} = 1$. This leads to $n_\Theta = 39$ if $N_{\text{harm}} = 3$. The last parameter to be modified is the added Gaussian noise by modifying the SNR value.

For SNR = 100, which is equal to add noise with $\sigma^2 = 4.69 \cdot 10^{-4}$ variance, the results are shown in Figure 5.2.

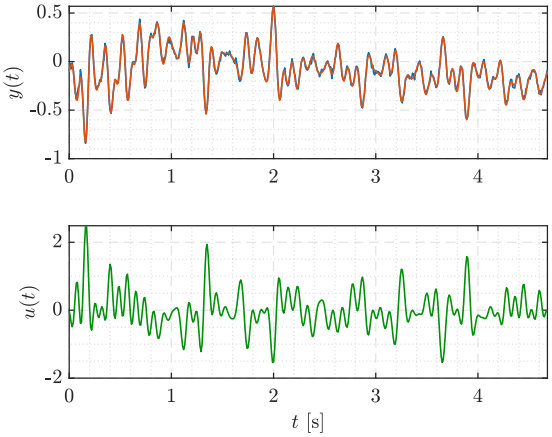

(a) Input-output chart

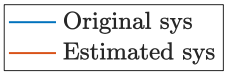

$$\rho_{\text{ref}} = \begin{bmatrix} 0.9954 + 0.0091i \\ 0.9954 - 0.0091i \end{bmatrix}$$

$$\rho_{\text{ident}} = \begin{bmatrix} 0.9954 + 0.0092i \\ 0.9954 - 0.0092i \end{bmatrix}$$

(b) $\hat{A}_d$ matrix eigenvalues comparison

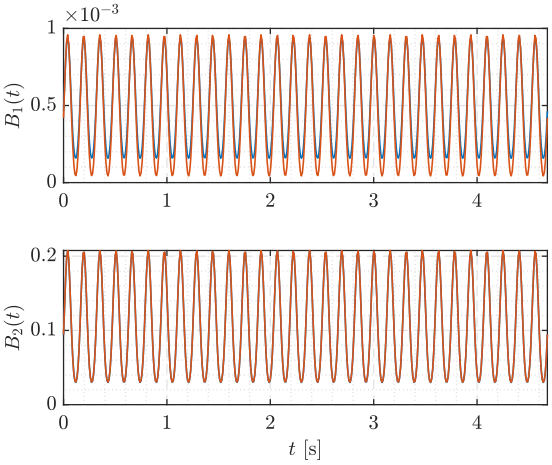

(c) $\hat{B}_d$ matrix in time domain

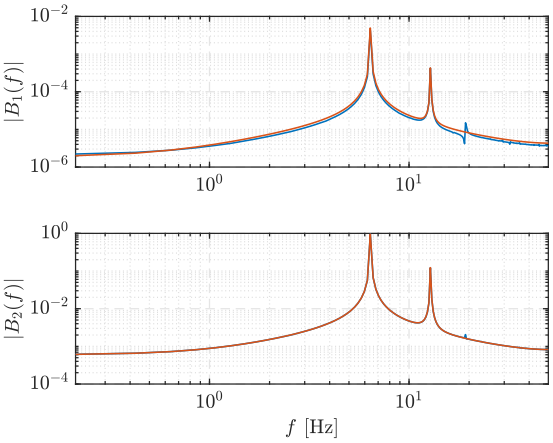

(d) $\hat{B}_d$ matrix in frequency domain

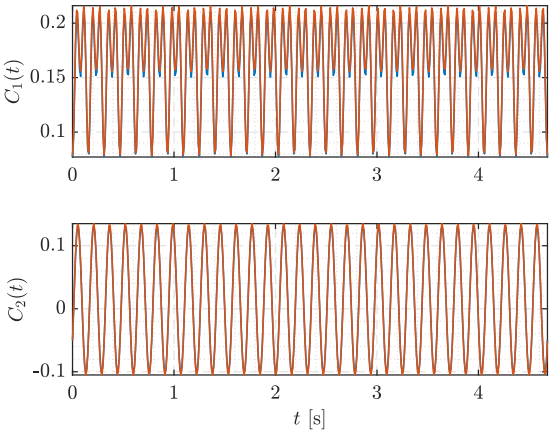

(e) $\hat{C}_d$ matrix in time domain

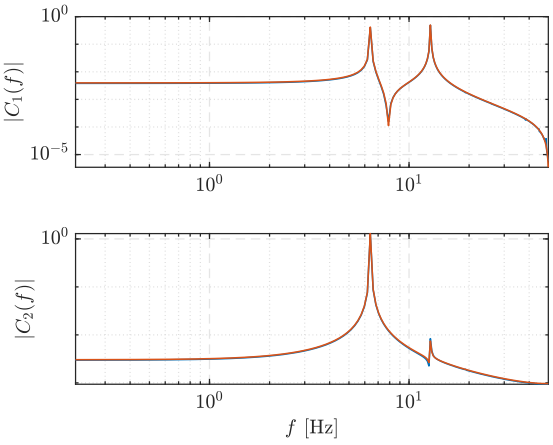

(f) $\hat{C}_d$ matrix in frequency domain

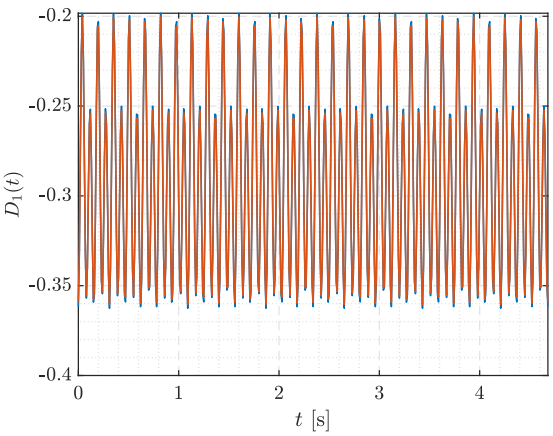

(g) $\hat{D}_d$ matrix in time domain

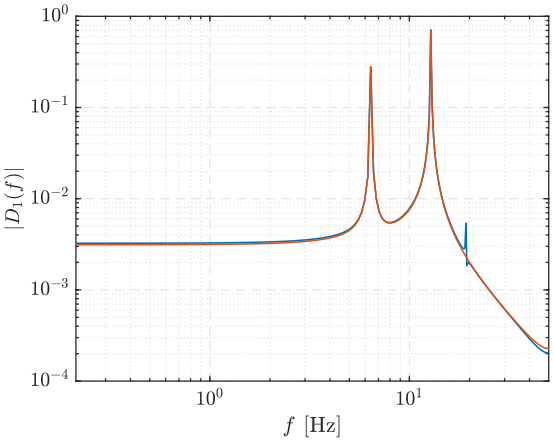

(h) $\hat{D}_d$ matrix in frequency domain

Figure 5.2: Bending model numerical example. $n_{\text{modes}} = 1$, SNR= 100

For SNR $= 10$, which is equal to add noise with $\sigma^2 = 4.69 \cdot 10^{-3}$ variance, the results are shown in Figure 5.3.

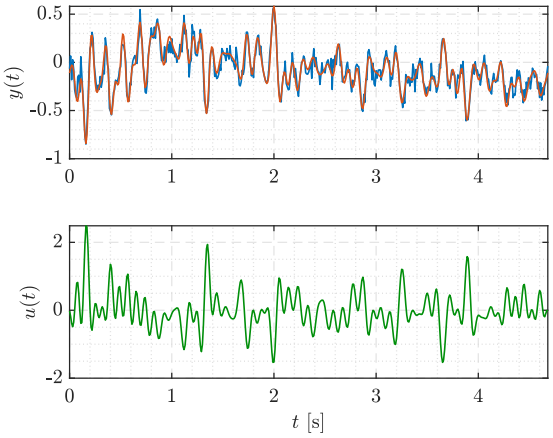

(a) Input-output chart

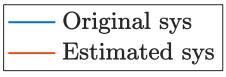

$$\rho_{\text{ref}} = \begin{bmatrix} 0.9954 + 0.0091i \\ 0.9954 - 0.0091i \end{bmatrix}$$

$$\rho_{\text{ident}} = \begin{bmatrix} 0.9954 + 0.0093i \\ 0.9954 - 0.0093i \end{bmatrix}$$

(b) $\hat{A}_d$ matrix eigenvalues comparison

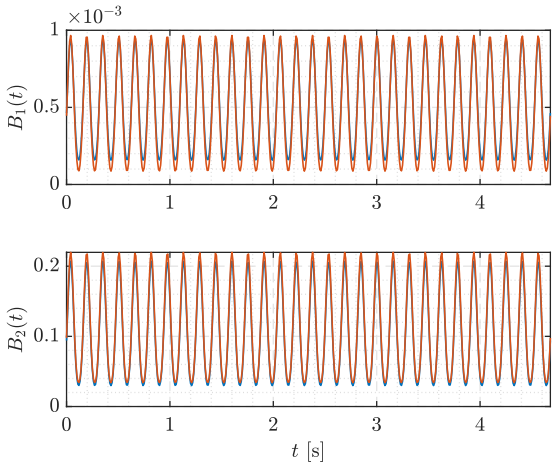

(c) $\hat{B}_d$ matrix in time domain

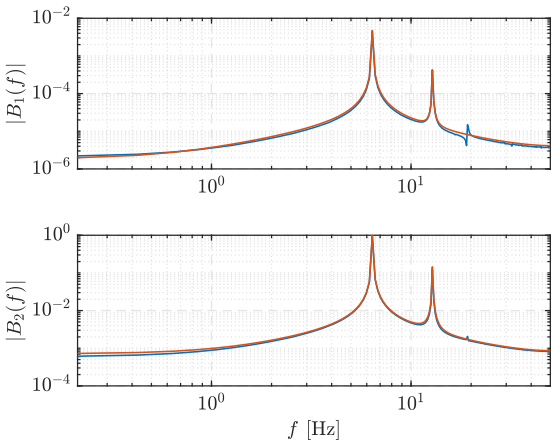

(d) $\hat{B}_d$ matrix in frequency domain

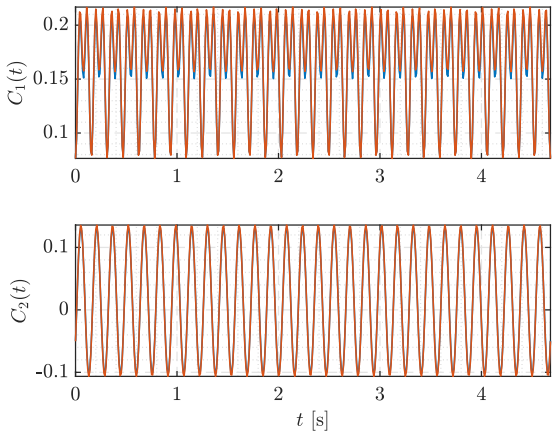

(e) $\hat{C}_d$ matrix in time domain

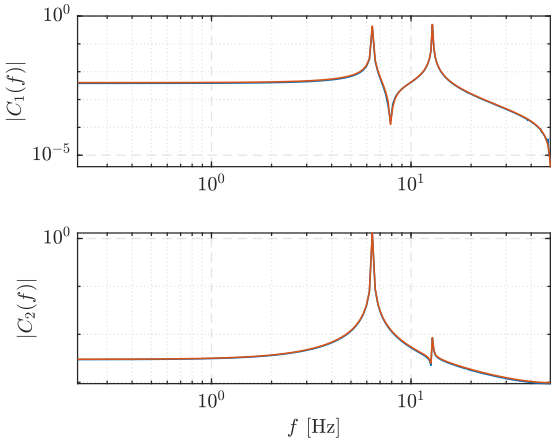

(f) $\hat{C}_d$ matrix in frequency domain

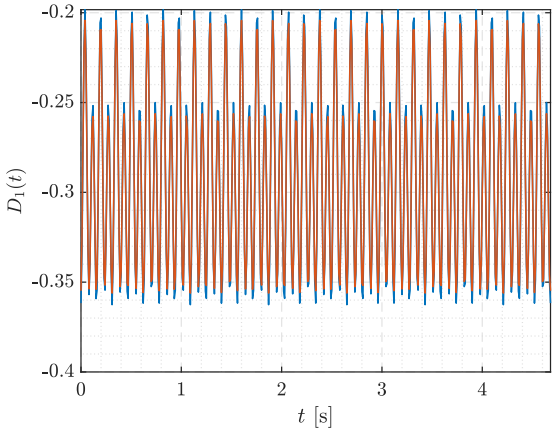

(g) $\hat{D}_d$ matrix in time domain

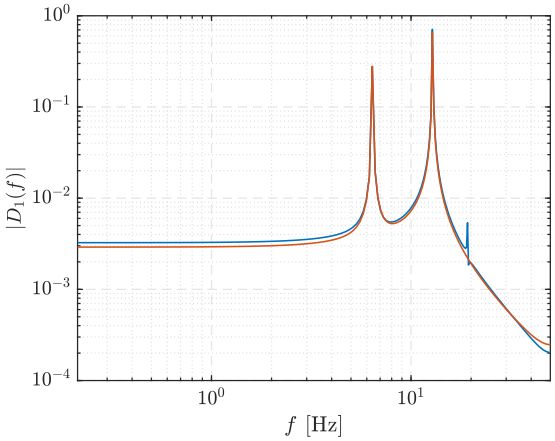

(h) $\hat{D}_d$ matrix in frequency domain

Figure 5.3: Bending model numerical example. $n_{\text{modes}} = 1$, SNR= 10

For SNR = 3, which is equal to add noise with $\sigma^2 = 1.57 \cdot 10^{-2}$ variance, the results are shown in Figure 5.4.

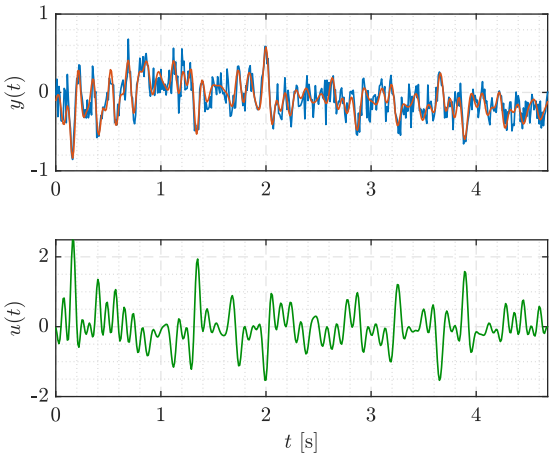

(a) Input-output chart

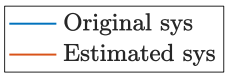

$$\rho_{\text{ref}} = \begin{bmatrix} 0.9954 + 0.0091i \\ 0.9954 - 0.0091i \end{bmatrix}$$

$$\rho_{\text{ident}} = \begin{bmatrix} 0.9954 + 0.0089i \\ 0.9954 - 0.0089i \end{bmatrix}$$

(b) $\hat{A}_d$ matrix eigenvalues comparison

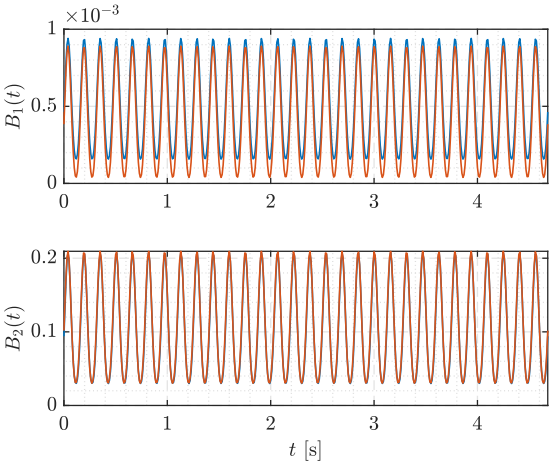

(c) $\hat{B}_d$ matrix in time domain

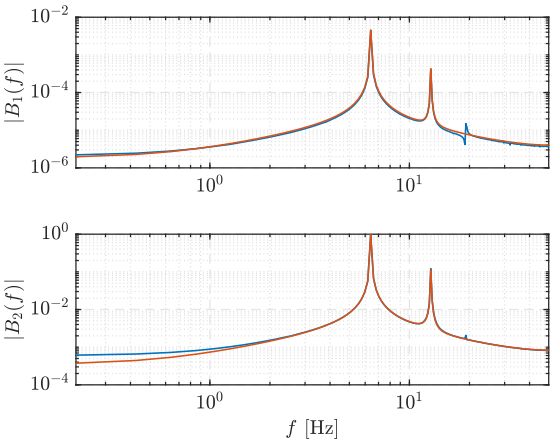

(d) $\hat{B}_d$ matrix in frequency domain

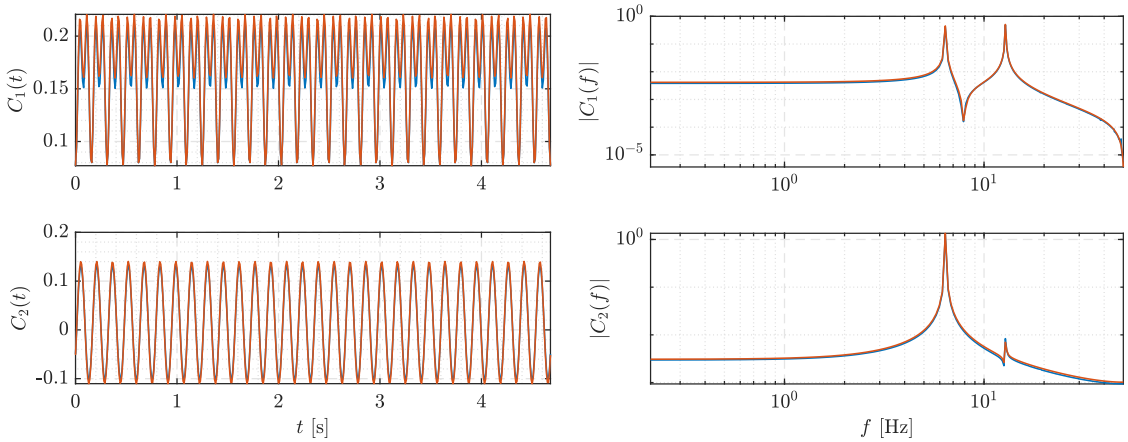

(e) $\hat{C}_d$ matrix in time domain (f) $\hat{C}_d$ matrix in frequency domain

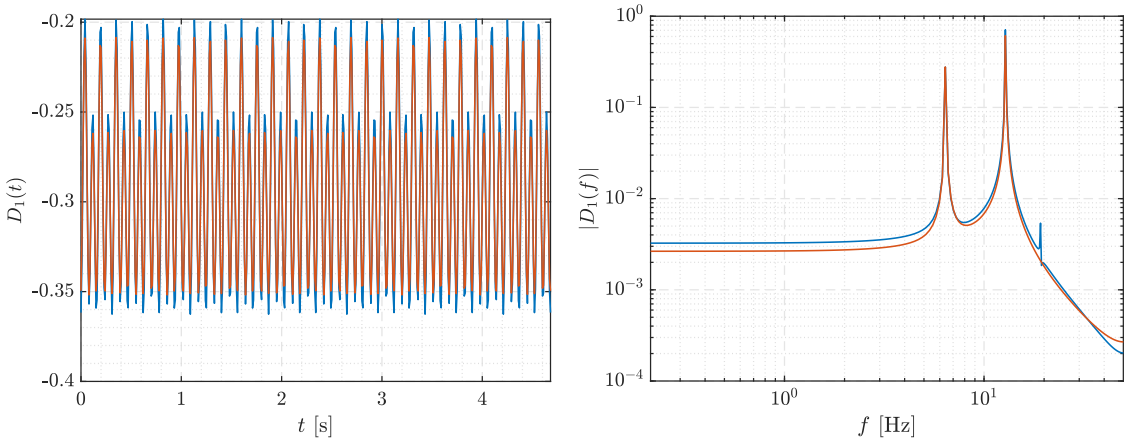

(g) $\hat{D}_d$ matrix in time domain (h) $\hat{D}_d$ matrix in frequency domain

Figure 5.4: Bending model numerical example. $n_{\text{modes}} = 1$, SNR= 3

For SNR = 1.6, which is equal to add noise with $\sigma^2 = 2.94 \cdot 10^{-2}$ variance, the results are shown in Figure 5.5.

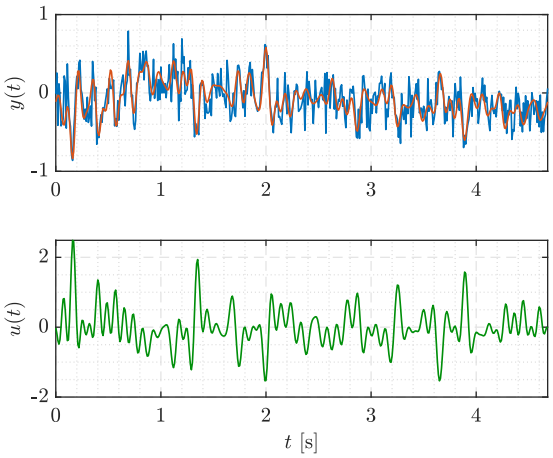

(a) Input-output chart

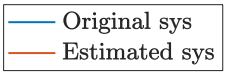

$$\rho_{\text{ref}} = \begin{bmatrix} 0.9954 + 0.0091i \\ 0.9954 - 0.0091i \end{bmatrix}$$

$$\rho_{\text{ident}} = \begin{bmatrix} 0.9954 + 0.0090i \\ 0.9954 - 0.0090i \end{bmatrix}$$

(b) $\hat{A}_d$ matrix eigenvalues comparison

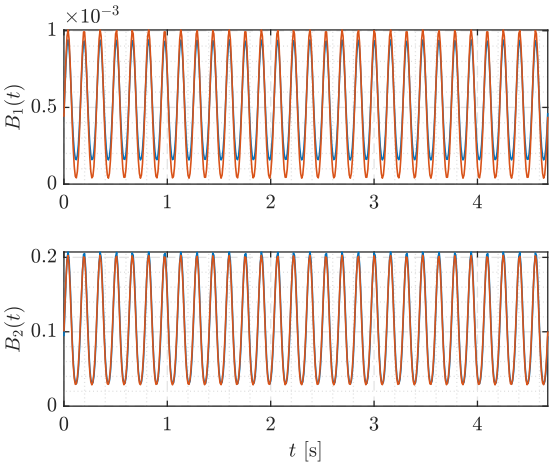

(c) $\hat{B}_d$ matrix in time domain

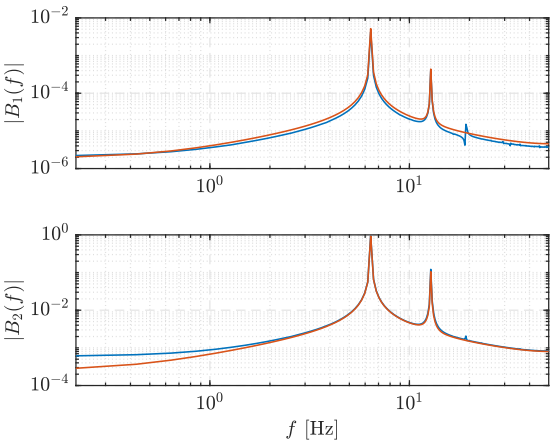

(d) $\hat{B}_d$ matrix in frequency domain

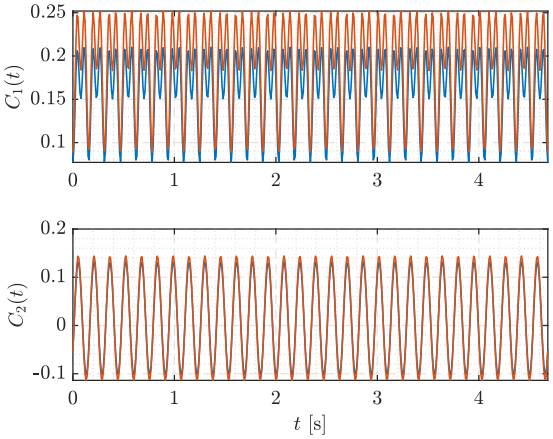

(e) $\hat{C}_d$ matrix in time domain

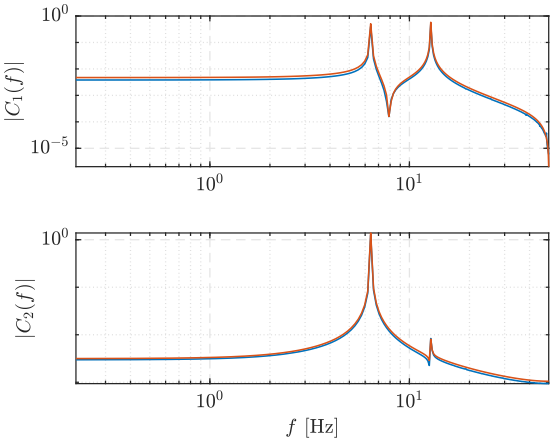

(f) $\hat{C}_d$ matrix in frequency domain

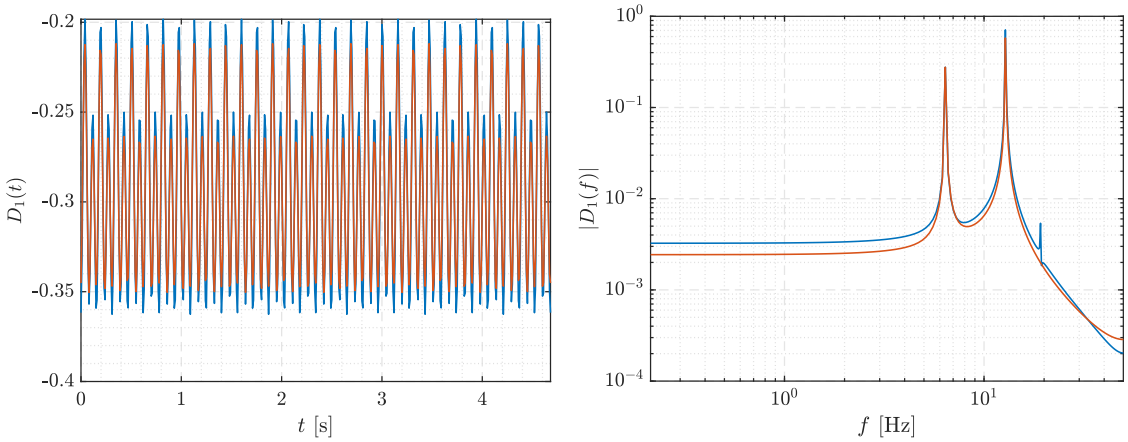

(g) $\hat{D}_d$ matrix in time domain

(h) $\hat{D}_d$ matrix in frequency domain

Figure 5.5: Bending model numerical example. $n_{\text{modes}} = 1$, SNR= 1.6

The charts show that in all the cases, the output signal is recovered, as well as the harmonics that compose the state-space matrices. In fact, the presence of noise disturbs the model identification, but keeping always the magnitude. In general, it has been proved that for small systems, the method is very reliable, because the number of parameters is relatively small. It is also remarkable that the eigenvalues are successfully recovered, which is an important part in the system characterisation.

As it was explained in the previous chapter, for each computation, a Monte Carlo analysis was performed, changing the added-noise realisation, but maintaining its SNR. By doing this, the mean and the variance of each value can be computed by using standard formulas (see equation (5.7)). In this case, N_{mont} was set to 20.

$$\mu_p = \frac{1}{N_{\text{mont}}} \sum_{i=1}^{N_{\text{mont}}} \hat{\Theta}_{p_i}, \quad \sigma_p^2 = \frac{1}{N_{\text{mont}} - 1} \sum_{i=1}^{N_{\text{mont}}} \left(\hat{\Theta}_{p_i} - \mu_p \right)^2 \tag{5.7}$$

Since the number of non-zero parameters is not very large for each matrix, the computed variance for each one can be plotted with respect to the SNR, to understand the behaviour of the optimizer when the added-noise increases. The fact of plotting the variance, and also the coefficient of variation (CV), may help to discard some non-zero mean parameters that are not relevant for the system. This means to discard, for example, those parameters which have a CV higher than a threshold.

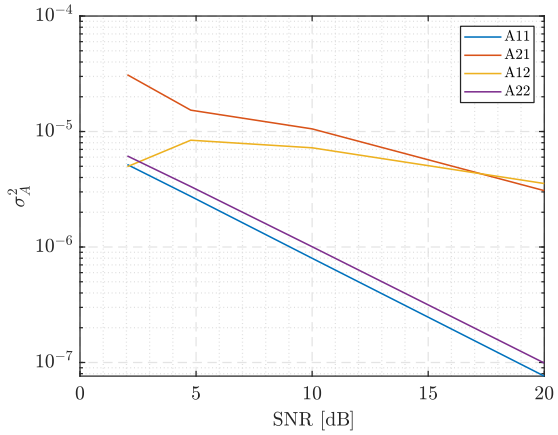

(a) $\hat{A}_d$ matrix variance

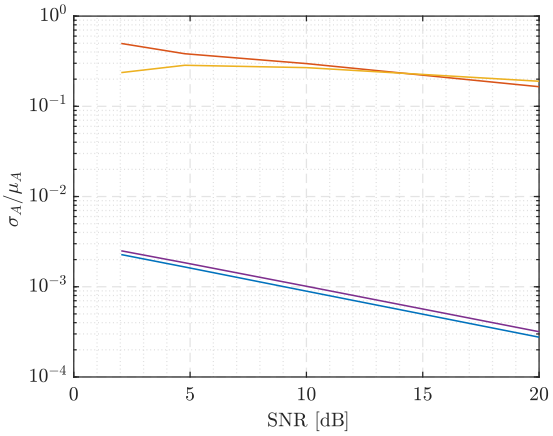

(b) $\hat{A}_d$ matrix CV

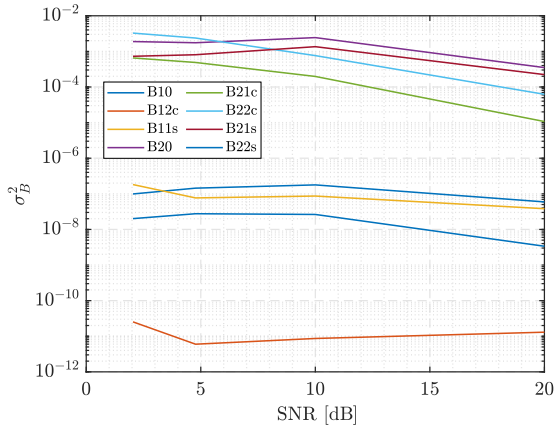

(a) $\hat{B}_d$ matrix variance

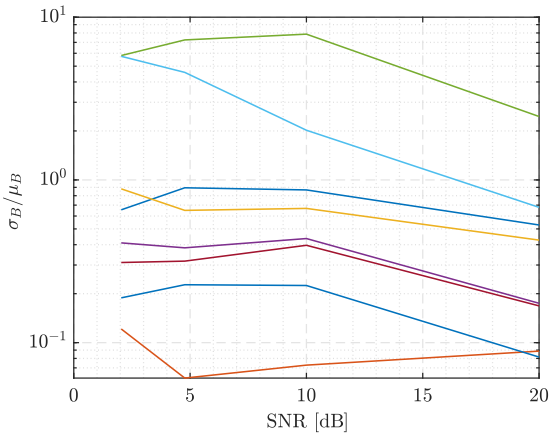

(b) $\hat{B}_d$ matrix CV

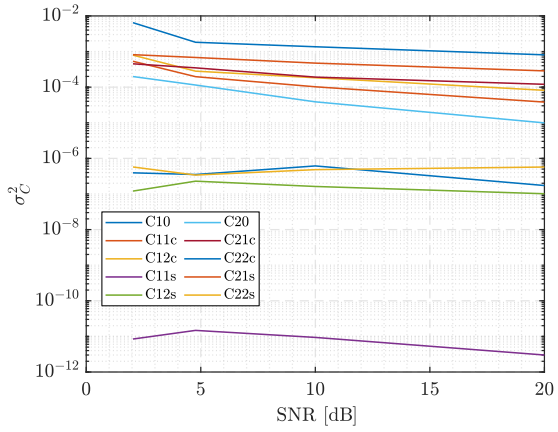

(c) $\hat{C}_d$ matrix variance

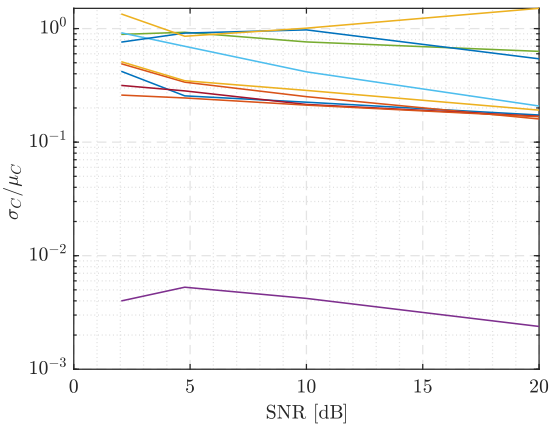

(d) $\hat{C}_d$ matrix CV

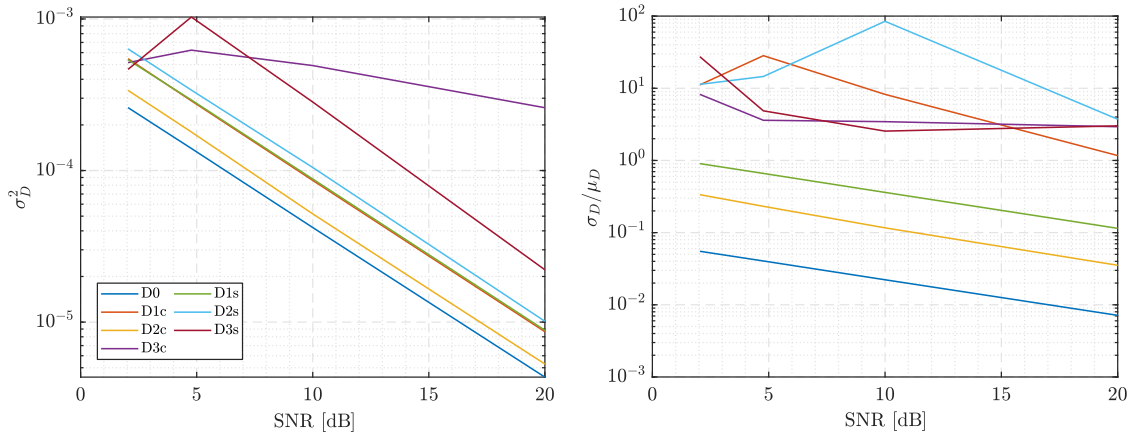

(e) $\hat{D}_d$ matrix variance (f) $\hat{D}_d$ matrix CV

Figure 5.6: Bending model numerical example. Variance and CV. $n_{\text{modes}} = 1$

As expected, in the majority of the cases, the variance and the CV decrease as the SNR increases. Nevertheless, some parameters as B_{21c}, B_{22c}, D_{3s} and D_{3c} may be discarded due to their high CV.

At last, as it may be difficult to evaluate an identification taking into account all of those charts, (taking into account that for higher systems, the number of charts will incrase exponentially), a measurement of the error between the identified and the reference model can be computed through some definitions, that will help to rate the algorithm performance.

$$\varepsilon_A = \|A_{\text{ref}} - \hat{A}_{\text{ident}}\|_2 \tag{5.8a}$$

$$\varepsilon_{Q\,i} = \int_0^{f_{\text{max input}}} \left| |Q_i|_{\text{ref}}(f) - |\hat{Q}_i|_{\text{ident}}(f) \right| \mathrm{d}f, \quad \begin{matrix} i = 1, ..., n_p \\ Q = B, C, D \end{matrix} \tag{5.8b}$$

$$\varepsilon_{\text{Tot}} = \|\sum \varepsilon_{Q\,i}\|_2. \tag{5.8c}$$

Then, a trend of the errors with respect to the SNR added-noise value can be plotted so as to understand the range of SNR value in which the method provides reasonable results.

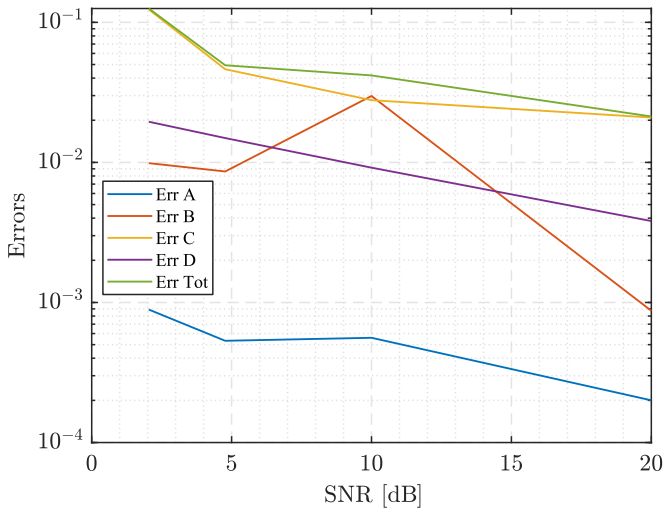

Figure 5.7: Bending model numerical example. Errors. $n_{\text{modes}} = 1$

Except for the $\hat{B}_d$ matrix, the rest of the matrices show an almost logarithmic behaviour with respect to the SNR increasement. This unexpected behaviour of $\hat{B}_d$ may become from a relative low value considered for N_{mont}, which value was selected mosly due to computation power reasoning.

5.4 Identification with $n_{\text{modes}} = 2$

The following case to be considered is the one with $n_{\text{modes}} = 2$. This leads to $n_\Theta = 79$ leaving $N_{\text{harm}} = 3$.

For SNR = 100, which is equal to add noise with $\sigma^2 = 4.29 \cdot 10^{-4}$ variance, the results are shown in Figure 5.8.

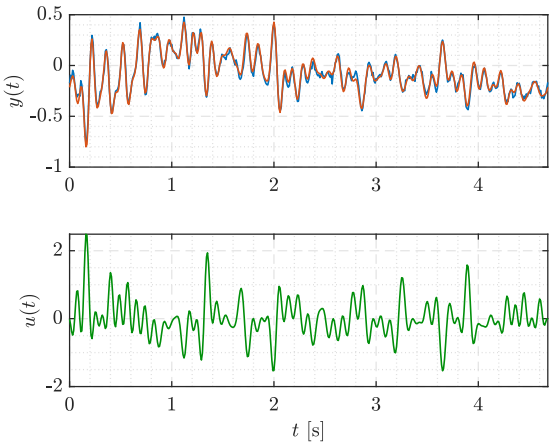

(a) Input-output chart

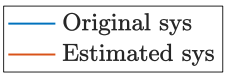

$$\rho_{\text{ref}} = \begin{bmatrix} 0.9954 \pm 0.0091i \\ 0.9964 \pm 0.0264i \end{bmatrix}$$

$$\rho_{\text{ident}} = \begin{bmatrix} 0.9945 \pm 0.0065i \\ 0.9964 \pm 0.0275i \end{bmatrix}$$

(b) $\hat{A}_d$ matrix eigenvalues comparison

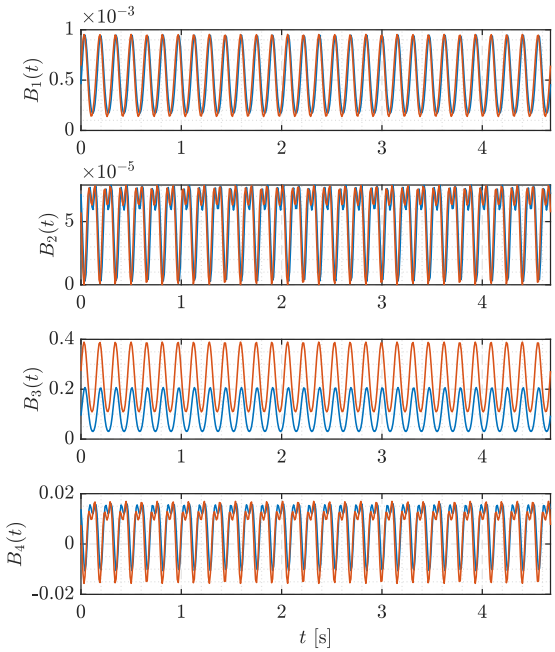

(c) $\hat{B}_d$ matrix in time domain

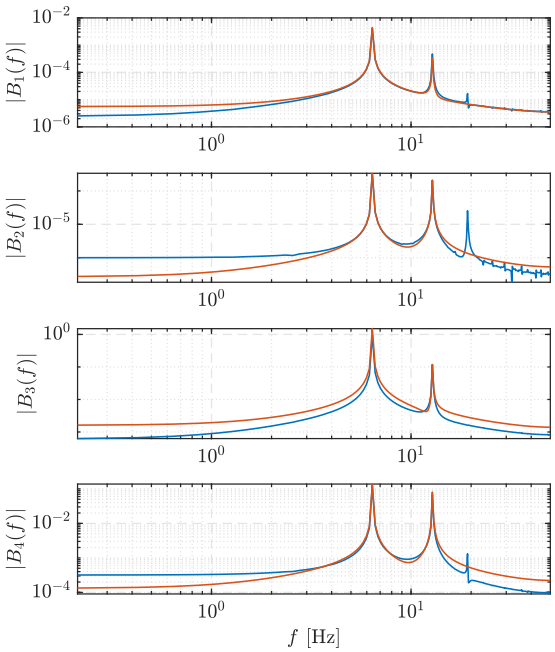

(d) $\hat{B}_d$ matrix in frequency domain

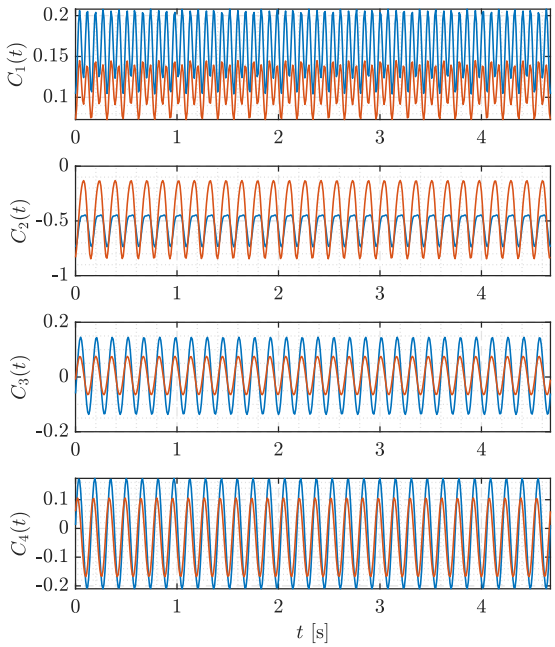

(e) $\hat{C}_d$ matrix in time domain

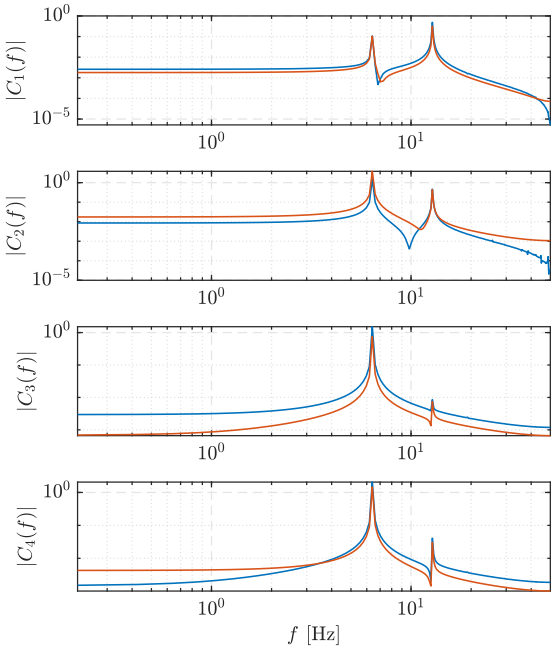

(f) $\hat{C}_d$ matrix in frequency domain

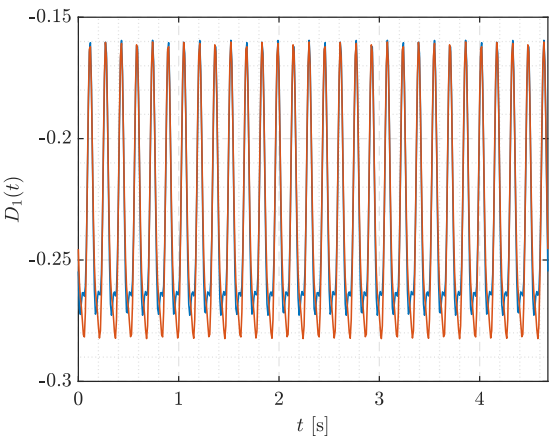

(g) $\hat{D}_d$ matrix in time domain

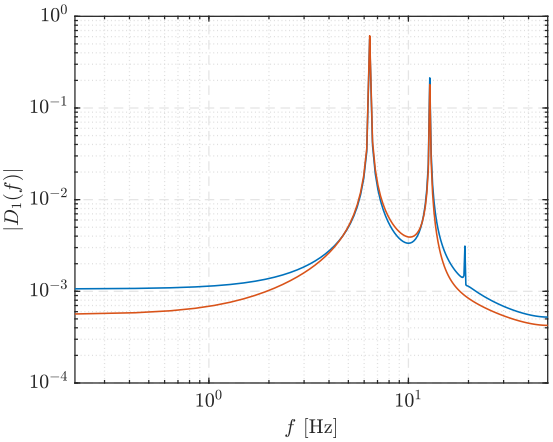

(h) $\hat{D}_d$ matrix in frequency domain

Figure 5.8: Bending model numerical example. $n_{\text{modes}} = 2$, SNR= 100

For SNR $= 10$, which is equal to add noise with $\sigma^2 = 4.29 \cdot 10^{-3}$ variance, the results are shown in Figure 5.9.

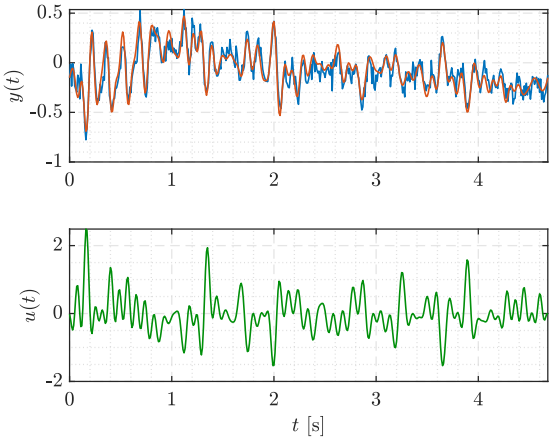

(a) Input-output chart

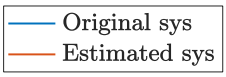

$$\rho_{\text{ref}} = \begin{bmatrix} 0.9954 \pm 0.0091i \\ 0.9964 \pm 0.0264i \end{bmatrix}$$

$$\rho_{\text{ident}} = \begin{bmatrix} 0.9949 \pm 0.0066i \\ 0.9965 \pm 0.0289i \end{bmatrix}$$

(b) $\hat{A}_d$ matrix eigenvalues comparison

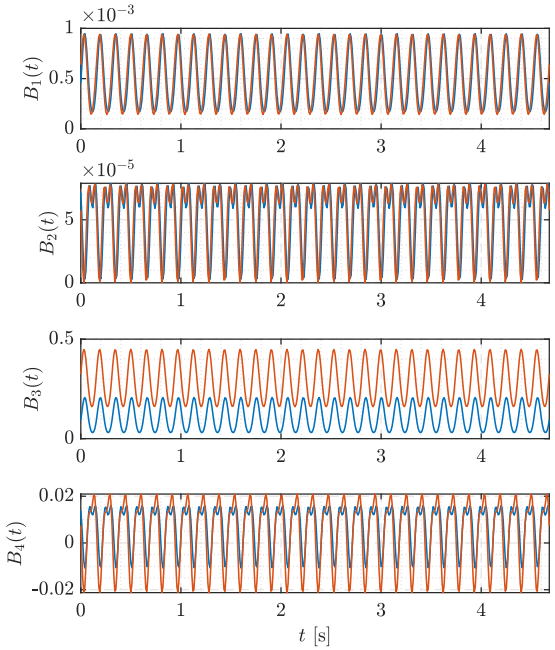

(c) $\hat{B}_d$ matrix in time domain

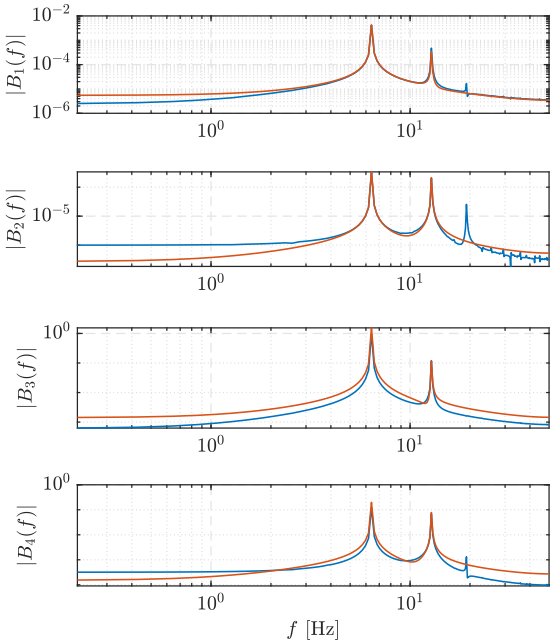

(d) $\hat{B}_d$ matrix in frequency domain

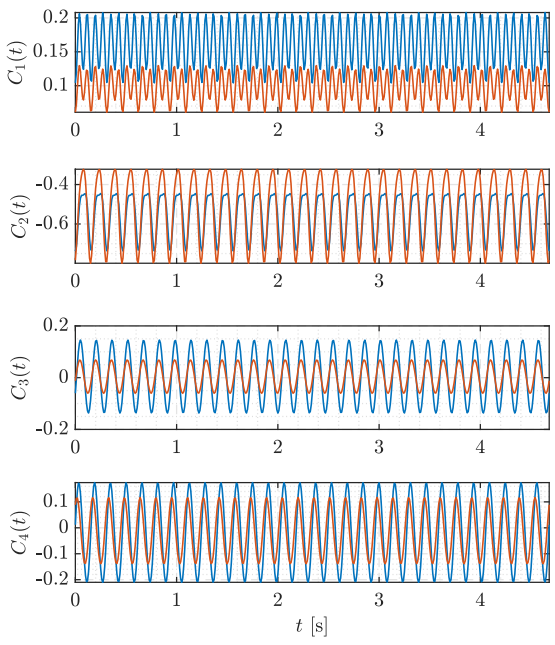

(e) $\hat{C}_d$ matrix in time domain

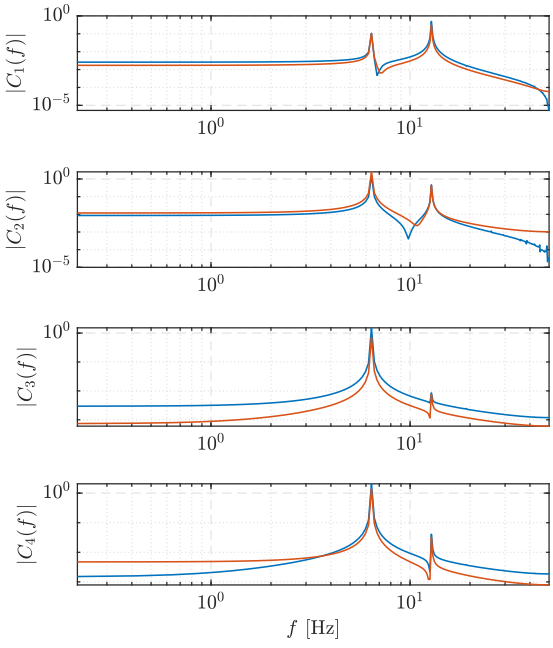

(f) $\hat{C}_d$ matrix in frequency domain

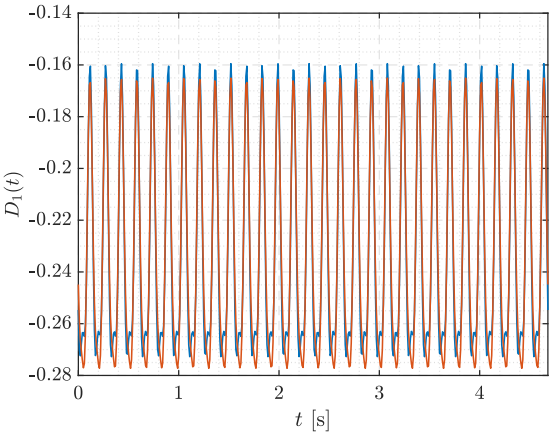

(g) $\hat{D}_d$ matrix in time domain

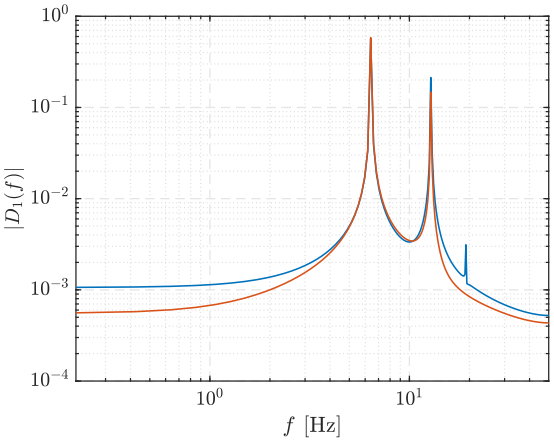

(h) $\hat{D}_d$ matrix in frequency domain

Figure 5.9: Bending model numerical example. $n_{\text{modes}} = 2$, SNR= 10

For SNR $= 3$, which is equal to add noise with $\sigma^2 = 1.43 \cdot 10^{-2}$ variance, the results are shown in Figure 5.10.

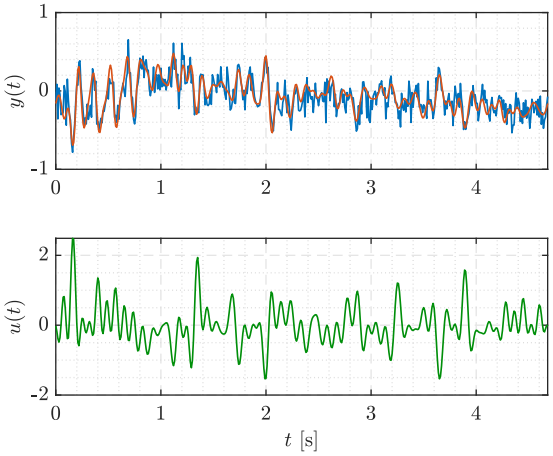

(a) Input-output chart

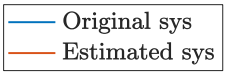

$$\rho_{\text{ref}} = \begin{bmatrix} 0.9954 \pm 0.0091i \\ 0.9964 \pm 0.0264i \end{bmatrix}$$

$$\rho_{\text{ident}} = \begin{bmatrix} 0.9948 \pm 0.0065i \\ 0.9958 \pm 0.0286i \end{bmatrix}$$

(b) $\hat{A}_d$ matrix eigenvalues comparison

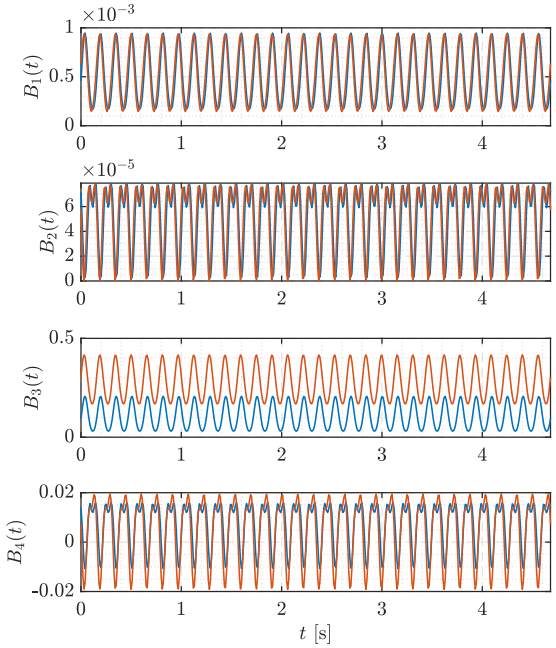

(c) $\hat{B}_d$ matrix in time domain

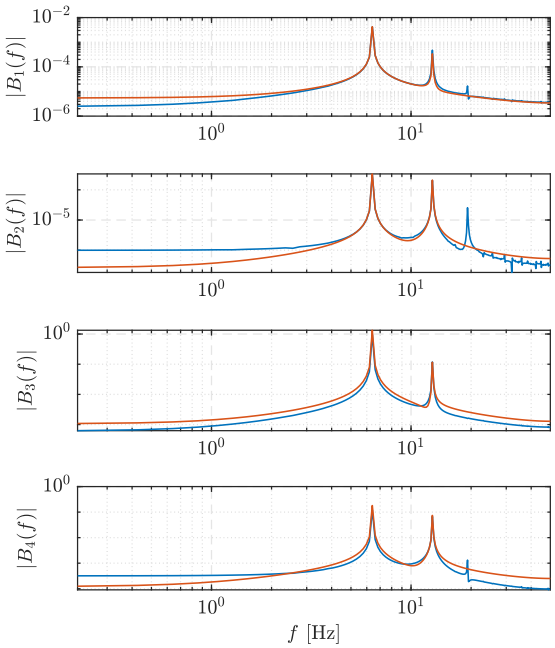

(d) $\hat{B}_d$ matrix in frequency domain

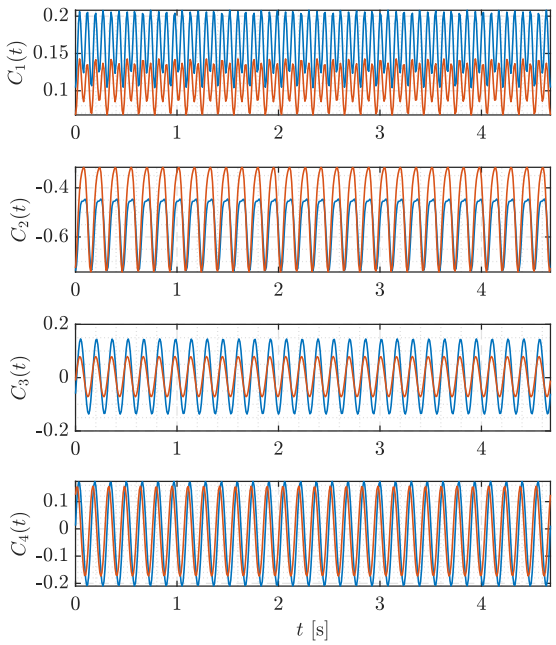

(e) $\hat{C}_d$ matrix in time domain

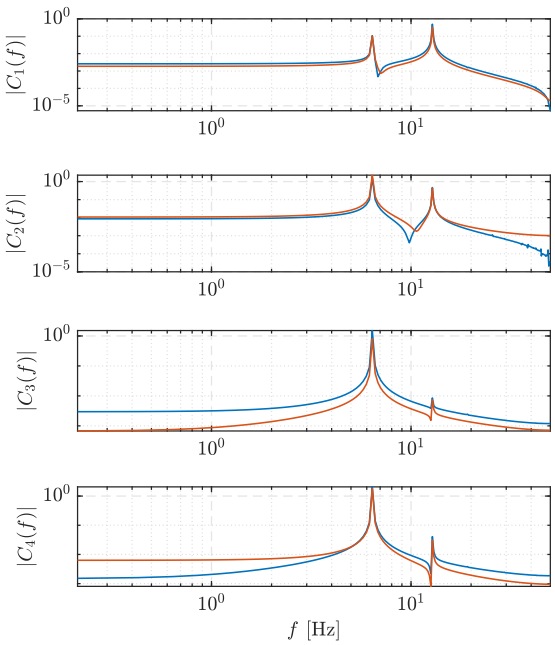

(f) $\hat{C}_d$ matrix in frequency domain

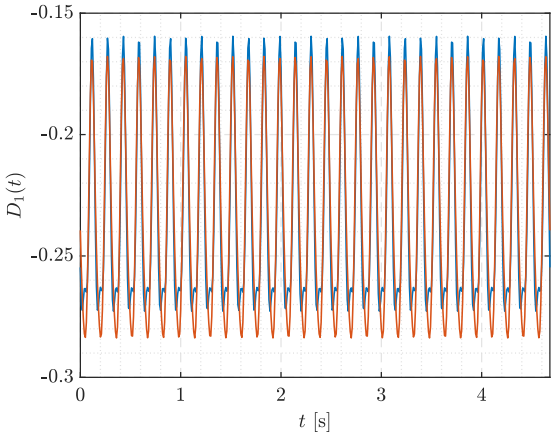

(g) $\hat{D}_d$ matrix in time domain

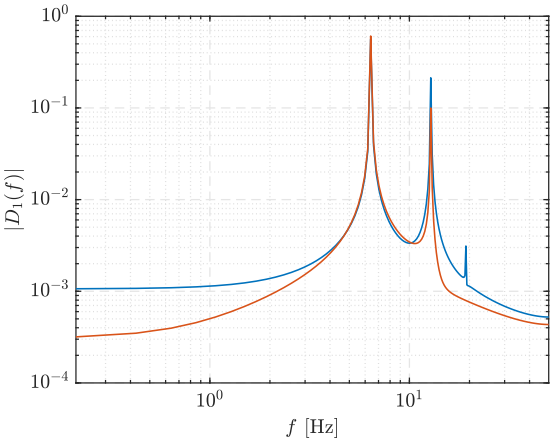

(h) $\hat{D}_d$ matrix in frequency domain

Figure 5.10: Bending model numerical example. $n_{\text{modes}} = 2$, SNR= 3

For SNR $= 1.6$, which is equal to add noise with $\sigma^2 = 2.68 \cdot 10^{-2}$ variance, the results are shown in Figure 5.11.

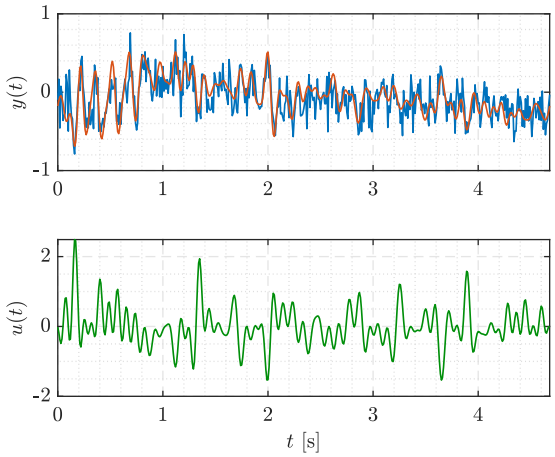

(a) Input-output chart

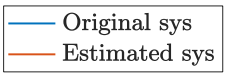

$$\rho_{\text{ref}} = \begin{bmatrix} 0.9954 \pm 0.0091i \\ 0.9954 \pm 0.0091i \end{bmatrix}$$

$$\rho_{\text{ident}} = \begin{bmatrix} 0.9950 \pm 0.0071i \\ 0.9948 \pm 0.0279i \end{bmatrix}$$

(b) $\hat{A}_d$ matrix eigenvalues comparison

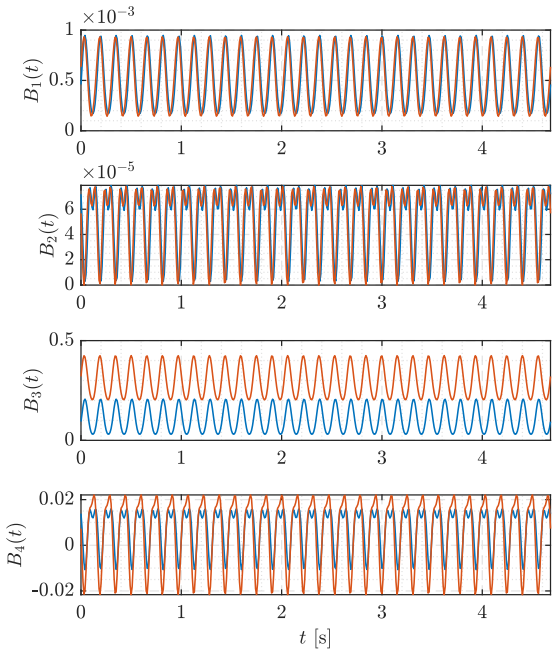

(c) $\hat{B}_d$ matrix in time domain

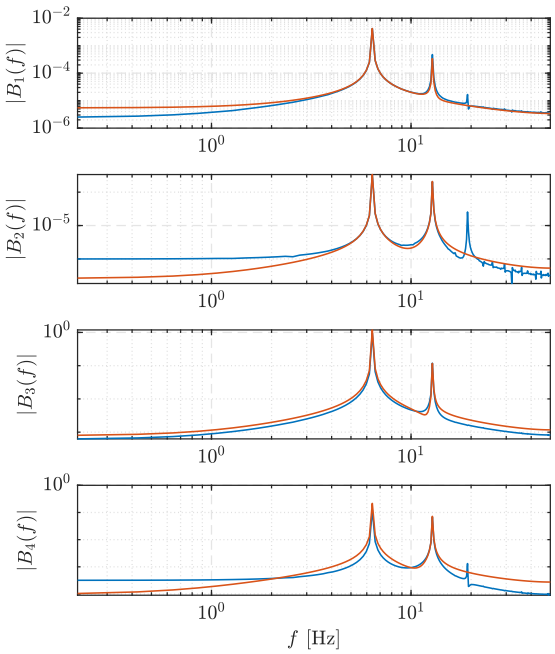

(d) $\hat{B}_d$ matrix in frequency domain

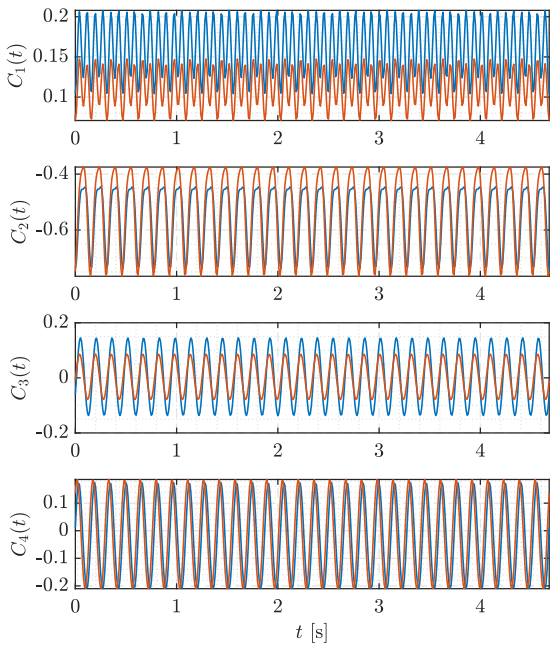

(e) $\hat{C}_d$ matrix in time domain

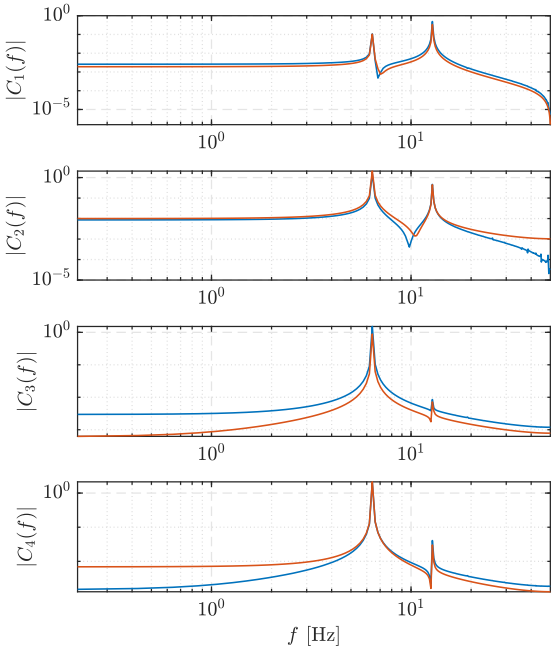

(f) $\hat{C}_d$ matrix in frequency domain

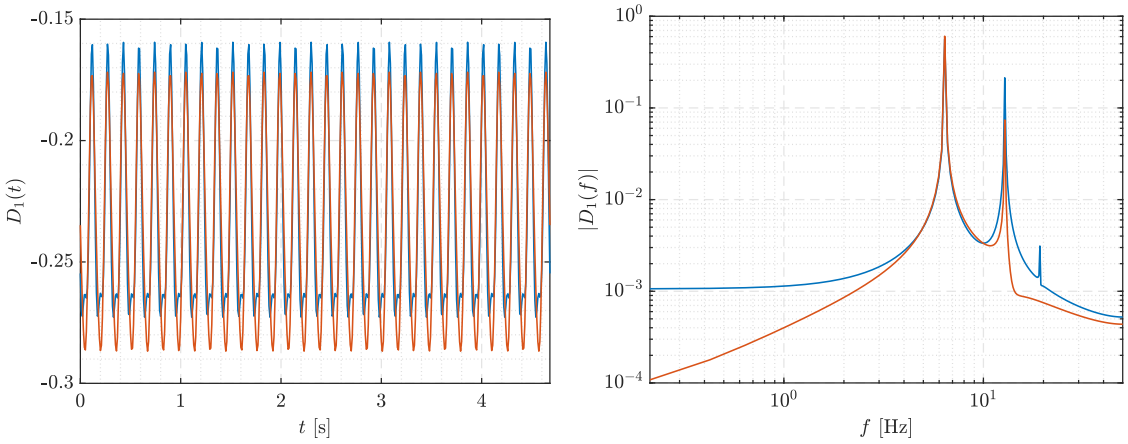

(g) $\hat{D}_d$ matrix in time domain

(h) $\hat{D}_d$ matrix in frequency domain

Figure 5.11: Bending model numerical example. $n_{\text{modes}} = 2$, SNR= 1.6

In this case, also a Monte Carlo analysis was performed, as it was explained in the $n_{\text{modes}} = 1$ case, maintaining $N_{\text{mont}} = 20$. Despite the number of non-zero parameters is much higher in this case, the uncertainty plots are provided, for each matrix, just to understand the general trend.

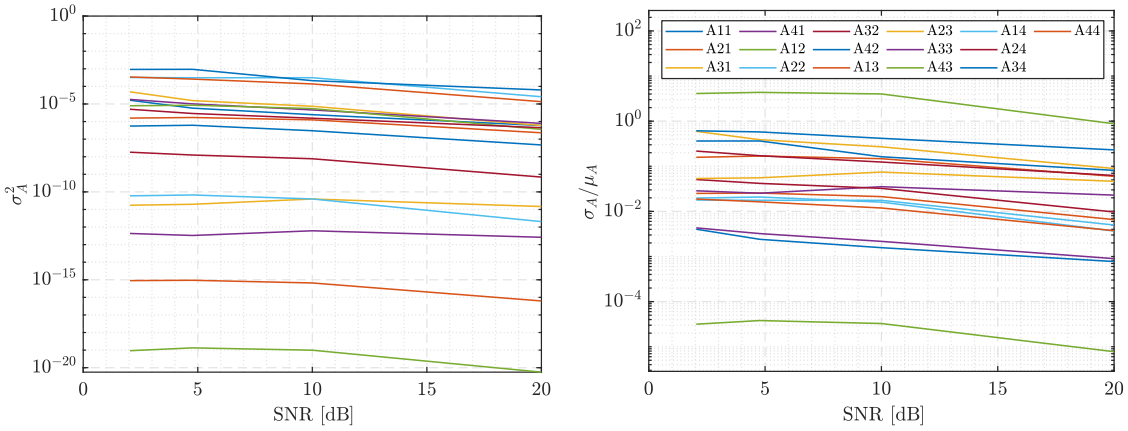

(a) $\hat{A}_d$ matrix variance

(b) $\hat{A}_d$ matrix CV

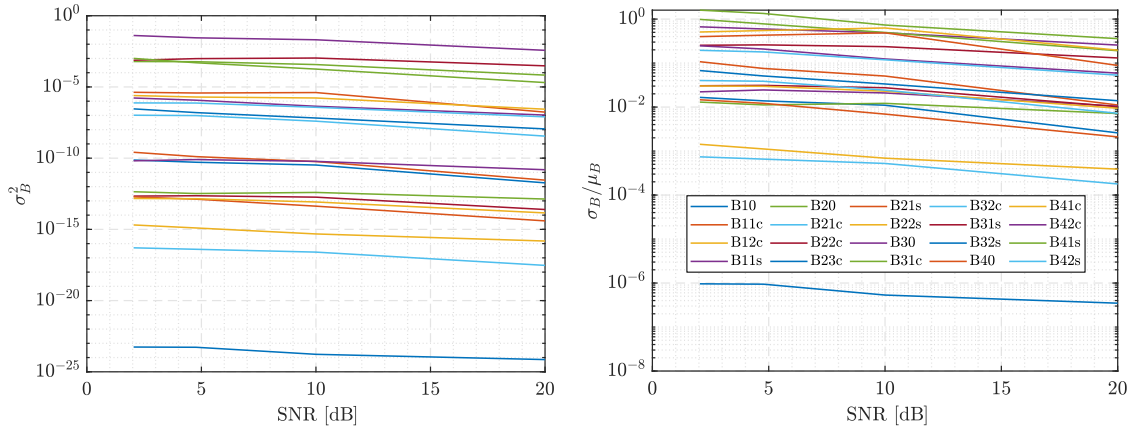

(a) $\hat{B}_d$ matrix variance (b) $\hat{B}_d$ matrix CV

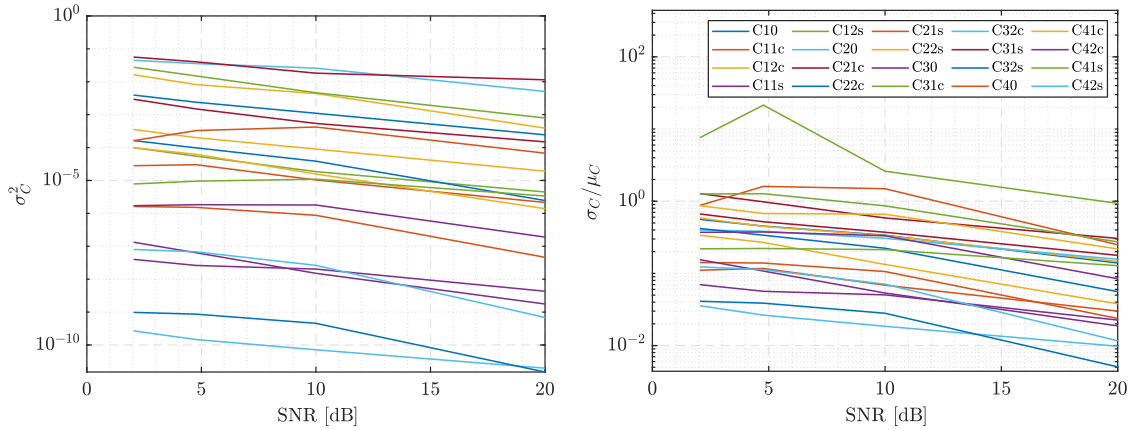

(c) $\hat{C}_d$ matrix variance (d) $\hat{C}_d$ matrix CV

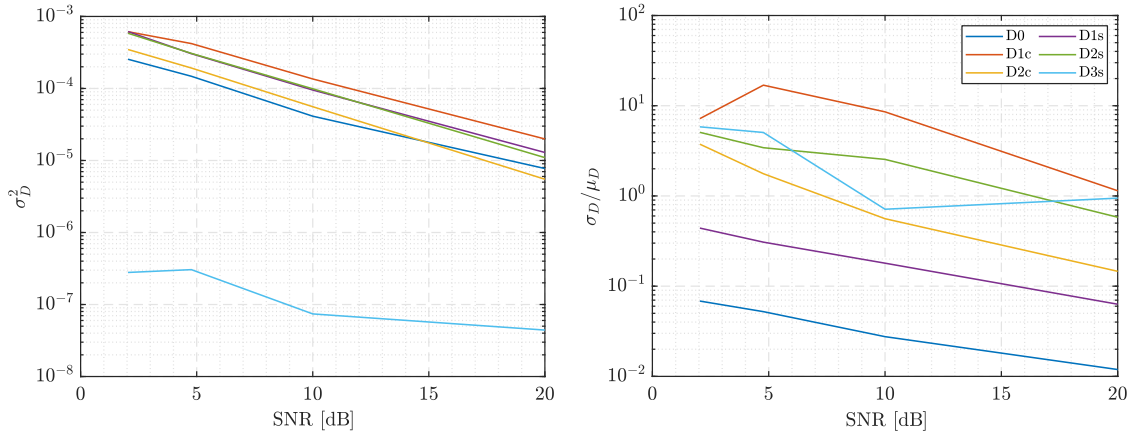

(e) $\hat{D}_d$ matrix variance (f) $\hat{D}_d$ matrix CV

Figure 5.12: Bending model numerical example. Variance and CV. $n_{\text{modes}} = 2$

As in the previous case, many parameters are likely to be discarded, due to their high standard deviation with respect to their low mean value (high CV). However, many parameters show a very small variation with respect to the SNR value, which would mean that the estimated value is not noise sensitive.

Finally, as in the previous case, the trend of the errors of the identified system with respect to the reference one is provided in Figure 5.13

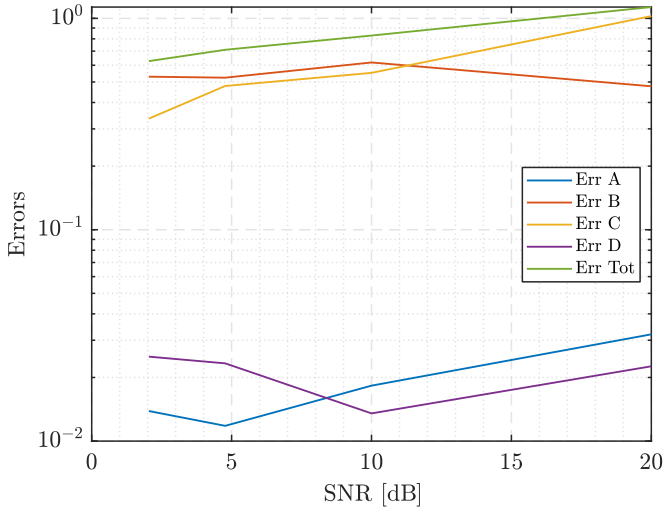

Figure 5.13: Bending model numerical example. Errors. $n_{\text{modes}} = 2$

With respect to the $n_{\text{modes}} = 1$ results, the errors have grown, due to the increase of parameters to identify, the double. These errors are mostly in the $\hat{B}_d$ and $\hat{C}_d$ matrices, where the amplitude of the harmonics is not perfectly captured. It is also remarkable that the error in the eigenvalues of the identified system with respect to the reference one has grown in this case. However, despite these errors, the identified matrices are still similar to the reference ones, in the sense of maintaining the same order of magnitude, and the estimated output is still close to the reference one, even in the worst-noise case.

5.5 Identification with $n_{\text{modes}} = 1$ system and $n_{\text{modes}} = 2$ signal

So far, the identification has been performed using the same n_{modes} value for the computed output signal and for the identified state-space system. However, considering the application of this example to real life, the blade will have an infinite number of modes. Therefore, the next step will be testing the behaviour of the method identifying a system which is not exactly the same as the obtained output. To perform this, in the following case, $n_{\text{modes}} = 2$ to compute the output signal

and the identified system will have the $n_{\text{modes}} = 1$ size.

In this analysis, an identification with an added-noise signal in which SNR = 10000 ($\sigma^2 = 4.29 \cdot 10^{-6}$) to test a case with a very low amount of added noise. In this case, the results are shown in Figure 5.14.

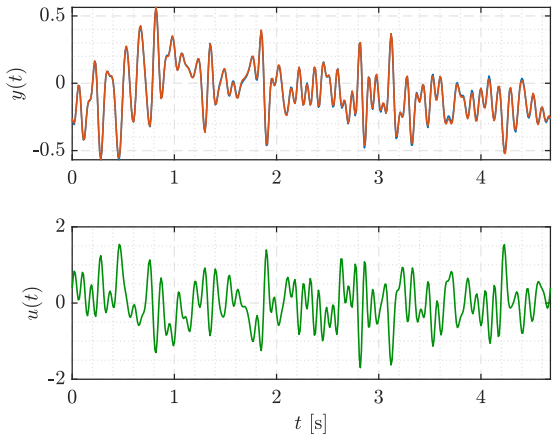

(a) Input-output chart

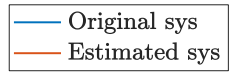

$$\rho_{\text{ref}} = \begin{bmatrix} 0.9954 \pm 0.0091i \\ 0.9964 \pm 0.0264i \end{bmatrix}$$

$$\rho_{\text{ident}} = \begin{bmatrix} 0.9958 \pm 0.0082i \end{bmatrix}$$

(b) $\hat{A}_d$ matrix eigenvalues comparison

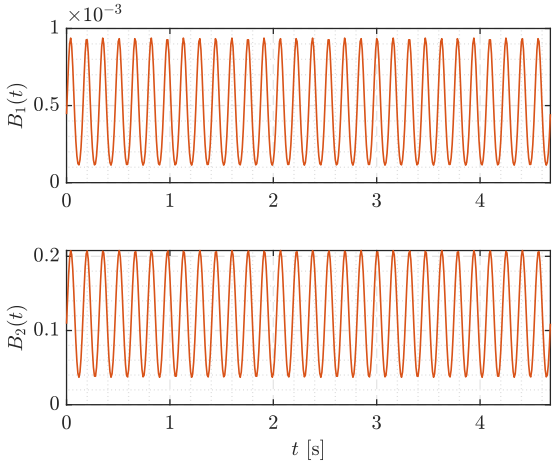

(c) $\hat{B}_d$ matrix in time domain

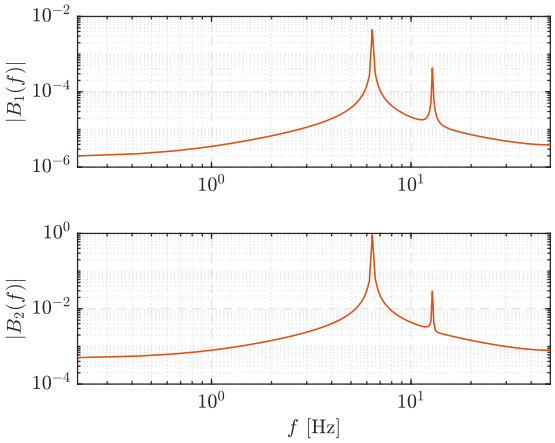

(d) $\hat{B}_d$ matrix in frequency domain

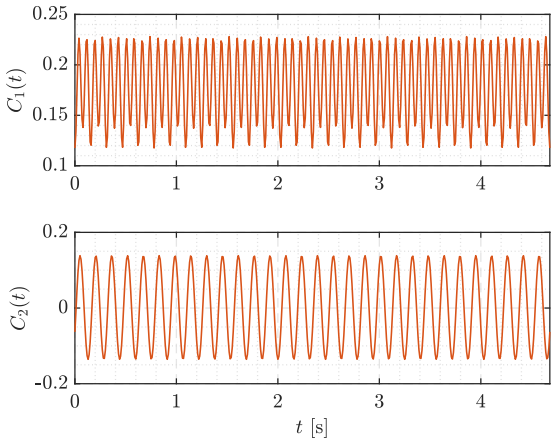

(e) $\hat{C}_d$ matrix in time domain

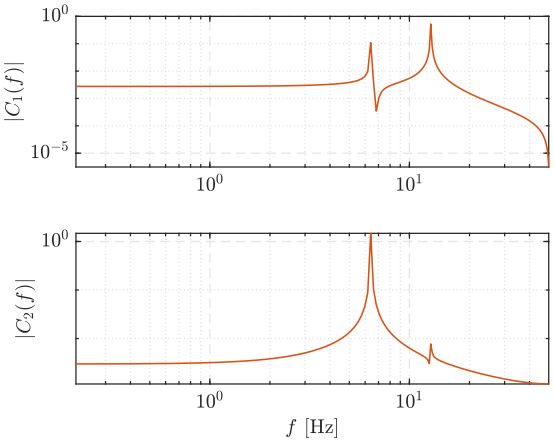

(f) $\hat{C}_d$ matrix in frequency domain

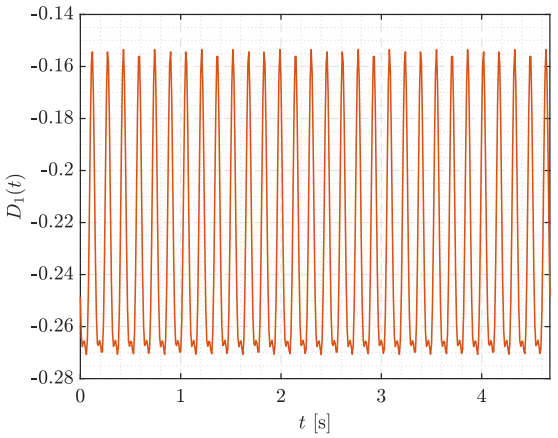

(g) $\hat{D}_d$ matrix in time domain

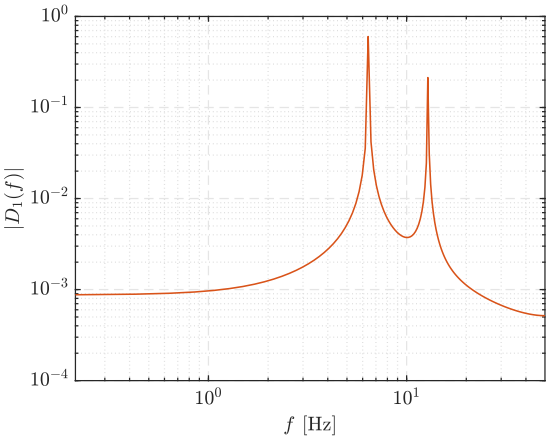

(h) $\hat{D}_d$ matrix in frequency domain

Figure 5.14: Bending model numerical example. $n_{\text{modes signal}} = 2$, $n_{\text{modes system}} = 1$, SNR= 10000

For SNR = 100, which is equal to add noise with $\sigma^2 = 4.29 \cdot 10^{-4}$ variance, the results are shown in Figure 5.15.

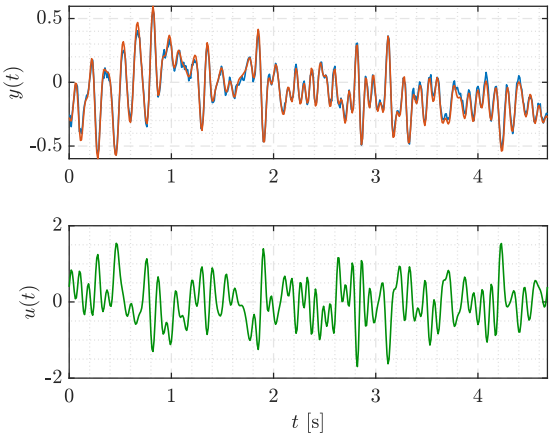

(a) Input-output chart

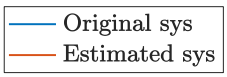

$$\rho_{\text{ref}} = \begin{bmatrix} 0.9954 \pm 0.0091i \\ 0.9964 \pm 0.0264i \end{bmatrix}$$

$$\rho_{\text{ident}} = \begin{bmatrix} 0.9959 \pm 0.0082i \end{bmatrix}$$

(b) $\hat{A}_d$ matrix eigenvalues comparison

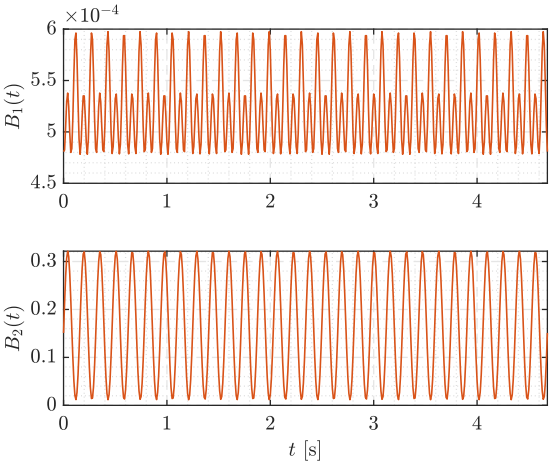

(c) $\hat{B}_d$ matrix in time domain

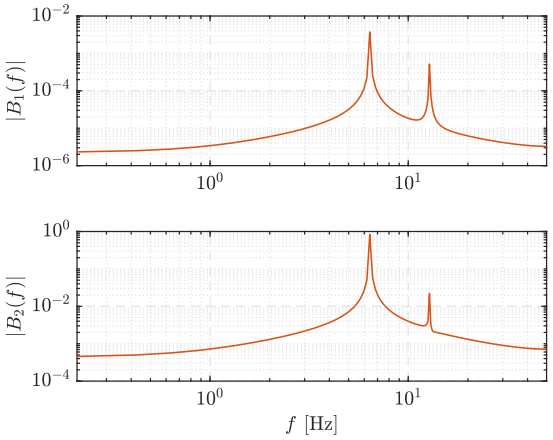

(d) $\hat{B}_d$ matrix in frequency domain

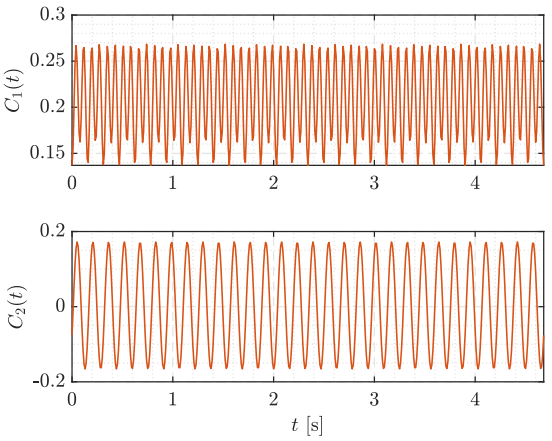

(e) $\hat{C}_d$ matrix in time domain

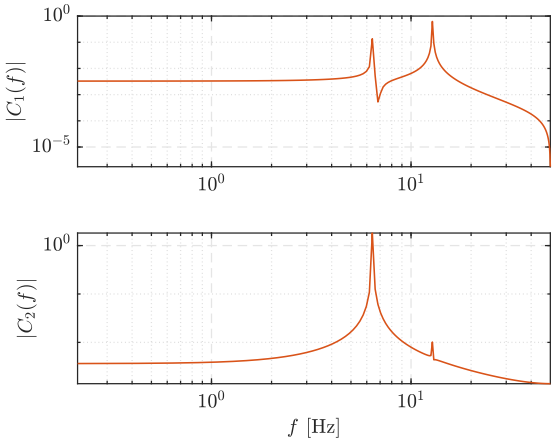

(f) $\hat{C}_d$ matrix in frequency domain

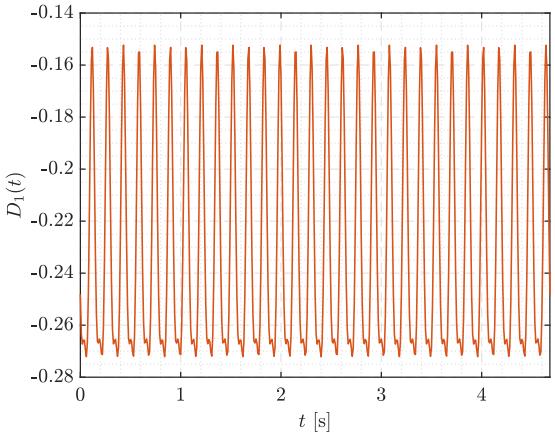

(g) $\hat{D}_d$ matrix in time domain

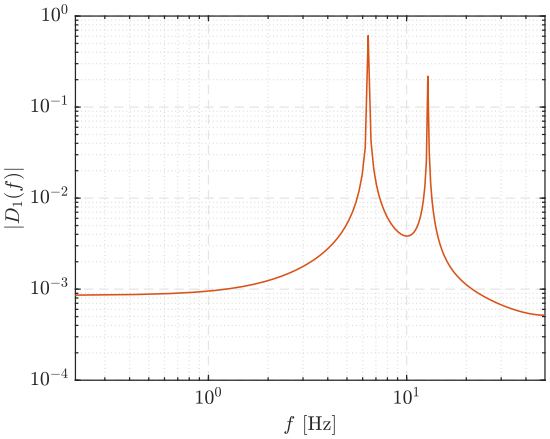

(h) $\hat{D}_d$ matrix in frequency domain

Figure 5.15: Bending model numerical example. $n_{\text{modes signal}} = 2$, $n_{\text{modes system}} = 1$, SNR= 100

For SNR $= 10$, which is equal to add noise with $\sigma^2 = 4.29 \cdot 10^{-3}$ variance, the results are shown in Figure 5.16.

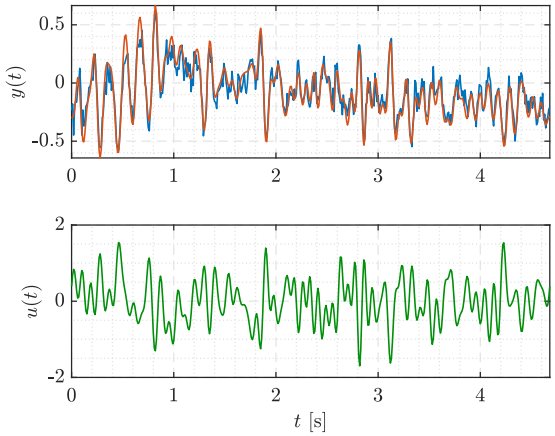

(a) Input-output chart

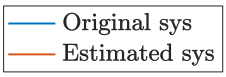

$$\rho_{\text{ref}} = \begin{bmatrix} 0.9954 \pm 0.0091i \\ 0.9964 \pm 0.0264i \end{bmatrix}$$

$$\rho_{\text{ident}} = \begin{bmatrix} 0.9950 \pm 0.0094i \end{bmatrix}$$

(b) $\hat{A}_d$ matrix eigenvalues comparison

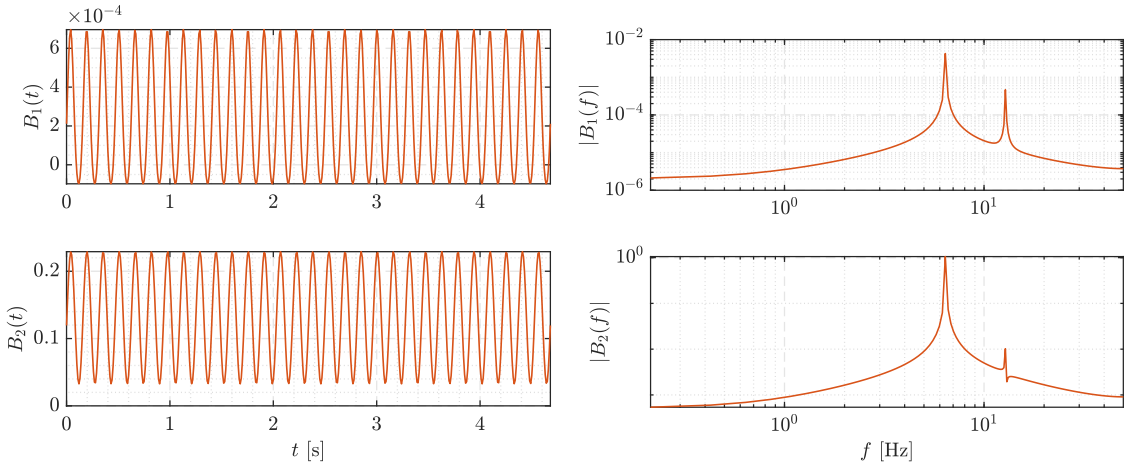

(c) $\hat{B}_d$ matrix in time domain (d) $\hat{B}_d$ matrix in frequency domain

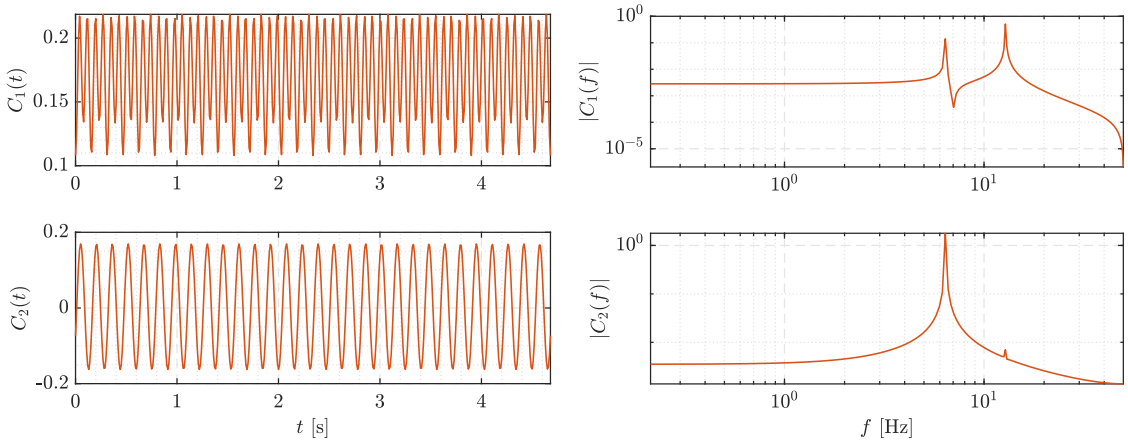

(e) $\hat{C}_d$ matrix in time domain (f) $\hat{C}_d$ matrix in frequency domain

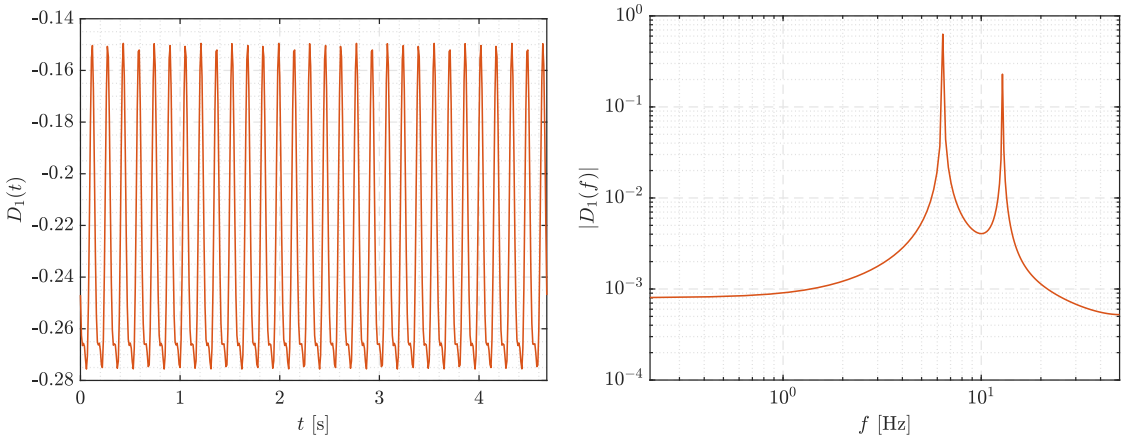

(g) $\hat{D}_d$ matrix in time domain (h) $\hat{D}_d$ matrix in frequency domain

Figure 5.16: Bending model numerical example. $n_{\text{modes signal}} = 2$, $n_{\text{modes system}} = 1$, SNR= 10

For SNR = 3, which is equal to add noise with $\sigma^2 = 1.43 \cdot 10^{-2}$ variance, the results are shown in Figure 5.17.

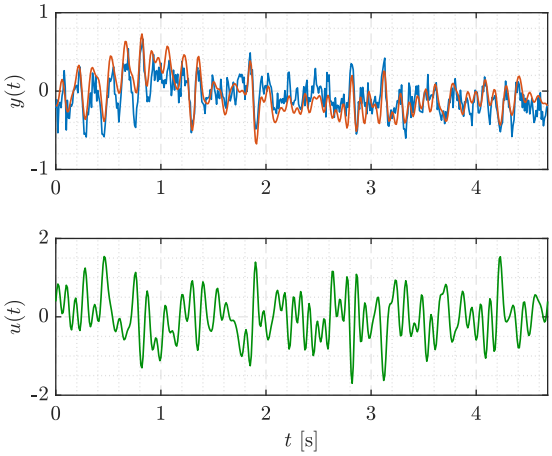

(a) Input-output chart

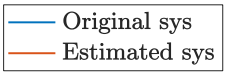

$$\rho_{\text{ref}} = \begin{bmatrix} 0.9954 \pm 0.0091i \\ 0.9964 \pm 0.0264i \end{bmatrix}$$

$$\rho_{\text{ident}} = \begin{bmatrix} 0.9952 \pm 0.0143i \end{bmatrix}$$

(b) $\hat{A}_d$ matrix eigenvalues comparison

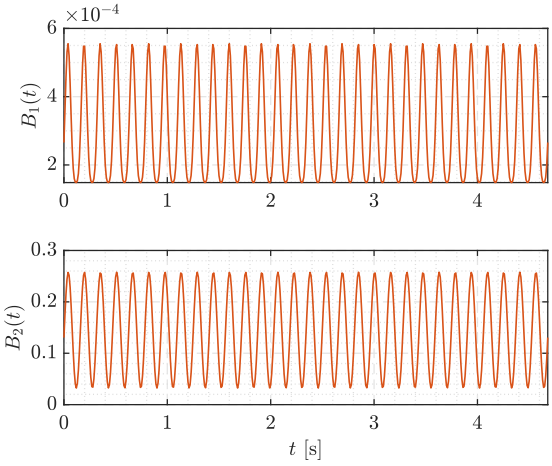

(c) $\hat{B}_d$ matrix in time domain

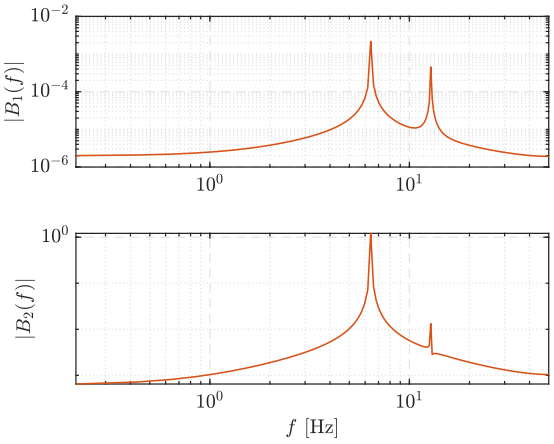

(d) $\hat{B}_d$ matrix in frequency domain

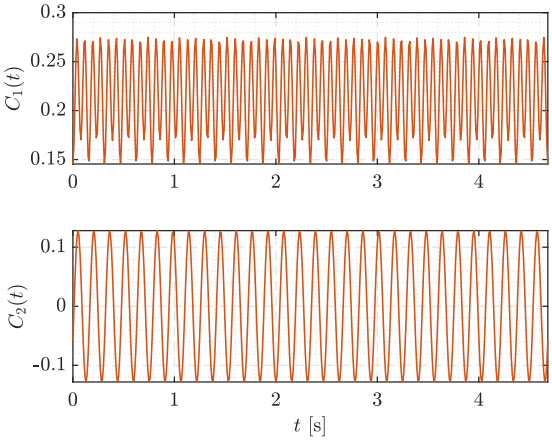

(e) $\hat{C}_d$ matrix in time domain

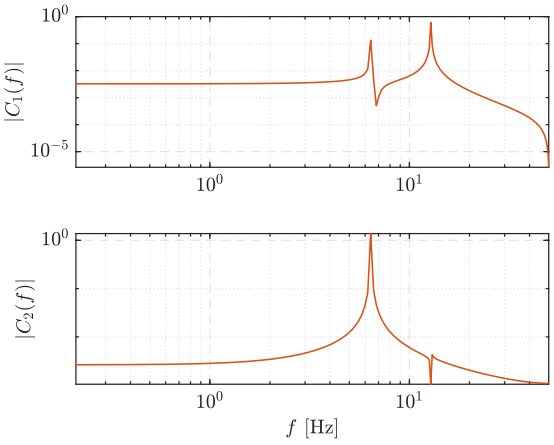

(f) $\hat{C}_d$ matrix in frequency domain

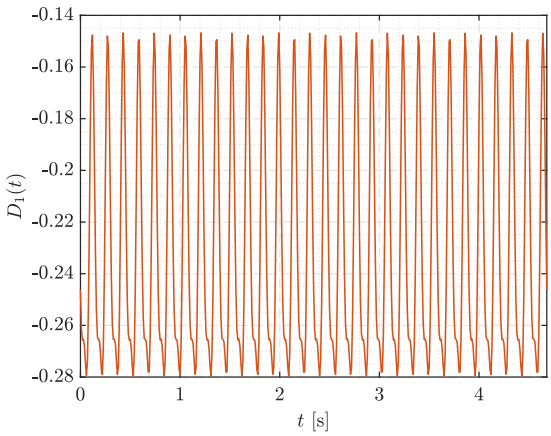

(g) $\hat{D}_d$ matrix in time domain

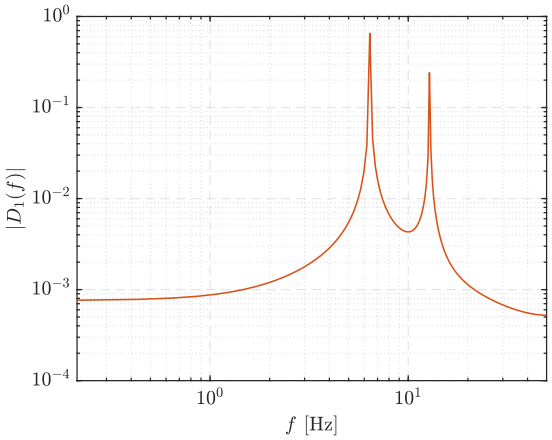

(h) $\hat{D}_d$ matrix in frequency domain

Figure 5.17: Bending model numerical example. $n_{\text{modes signal}} = 2$, $n_{\text{modes system}} = 1$, SNR= 3

For SNR = 1.6, which is equal to add noise with $\sigma^2 = 2.68 \cdot 10^{-2}$ variance, the results are shown in Figure 5.18.

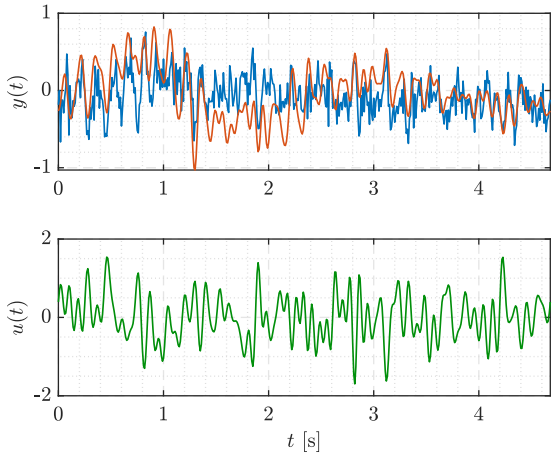

(a) Input-output chart

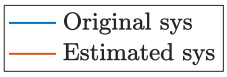

$$\rho_{\text{ref}} = \begin{bmatrix} 0.9954 \pm 0.0091i \\ 0.9964 \pm 0.0264i \end{bmatrix}$$

$$\rho_{\text{ident}} = \begin{bmatrix} 0.9955 \pm 0.0241i \end{bmatrix}$$

(b) $\hat{A}_d$ matrix eigenvalues comparison

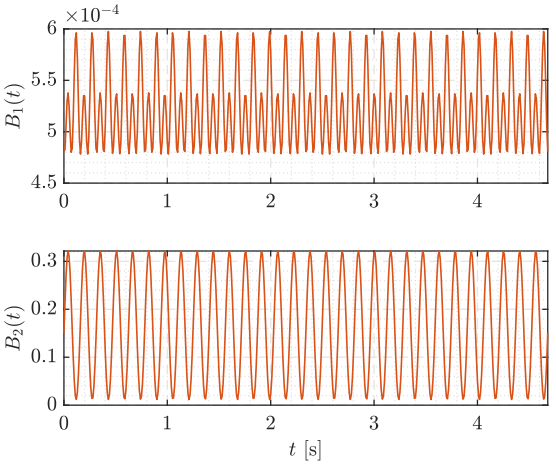

(c) $\hat{B}_d$ matrix in time domain

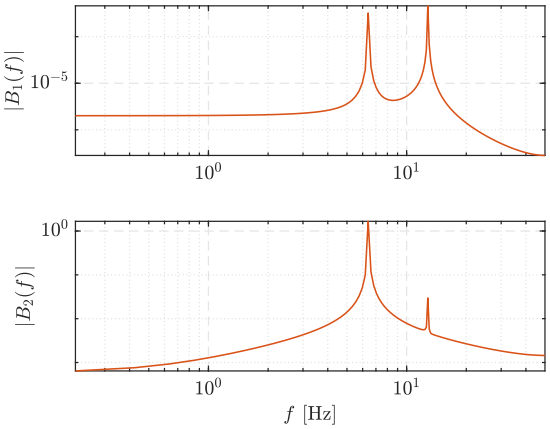

(d) $\hat{B}_d$ matrix in frequency domain

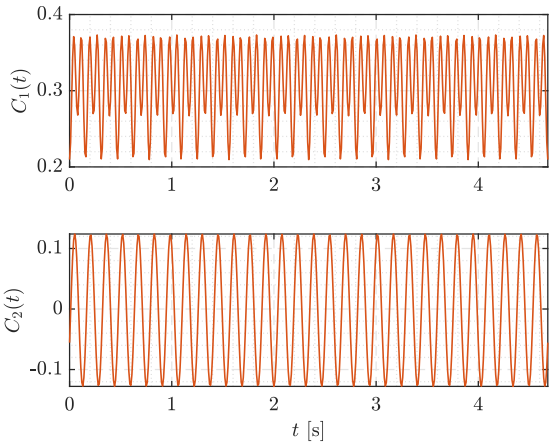

(e) $\hat{C}_d$ matrix in time domain

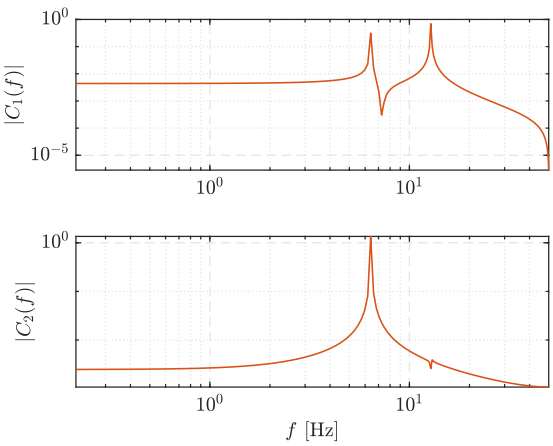

(f) $\hat{C}_d$ matrix in frequency domain

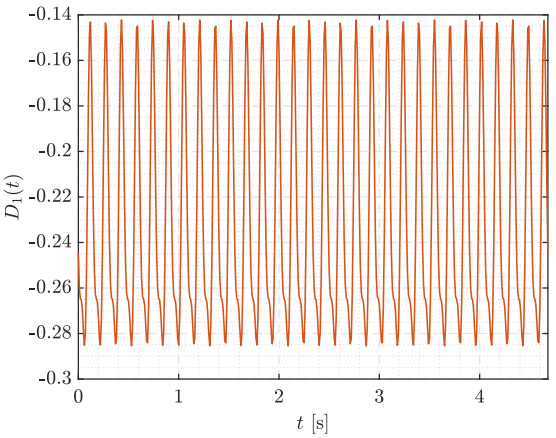

(g) $\hat{D}_d$ matrix in time domain

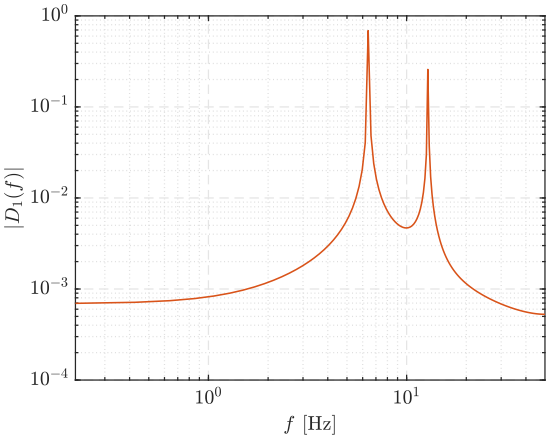

(h) $\hat{D}_d$ matrix in frequency domain

Figure 5.18: Bending model numerical example. $n_{\text{modes signal}} = 2$, $n_{\text{modes system}} = 1$, SNR= 1.6

In this case, the presence of noise is more relevant than in the previous cases. When the noise is such that SNR ≤ 3, the method cannot find the combination of parameters such that the difference between the system output and the simulated output is minimum with respect to the required tolerance. Therefore, it would be necessary to apply some filtering. A good option for this would be to use a periodic filter.

The reasoning for this periodic filter resides in what explained in Figure 2.1. Since each harmonic in the input excites all the rest of the harmonics in the output, to delete a frequency in the input would mean to modify all the amplitudes of the frequencies in the output signal. However, the study and application of a periodic filter will not be discussed in this thesis.

After the Monte Carlo analysis, maintaining the same configuration as the previous cases, the uncertainty results are provided in Figure 5.19.

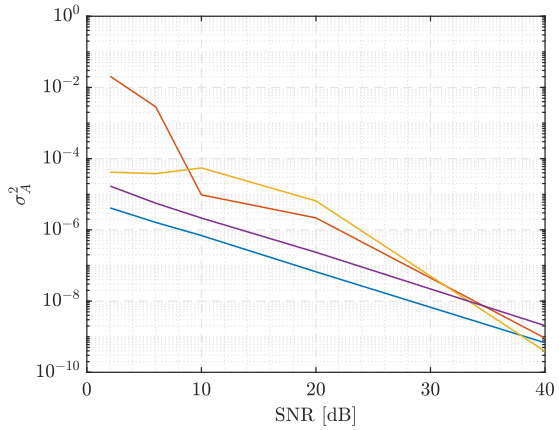

(a) $\hat{A}_d$ matrix variance

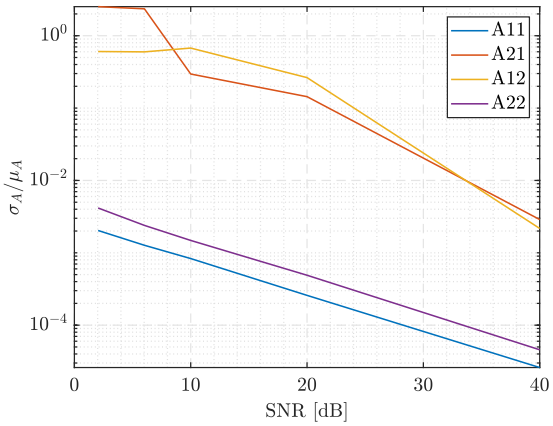

(b) $\hat{A}_d$ matrix CV

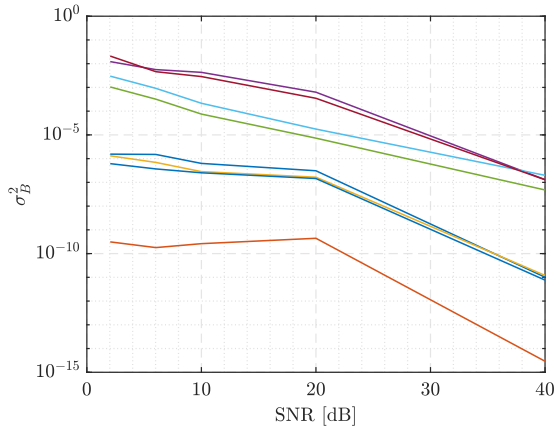

(c) $\hat{B}_d$ matrix variance

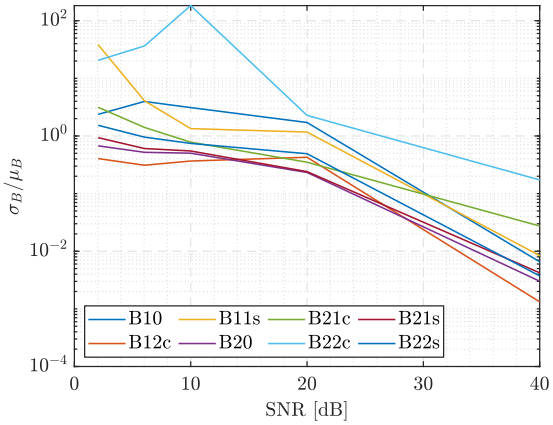

(d) $\hat{B}_d$ matrix CV

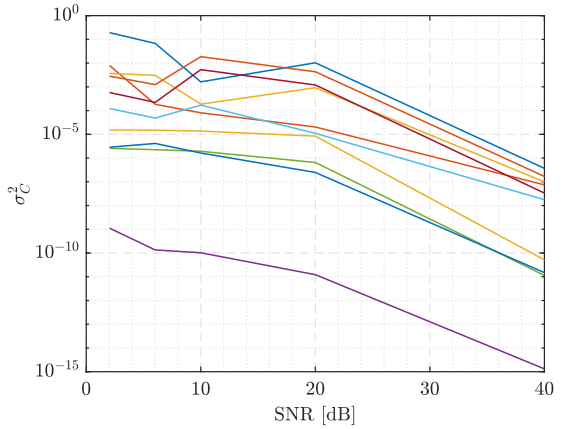

(e) $\hat{C}_d$ matrix variance

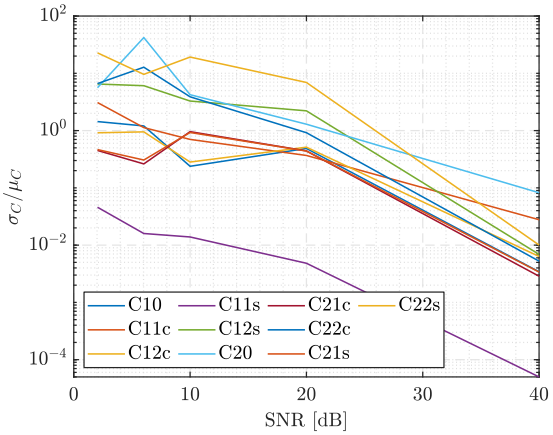

(f) $\hat{C}_d$ matrix CV

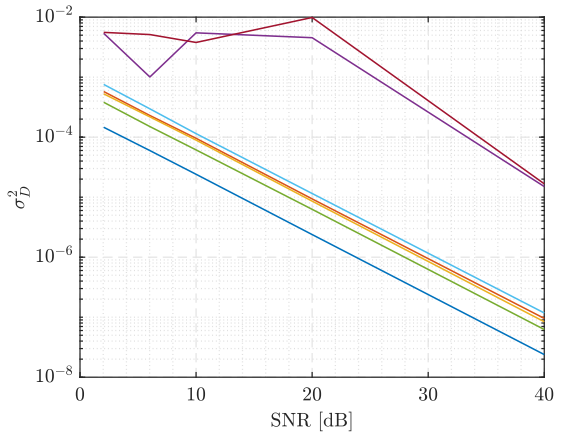

(g) $\hat{D}_d$ matrix variance

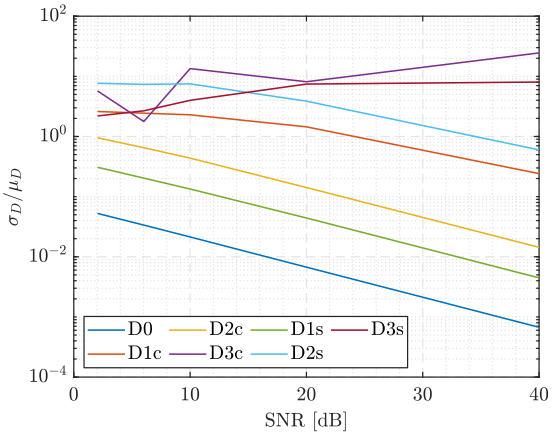

(h) $\hat{D}_d$ matrix CV

Figure 5.19: Bending model numerical example. Variance and CV. $n_{\text{modes signal}} = 2$, $n_{\text{modes system}} = 1$

As in the previous cases, it may be desired to discard some parameters, as the ones that increase their CV with the SNR, but it is also noticeable that the uncertainty of the parameters are more sensitive to the reference output signal noise.

To conclude this section, as in this case it would not make sense to study the trend of the errors of the identified system with respect to the reference one because of the structural difference, to perform a comparison, the HTF should be reviewed, in order to understand the dynamics that are not captured by the identified model. A primary idea would be to plot the magnitude and the phase of each element of the HTF matrix, in order to perform the comparison.

To construct a chart to perform the comparison, it is necessary to shift some columns of the HTF matrix. Coming back to equation (2.36), and taking into account the provided definitions in Section 2.4.4, it is possible to shift the columns so as, for each $G_{a\,b}$, the same index a will be in the same row, mantaining that the same index b will be in the same column. Equation (5.9) can be illustrative. This shifted matrix will be denoted as $G^*(s/z)$.

$$\mathcal{G}^*(s/z) = \begin{bmatrix} \ddots & \vdots & \vdots & \vdots & \\ \cdots & G_{-1}(s - s_m/z \cdot z_m^{-1}) & G_{-1}(s/z) & G_{-1}(s + s_m/z \cdot z_m) & \cdots \\ \cdots & G_0(s - s_m/z \cdot z_m^{-1}) & G_0(s/z) & G_0(s + s_m/z \cdot z_m) & \cdots \\ \cdots & G_1(s - s_m/z \cdot z_m^{-1}) & G_1(s/z) & G_1(s + s_m/z \cdot z_m) & \cdots \\ & \vdots & \vdots & \vdots & \ddots \end{bmatrix} \tag{5.9}$$

However, due to high amount of information that it shows, it is not practical. Another possibility would be to study the main system modes, that can be defined as the ration of the output signal period and the system period,

$$H_n = n\,\frac{T_\text{o}}{T_\text{m}} = 30\,n, \quad n \in \mathbb{Z}, \tag{5.10}$$

where T_o stands for the period of the output signal. These modes correspond to $G_{a\,H_n}$. Since the magnitude of the main system modes is higher than the other values, it is justified to compare just them.

This comparison can be done using Bode-like charts. Also, as the magnitude of H_n will decrease as n increases, only H_0 and H_1 will be studied. Physically, in this case, the meaning of H_0 would mean applying a collective input to the rotor, in which the system would behave as a LTI one, because the resultant force is time-invariant. In the case of H_1, the physical meaning would be a cyclic input to the rotor. Hence, these charts are provided in Figure 5.20.

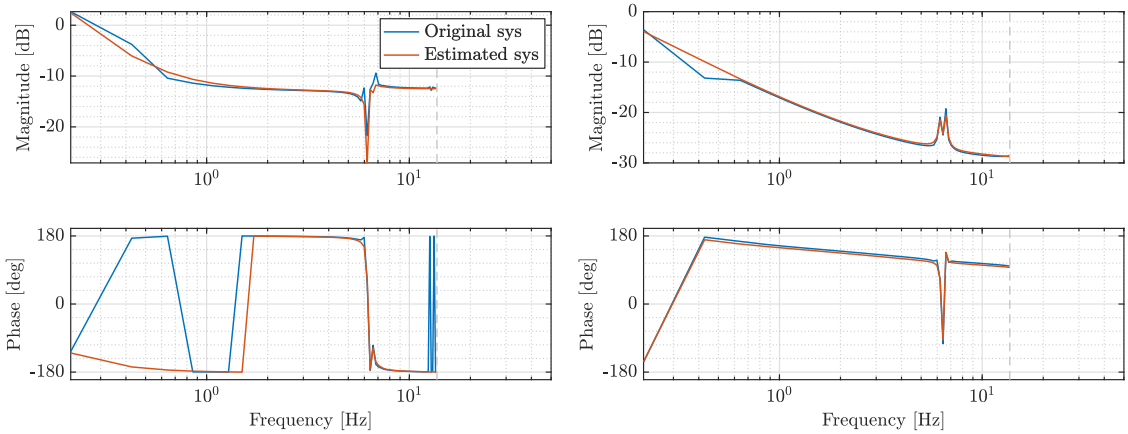

(a) H_0, SNR = 10000 (b) H_1, SNR = 10000

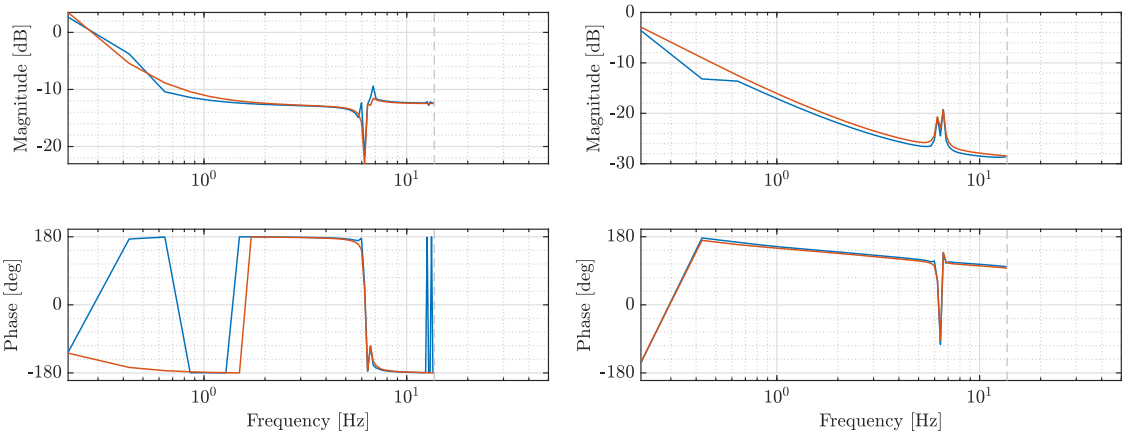

(c) H_0, SNR = 100

(d) H_1, SNR = 100

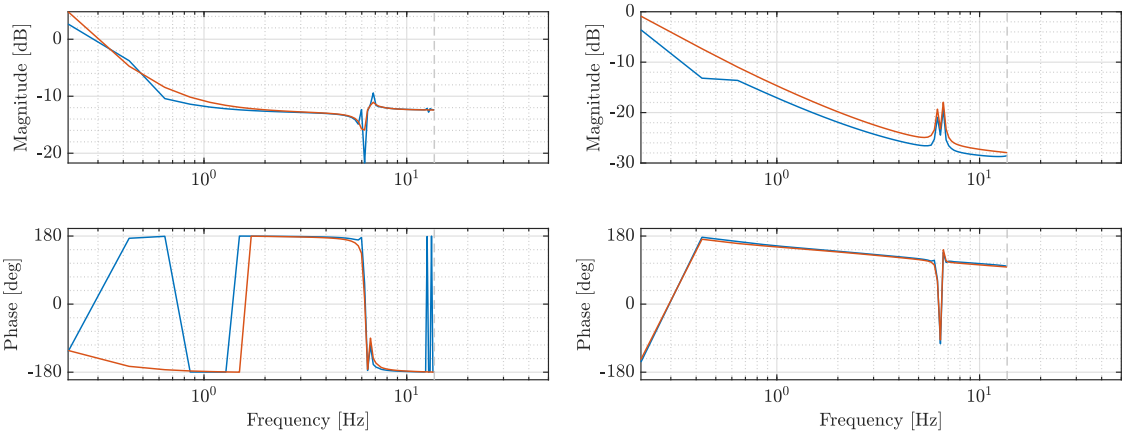

(e) H_0, SNR = 10

(f) H_1, SNR = 10

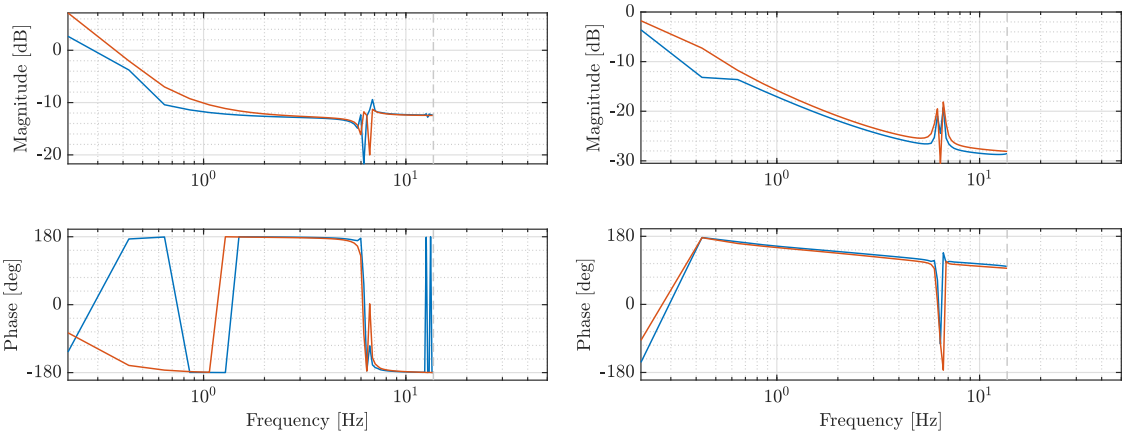

(g) H_0, SNR = 3

(h) H_1, SNR = 3

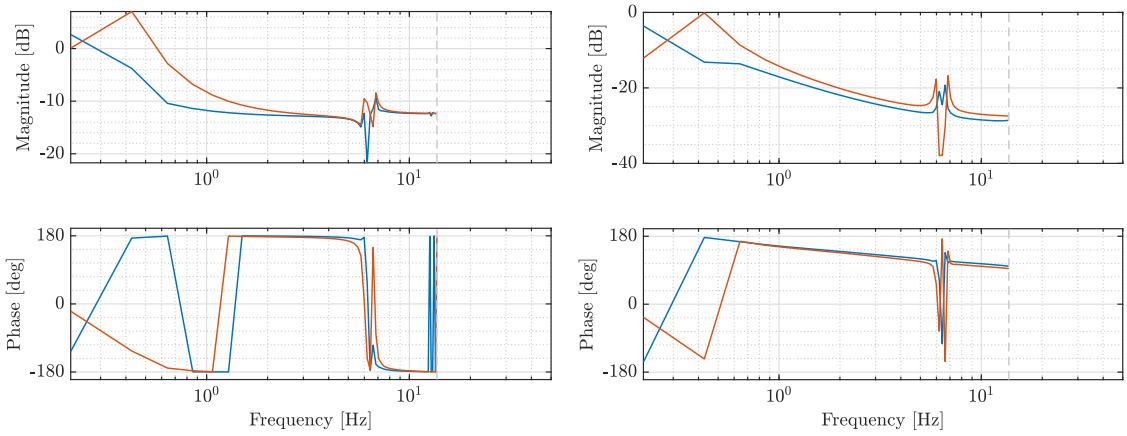

(i) H_0, SNR = 1.6 (j) H_1, SNR = 1.6

Figure 5.20: Bending model numerical example. H_0 and H_1 Bode-like charts. $n_{\text{modes signal}} = 2$, $n_{\text{modes system}} = 1$

As it can be noticed, a better comparison can be performed regarding H_0 and H_1. In these charts, it must be taken into account that, despite the Nyquist frequency is 50 Hz due to the chosen sampling time (0.01 s), the charts only show the range of frequencies of the input, which is lower than the total available range. As it was expected, the lower the noise, the better the results. However, at some frequencies, mostly at those lower than 1 Hz and those higher than 10 Hz, the phase is not well captured. Even so, it can be said that the entire system is well captured by the method, which motivates the try with a higher modes signal.

5.6 Identification with $n_{\text{modes}} = 1$ system and $n_{\text{modes}} = 5$ signal

According to [25], a reasonable modal expansion would take the first 5 modes to consider the behaviour of the blade. Therefore, to perform case, $n_{\text{modes}} = 5$ to compute the output signal and the identified system will have the $n_{\text{modes}} = 1$ size.

For SNR = 10000, which is equal to add noise with $\sigma^2 = 4.79 \cdot 10^{-6}$ variance, the results are shown in Figure 5.21.

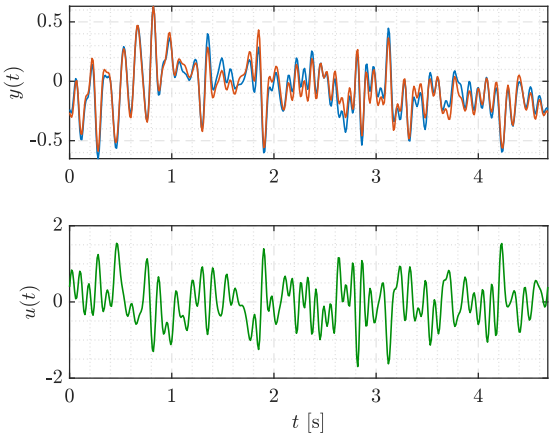

(a) Input-output chart

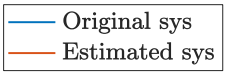

$$\rho_{\text{ref}} = \begin{bmatrix} 0.9901 \pm 0.1172i \\ 0.9939 \pm 0.0791i \\ 0.9958 \pm 0.0492i \\ 0.9954 \pm 0.0091i \\ 0.9963 \pm 0.0265i \end{bmatrix}$$

$$\rho_{\text{ident}} = \begin{bmatrix} 0.9958 \pm 0.0082i \end{bmatrix}$$

(b) $\hat{A}_d$ matrix eigenvalues comparison

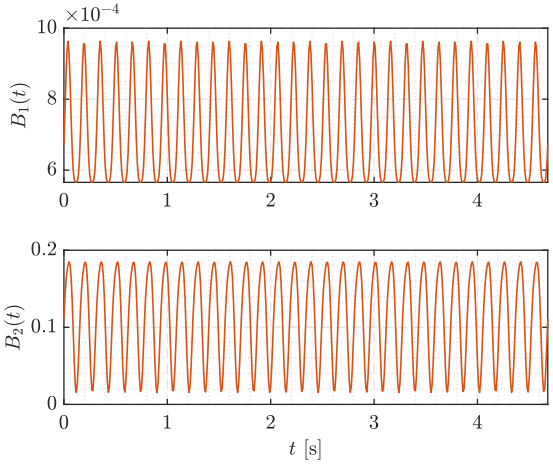

(c) $\hat{B}_d$ matrix in time domain

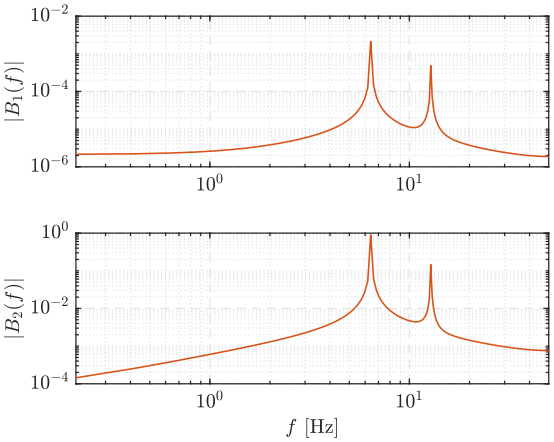

(d) $\hat{B}_d$ matrix in frequency domain

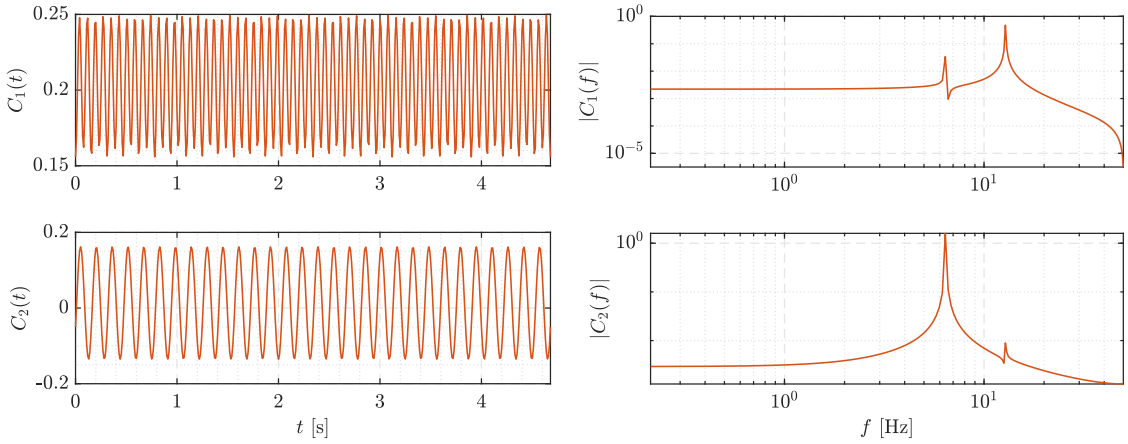

(e) $\hat{C}_d$ matrix in time domain

(f) $\hat{C}_d$ matrix in frequency domain

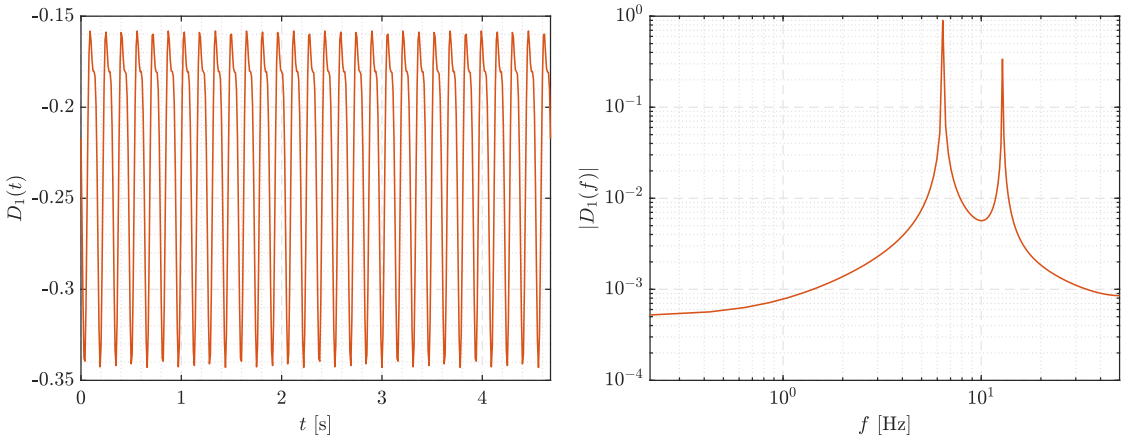

(g) $\hat{D}_d$ matrix in time domain

(h) $\hat{D}_d$ matrix in frequency domain

Figure 5.21: Bending model numerical example. $n_{\text{modes signal}} = 5$, $n_{\text{modes system}} = 1$, SNR= 10000

For SNR = 100, which is equal to add noise with $\sigma^2 = 4.79 \cdot 10^{-4}$ variance, the results are shown in Figure 5.22.

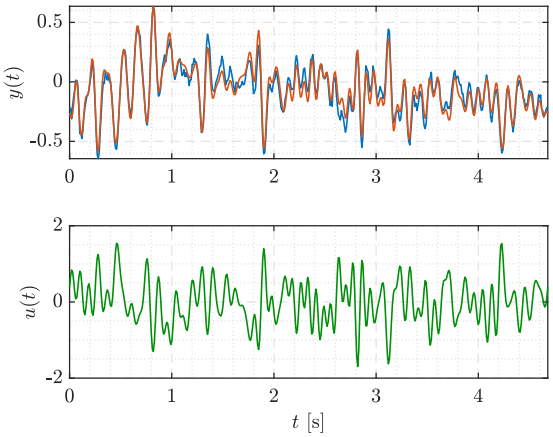

(a) Input-output chart

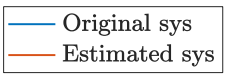

$$\rho_{\text{ref}} = \begin{bmatrix} 0.9901 \pm 0.1172i \\ 0.9939 \pm 0.0791i \\ 0.9958 \pm 0.0492i \\ 0.9954 \pm 0.0091i \\ 0.9963 \pm 0.0265i \end{bmatrix}$$

$$\rho_{\text{ident}} = \begin{bmatrix} 0.9959 \pm 0.0082i \end{bmatrix}$$

(b) $\hat{A}_d$ matrix eigenvalues comparison

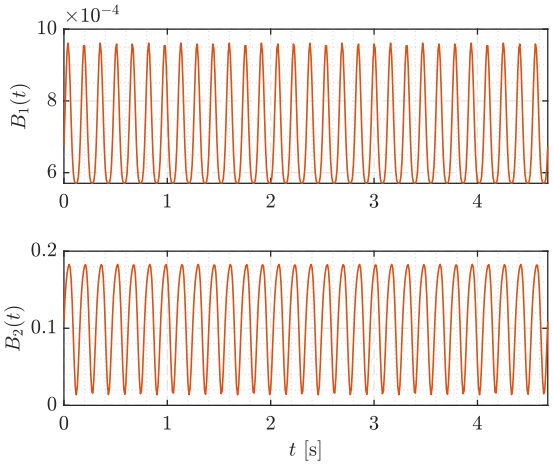

(c) $\hat{B}_d$ matrix in time domain

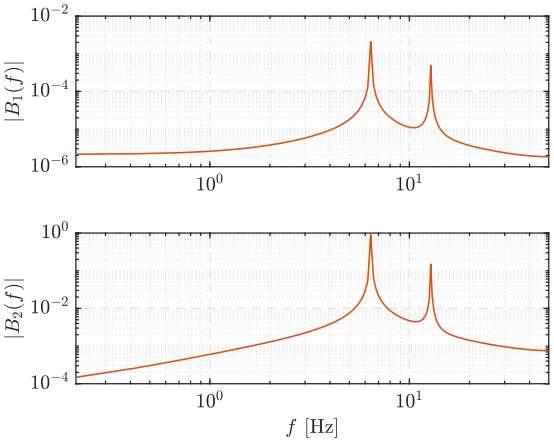

(d) $\hat{B}_d$ matrix in frequency domain

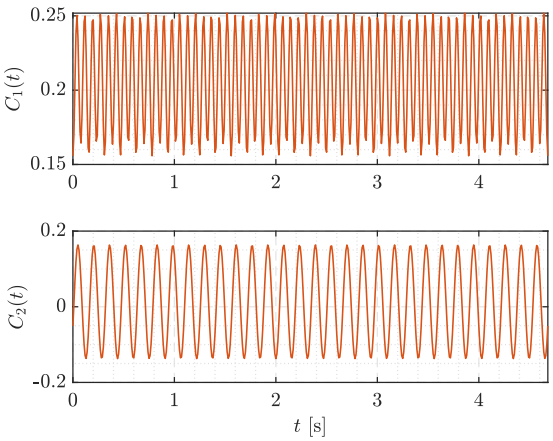

(e) $\hat{C}_d$ matrix in time domain

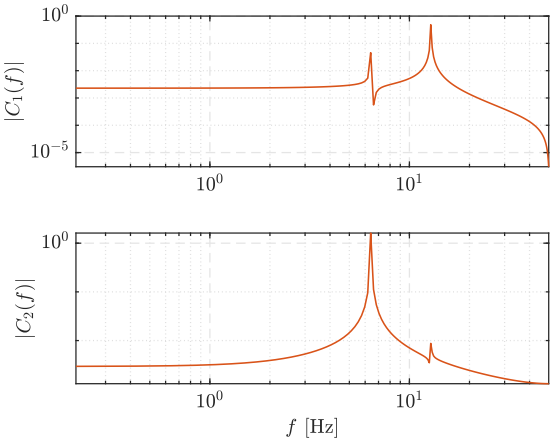

(f) $\hat{C}_d$ matrix in frequency domain

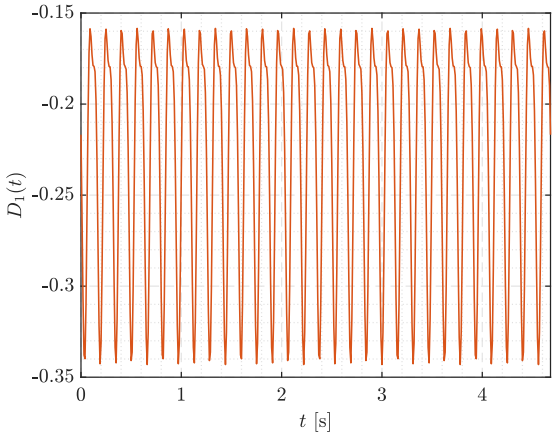

(g) $\hat{D}_d$ matrix in time domain

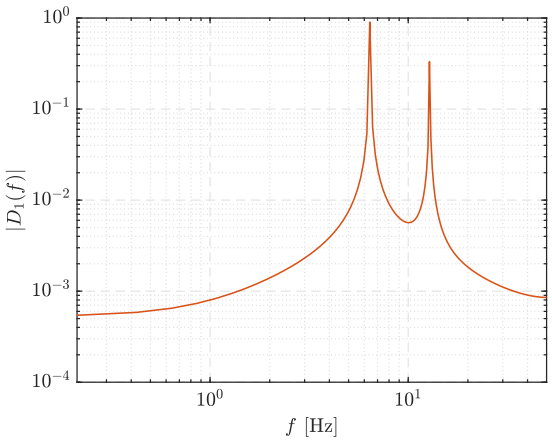

(h) $\hat{D}_d$ matrix in frequency domain

Figure 5.22: Bending model numerical example. $n_{\text{modes signal}} = 5$, $n_{\text{modes system}} = 1$, SNR= 100

For SNR = 10, which is equal to add noise with $\sigma^2 = 4.79 \cdot 10^{-3}$ variance, the results are shown in Figure 5.23.

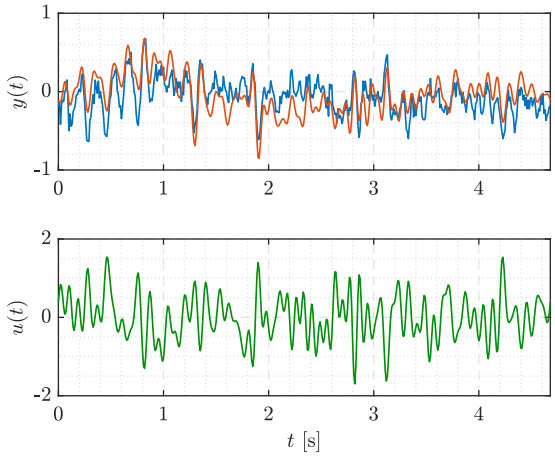

(a) Input-output chart

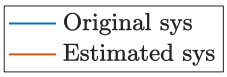

$$\rho_{\text{ref}} = \begin{bmatrix} 0.9901 \pm 0.1172i \\ 0.9939 \pm 0.0791i \\ 0.9958 \pm 0.0492i \\ 0.9954 \pm 0.0091i \\ 0.9963 \pm 0.0265i \end{bmatrix}$$

$$\rho_{\text{ident}} = \begin{bmatrix} 0.9961 \pm 0.0165i \end{bmatrix}$$

(b) $\hat{A}_d$ matrix eigenvalues comparison

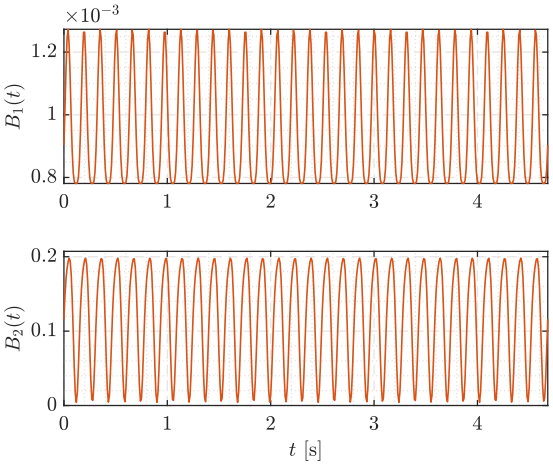

(c) $\hat{B}_d$ matrix in time domain

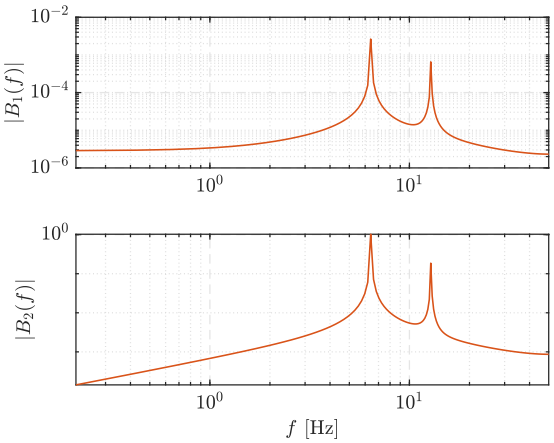

(d) $\hat{B}_d$ matrix in frequency domain

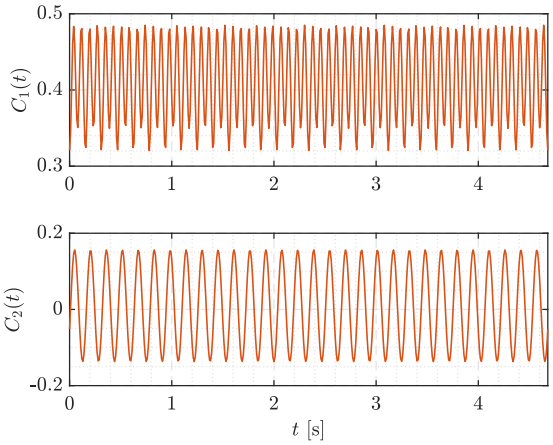

(e) $\hat{C}_d$ matrix in time domain

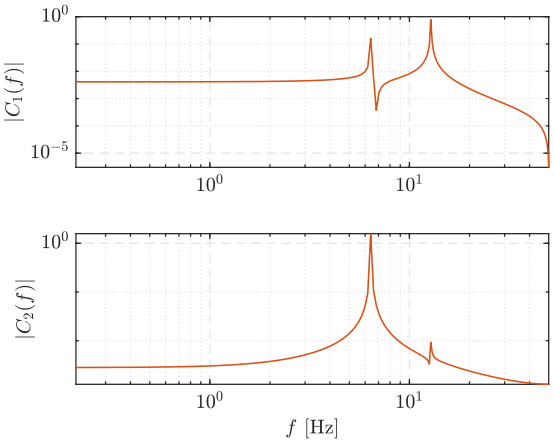

(f) $\hat{C}_d$ matrix in frequency domain

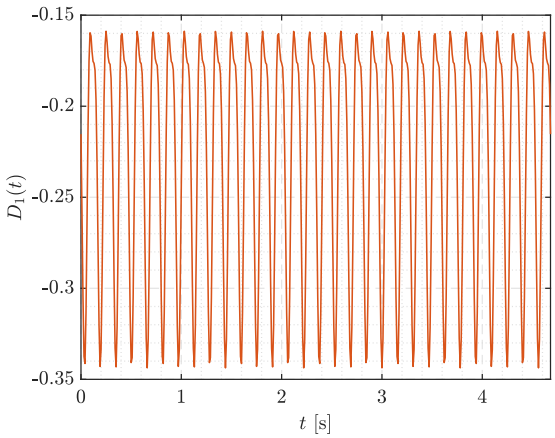

(g) $\hat{D}_d$ matrix in time domain

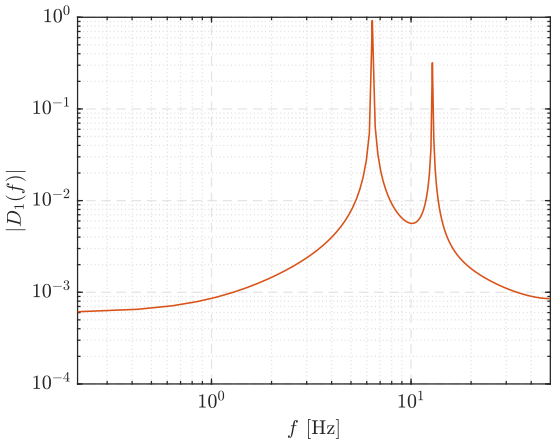

(h) $\hat{D}_d$ matrix in frequency domain

Figure 5.23: Bending model numerical example. $n_{\text{modes signal}} = 5$, $n_{\text{modes system}} = 1$, SNR= 10

For SNR = 3, which is equal to add noise with $\sigma^2 = 1.60 \cdot 10^{-2}$ variance, the results are shown in Figure 5.24.

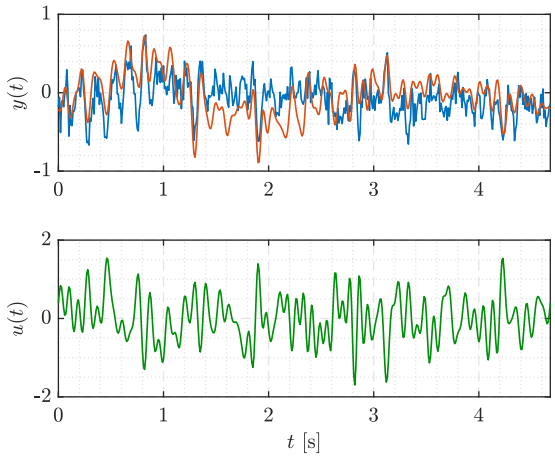

(a) Input-output chart

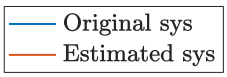

$$\rho_{\text{ref}} = \begin{bmatrix} 0.9901 \pm 0.1172i \\ 0.9939 \pm 0.0791i \\ 0.9958 \pm 0.0492i \\ 0.9954 \pm 0.0091i \\ 0.9963 \pm 0.0265i \end{bmatrix}$$

$$\rho_{\text{ident}} = \begin{bmatrix} 0.9963 \pm 0.0213i \end{bmatrix}$$

(b) $\hat{A}_d$ matrix eigenvalues comparison

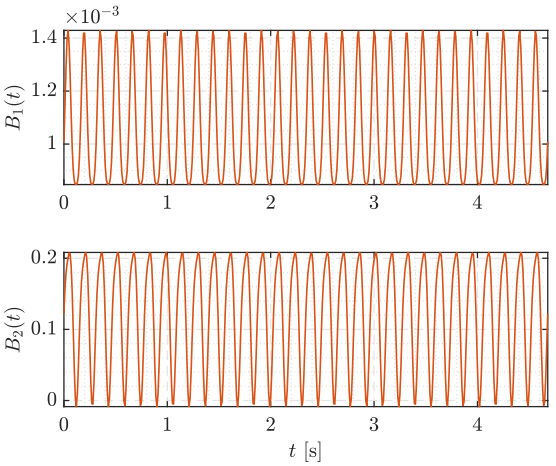

(c) $\hat{B}_d$ matrix in time domain

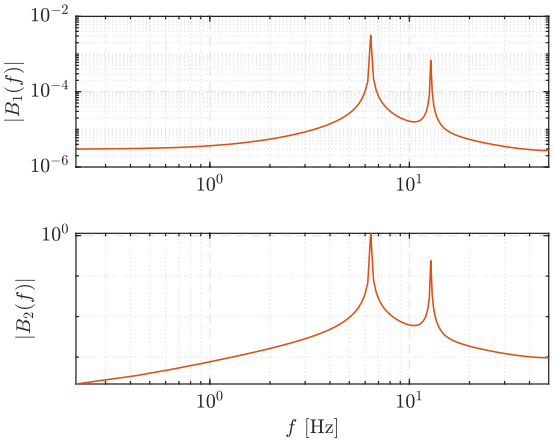

(d) $\hat{B}_d$ matrix in frequency domain

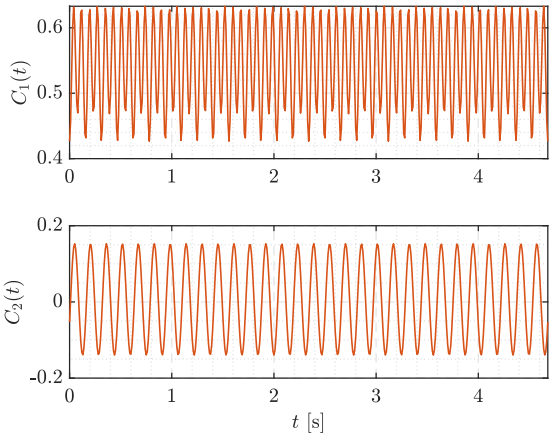

(e) $\hat{C}_d$ matrix in time domain

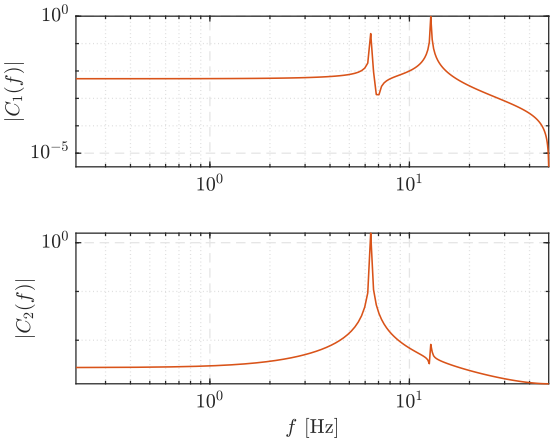

(f) $\hat{C}_d$ matrix in frequency domain

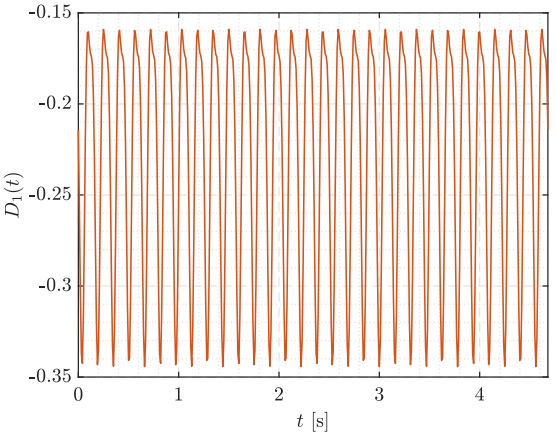

(g) $\hat{D}_d$ matrix in time domain

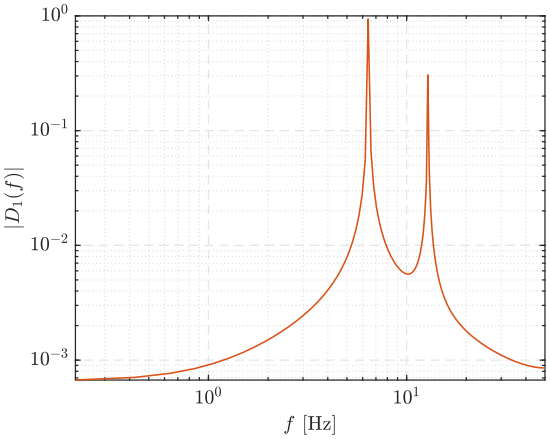

(h) $\hat{D}_d$ matrix in frequency domain

Figure 5.24: Bending model numerical example. $n_{\text{modes signal}} = 5$, $n_{\text{modes system}} = 1$, SNR= 3

For SNR = 1.6, which is equal to add noise with $\sigma^2 = 3.00 \cdot 10^{-2}$ variance, the results are shown in Figure 5.25.

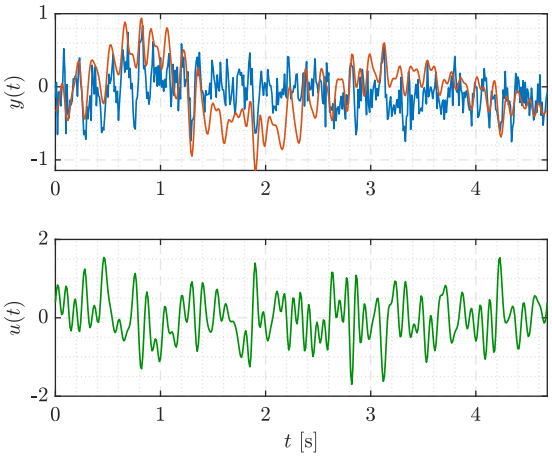

(a) Input-output chart

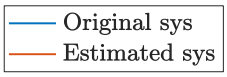

$$\rho_{\text{ref}} = \begin{bmatrix} 0.9901 \pm 0.1172i \\ 0.9939 \pm 0.0791i \\ 0.9958 \pm 0.0492i \\ 0.9954 \pm 0.0091i \\ 0.9963 \pm 0.0265i \end{bmatrix}$$

$$\rho_{\text{ident}} = \begin{bmatrix} 0.9955 \pm 0.0241i \end{bmatrix}$$

(b) $\hat{A}_d$ matrix eigenvalues comparison

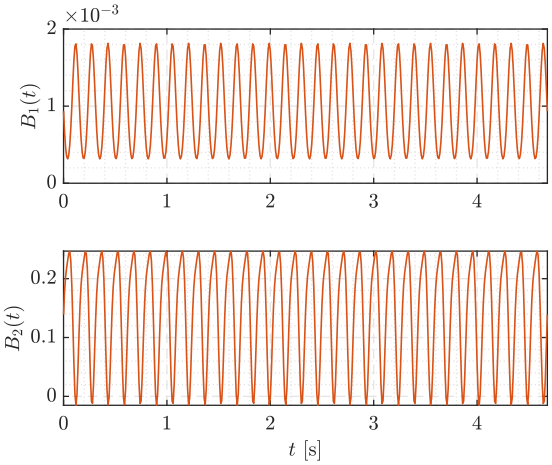

(c) $\hat{B}_d$ matrix in time domain

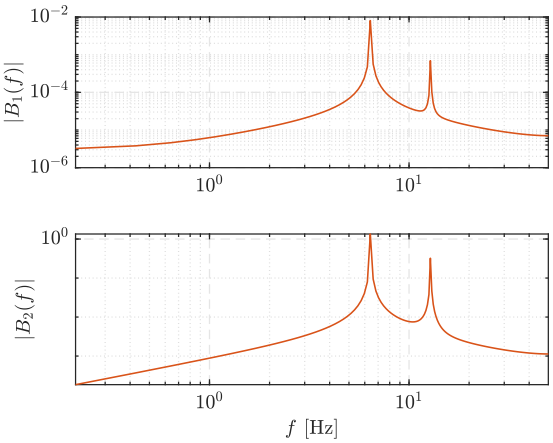

(d) $\hat{B}_d$ matrix in frequency domain

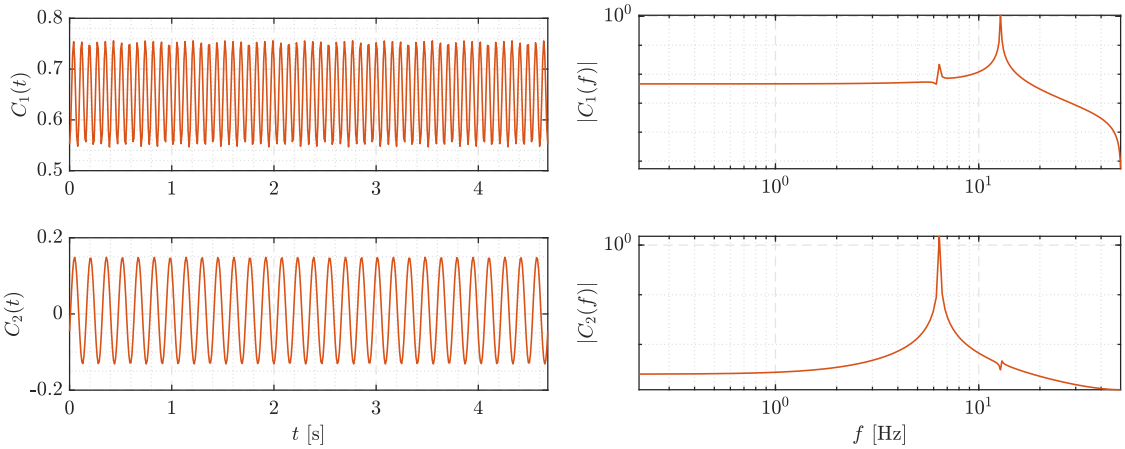

(e) $\hat{C}_d$ matrix in time domain

(f) $\hat{C}_d$ matrix in frequency domain

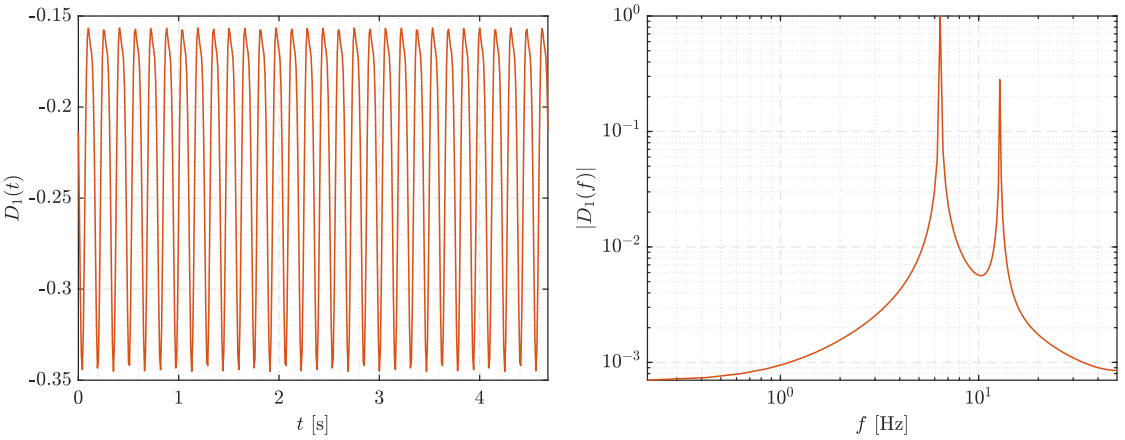

(g) $\hat{D}_d$ matrix in time domain

(h) $\hat{D}_d$ matrix in frequency domain

Figure 5.25: Bending model numerical example. $n_{\text{modes signal}} = 5$, $n_{\text{modes system}} = 1$, SNR= 1.6

After the Monte Carlo analysis, maintaining the same configuration as the previous cases, the uncertainty results are provided in Figure 5.26.

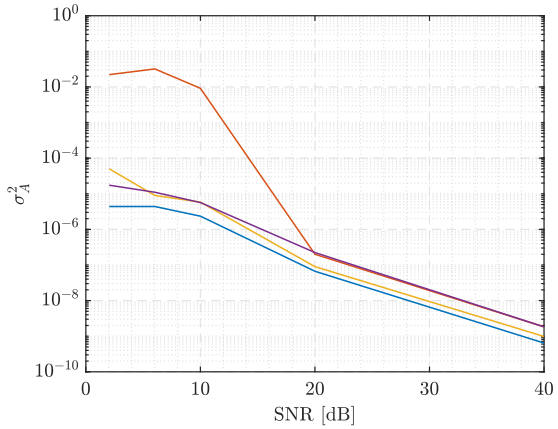

(a) $\hat{A}_d$ matrix variance

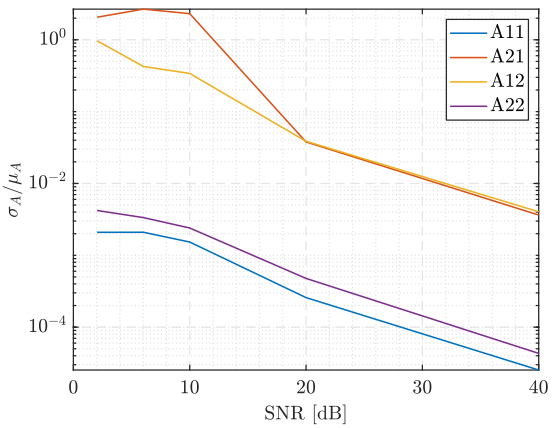

(b) $\hat{A}_d$ matrix CV

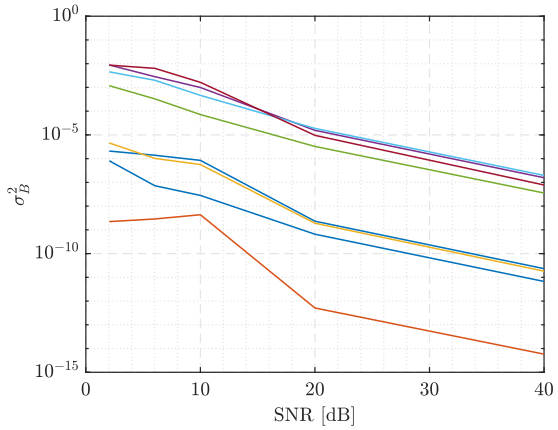

(a) $\hat{B}_d$ matrix variance

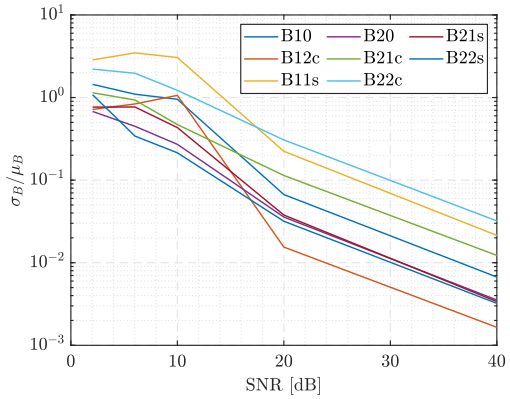

(b) $\hat{B}_d$ matrix CV

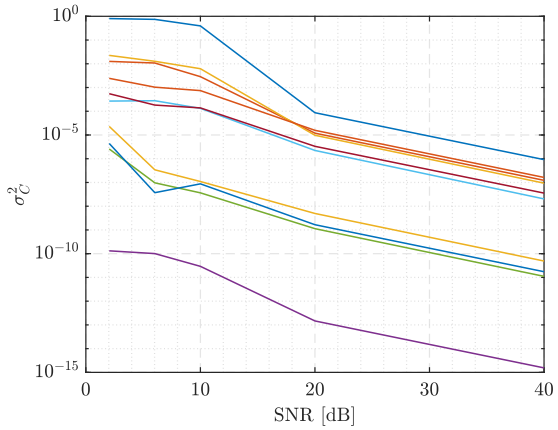

(c) $\hat{C}_d$ matrix variance

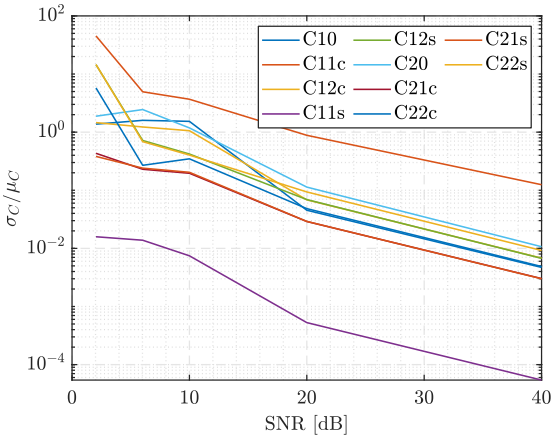

(d) $\hat{C}_d$ matrix CV

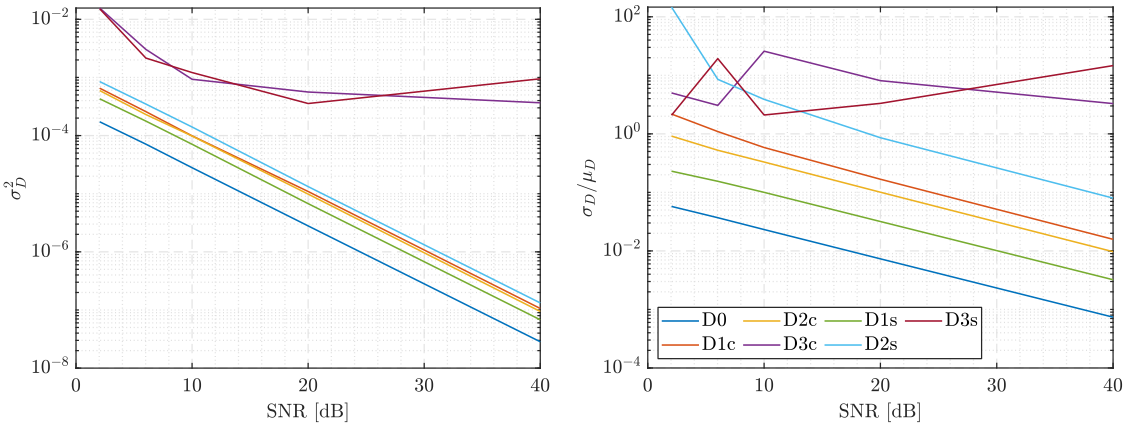

(e) $\hat{D}_d$ matrix variance (f) $\hat{D}_d$ matrix CV

Figure 5.26: Bending model numerical example. Variance and CV. $n_{\text{modes signal}} = 5$, $n_{\text{modes system}} = 1$

The parameters uncertainty behave as in the previous case, being remarkable, also in this case, the sensitivity of the parameters variance and CV to the noise variation.

Finally, as in the previous case, Figure 5.27 provides the Bode-like charts of H_0 and H_1 of the identified and reference systems.

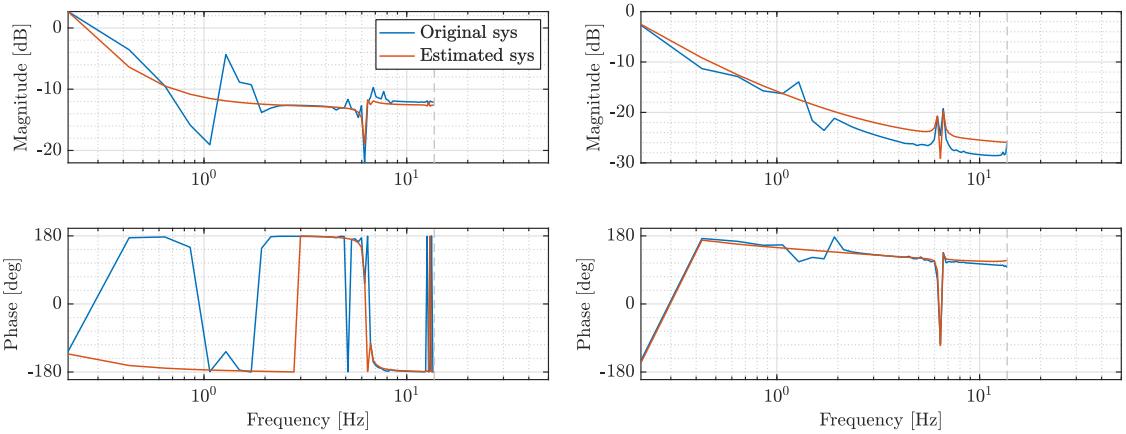

(a) H_0, SNR = 10000 (b) H_1, SNR = 10000

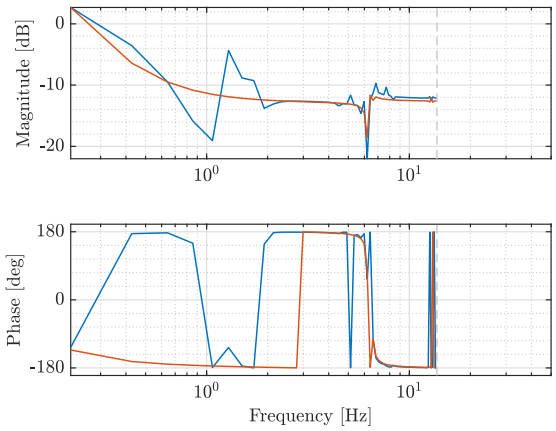

(c) H_0, SNR = 100

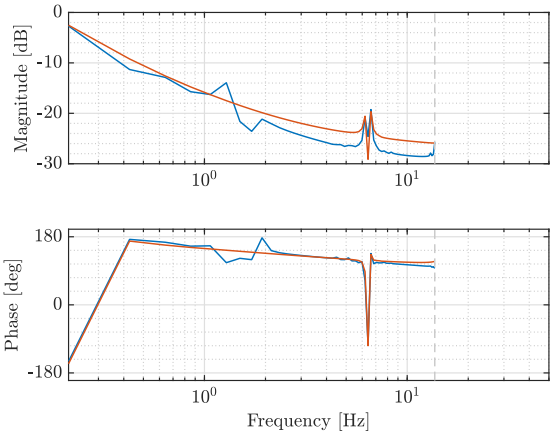

(d) H_1, SNR = 100

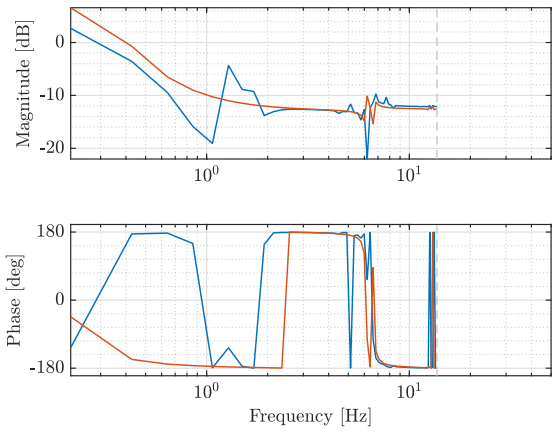

(e) H_0, SNR = 10

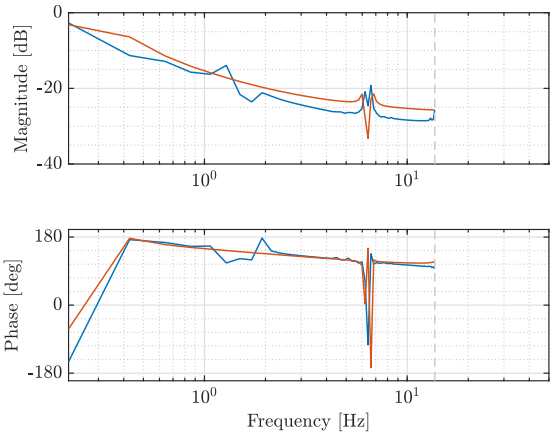

(f) H_1, SNR = 10

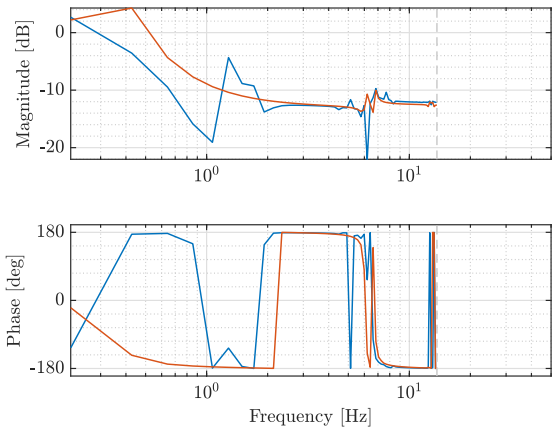

(g) H_0, SNR = 3

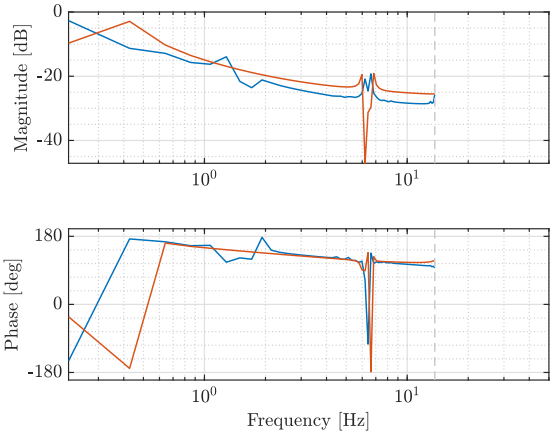

(h) H_1, SNR = 3

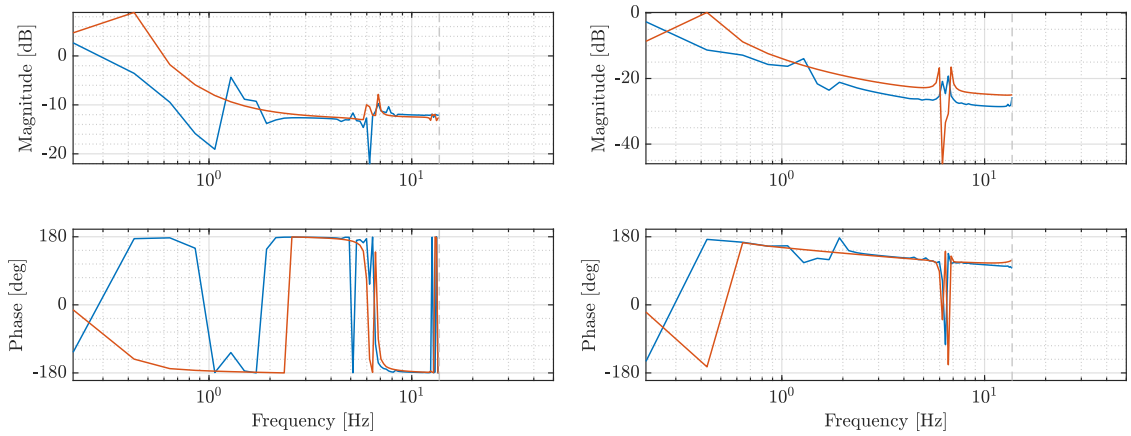

(i) H_0, SNR = 1.6 (j) H_1, SNR = 1.6

Figure 5.27: Bending model numerical example. H_0 and H_1 Bode-like charts. $n_{\text{modes signal}} = 5$, $n_{\text{modes system}} = 1$

In this case, much more differences can be noticed. This proves the existence of more non-negligible modes in the system. If there would be an interest into capturing the maximum number of modes as possible, without compromising the algorithm performance, a possible procedure would be to raise the identified model size until no variations in these Bode-like charts are noticed.

With respect to the results, for low-noise signals, the estimated system seems to capture the mean pattern of the reference one. Unfortunately, this behaviour is lost when the signal noise increases, which is consistent with the previous plots in which the recovered output signal was not close to the error tolerance required to stop the optimization.

Regarding the charts of this case and also the ones of the previous case, an error definition can be also made in order to rate the quality of the identified system with respect to the reference one, which is presented in equation (5.11).

$$\varepsilon_m = \sum_{i=0}^{1} \int_{f_{\text{min input}}}^{f_{\text{max input}}} |H_{i\,\text{ref}}(f) - H_{i\,\text{ident}}(f)|\,\mathrm{d}f. \tag{5.11}$$

This definition leads to Figure 5.28, which shows at a glance what has been commented before. With respect to the behaviour in noise presence, the algorithm performs worse as the SNR value decreases, which means that the added noise increases. However, it can be noticed that this behaviour is not logaritmic, but there is a point in which the error cannot be lower even if the reference output signal is noise-free. On the other part, with respect to the number of modes

considered in the reference output signal, increasing it without making the size of the identified model bigger, will mean that the errors will grow up.

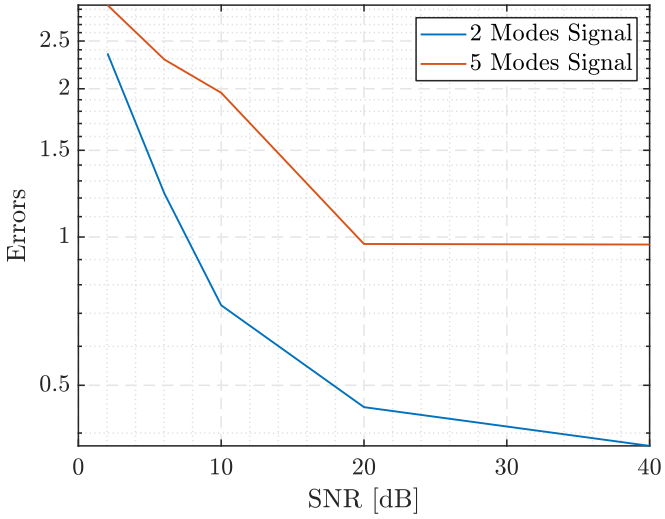

Figure 5.28: Bending model numerical example. Errors comparsion between $n_{\text{modes signal}} = 2$ and $n_{\text{modes signal}} = 5$

Conclusions

In this Thesis, a new method for a frequency-domain subspace-identification method for LPTV systems was developed. After reviewing some recent publications, one of them was chosen as reference but the others were used to select some procedures. Then, after developing it, it was tested using a physical-based rotorcraft model, with several cases to exploit a range of possibilities to prove its effectiveness and robustness in several cases of application. However, since the fields of application of LPTV systems are many and very different, the fact of testing this algorithm with a rotorcraft model does not mean it will not able to provide good results if it is used in other field. In fact, the intention was to develop a model in order to be used in any field of LPTV investigation.

With respect to the results, it has been proved that the method provides good results in the sense of recovering the original system in several modes and noise conditions. Regarding the added noise, a value of SNR ≥ 3 would be a reasonable value to consider the output measure as good, so as the method will be able to provide good results, in the sense of the defined errors. It must be also taken into account that the algorithm was developed in the output-error framework, and this approach may be modified if some other kind of considerations are desired. On the other hand, regarding the number of modes of the reference output signal, the method has shown ability to return an equivalent system that provides a very similar output with respect to the reference one. Later, it has been proved that the mean pattern of the modes is captured, since the degrees of freedom of the identified system are less than the reference one. Also, even if it has not been fully tested, this method also works well if a black-box identification is desired, providing also good results, but possibly, without any phyisical meaning.

Considering the possible future continuations of the present thesis, two main lines can be developed: the first one, to improve the algorithm, modifying the data processing as well as finding a better cost function for the optimizer. The objective of this is to reduce the computation time and to be able to increase the complexity of the problem, because this is the most counterpart of the developed algorithm. The computation time was about 20 min in the best case and 3 hours in the worst case using an Intel i7-9750H (@ 2.60 GHz). In fact, it testing this approach with a complete rotorcraft model would be a final test to show its effectiveness and robustness. On the other hand, it would be interesting, and also necessary, to

test it with real-life collected data, including sensors uncertainty, another type of noise, and some other cons that may raise when the identification is perfomed using real data.

Bibliography

[1] H. Yu, Y. Ran, G. Zhang, X. Li, and B. Li, "A time-varying comprehensive dynamic model for the rotor system with multiple bearing faults," *Journal of Sound and Vibration*, vol. 488, p. 115650, 2020.

[2] M. Maggia, S. Eisa, and H. Taha, "On higher-order averaging of time-periodic systems: reconciliation of two averaging techniques," *Nonlinear Dynamics*, vol. 99, 01 2020.

[3] C. Bottasso and S. Cacciola, "Model-independent periodic stability analysis of wind turbines," *Wind Energy*, vol. 18, no. 5, pp. 865–887.

[4] "V-280 in flight with rotors tilted to hover configuration," 2019, (Accessed on April, 19th 2022). [Online]. Available: https://en.wikipedia.org/wiki/Bell_V-280_Valor#/media/File:Bell_V-280_Valor_takeoff_demo,_2019_Alliance_Air_Show,_Fort_Worth,_TX.jpg

[5] Y. Xing, X. Cao, S. Zhang, H. Guo, and F. Wang, "Relative position and attitude estimation for satellite formation with coupled translational and rotational dynamics," *Acta Astronautica*, vol. 67, no. 3, pp. 455–467, 2010. [Online]. Available: https://www.sciencedirect.com/science/article/pii/S0094576510001190

[6] I. Uyanık, U. Saranl, M. M. Ankaral, N. J. Cowan, and O. Morgül, "Frequency-domain subspace identification of linear time-periodic (ltp) systems," *IEEE Transactions on Automatic Control*, vol. 64, no. 6, pp. 2529–2536, 2019.

[7] "A109 - riat 2012," 2012, (Accessed on June, 2th 2022). [Online]. Available: https://www.flickr.com/photos/24874528@N04/7549052866/

[8] N. Wereley, *Analysis and Control of Linear Periodically Time Varying Systems*. PhD dissertation, Massachusetts Institute of Technology, Department of Aeronautics and Astronautics, 1990.

[9] N. Tandon and A. Choudhury, "A review of vibration and acoustic measurement methods for the detection of defects in rolling element bearings," *Tribology International*, vol. 32, no. 8, pp. 469–480, 1999.

[10] H. E. Taha, M. R. Hajj, and A. H. Nayfeh, "Flight dynamics and control of flapping-wing mavs: a review," *Nonlinear Dynamics*, vol. 70, no. 2, pp. 907–939, 2012.

[11] C. Recchiuto, R. Molfino, A. Hedenström, H. Peremans, V. Cipolla, A. Frediani, E. Rizzo, and G. Muscolo, "Bioinspired mechanisms and sensorimotor schemes for flying: A preliminary study for a robotic bat," p. 37, 12 2014.

[12] M. Passaro, "Identification of a flapping-wing micro aerial vehicle using subspace methods," Master's thesis, Politecnico di Milano, 04 2021.

[13] F. Bullo, "Averaging and vibrational control of mechanical systems," *SIAM Journal on Control and Optimization*, vol. 41, no. 2, pp. 542–562, 2002.

[14] U. Saetti and M. Lovera, "Time-periodic and high-order time-invariant linearized models of rotorcraft: A survey," *Journal of the American Helicopter Society*, vol. 67, pp. 1–19, 01 2022.

[15] S. E. and M. Lovera, "Magnetic spacecraft attitude control: a survey and some new results," *Control Engineering Practice*, vol. 13, no. 3, pp. 357–371, 2005, aerospace IFAC 2002. [Online]. Available: https://www.sciencedirect.com/science/article/pii/S0967066103002922

[16] L. Mevel, I. Gueguen, and D. Tcherniak, "Lptv subspace analysis of wind turbines data," 07 2014.

[17] M. D. Pedersen and T. I. Fossen, "Efficient nonlinear wind-turbine modeling for control applications," *IFAC Proceedings Volumes*, vol. 45, no. 2, pp. 264–269, 2012, 7th Vienna International Conference on Mathematical Modelling. [Online]. Available: https://www.sciencedirect.com/science/article/pii/S1474667016306796

[18] I. Yavrucuk, J. Prasad, and A. Calise, "Carefree maneuvering using adaptive neural networks," *AIAA Atmospheric Flight Mechanics Conference and Exhibit*, 08 2002.

[19] S. S. Mulgund and G. L. Zacharias, "A hybrid neural network-fuzzy logic limit protection system for rotorcraft," *Proceedings of the AIAA Guidance, Navigation, and Control Conference, San Diego, CA*, 07 1996.

[20] C. E. Mballo and J. V. R. Prasad, "A real time scheme for rotating system component load estimation using fixed system measurements," *Proceedings of the 74th Annual Forum of the Vertical Flight Society, Phoenix, AZ*, 05 2018.

[21] R. L. Schoenman and H. A. Shomber, "Impact of active controls on future transport design, performance, and operation," *SAE Transactions*, vol. 84, pp. 2917–2932, 1975.

[22] P. Arcara, S. Bittanti, and M. Lovera, "Active control of vibrations in helicopters by periodic optimal control," pp. 730–735, 1997.

[23] S. Jacklin, A. Haber, G. Simone, T. Norman, C. Kitaplioglu, and P. Shinoda, "Full-scale wind tunnel test of an individual blade control system for a uh-60 helicopter," p. 13, 06 2002.

[24] P. Arcara, S. Bittanti, and M. Lovera, "Periodic control of helicopter rotors for attenuation of vibrations in forward flight," *IEEE Transactions on Control Systems Technology*, vol. 8, no. 6, pp. 883–894, 2000.

[25] S. Bittanti and M. Lovera, "On the zero dynamics of helicopter rotor loads," *European Journal of Control*, vol. 2, no. 1, pp. 57–68, 1996. [Online]. Available: https://www.sciencedirect.com/science/article/pii/S0947358096700298

[26] "Future vertical lift overview," 2016, (Accessed on April, 17th 2022). [Online]. Available: https://vtol.org/what-we-do/advocacy/future-vertical-lift

[27] A. Siddiqi, "Identification of the harmonic transfer functions of a helicopter rotor," Master's thesis, Massachusetts Institute of Technology, 02 2001.

[28] U. Saetti and J. Horn, "Load alleviation flight control design using high-order dynamic models," *Journal of the American Helicopter Society*, vol. 65, 05 2020.

[29] M. B. Cheng, R. P. Tischler and R. Celi, "A high-order, time invariant linearized model for application to hhc/afcs interaction studies," *Proceedings of the 59th Annual Forum of the American Helicopter Society, Phoenix, AZ*, vol. 65, 05 2003.

[30] G. Zeng, M. Hu, and H. Yao, "Relative orbit estimation and formation keeping control of satellite formations in low earth orbits," *Acta Astronautica*, vol. 76, pp. 164–175, 2012. [Online]. Available: https://www.sciencedirect.com/science/article/pii/S0094576512000598

[31] L. Vigano and M. Lovera, "Optimal orbit control of spacecraft on elliptical orbits," *IFAC Proceedings Volumes*, vol. 40, no. 7, pp. 13–18, 2007, 17th IFAC Symposium on Automatic Control in Aerospace. [Online]. Available: https://www.sciencedirect.com/science/article/pii/S1474667015332109

[32] W. Yin and A. S. Mehr, "Identification of linear periodically time-varying systems using periodic sequences," pp. 1455–1459, 2009.

[33] E. Louarroudi, R. Pintelon, and J. Lataire, "Nonparametric tracking of the time-varying dynamics of weakly nonlinear periodically time-varying systems using periodic inputs," *IEEE Transactions on Instrumentation and Measurement*, vol. 61, no. 5, pp. 1384–1394, 2012.

[34] J. Goos and R. Pintelon, "Continuous-time identification of periodically parameter-varying state space models," *Automatica*, vol. 71, pp. 254–263, 2016.

[35] T. A. Wood, "Model-based flight control of kites for wind power generation," Ph.D. dissertation, ETH Zurich, 2018.

[36] M. Yin, A. Iannelli, M. Khosravi, A. Parsi, and R. Smith, "Linear time-periodic system identification with grouped atomic norm regularization," *IFAC-PapersOnLine*, vol. 53, pp. 1237–1242, 01 2020.

[37] O. Fivel, "Analysis of linear time-varying & periodic systems," Master's thesis, University of the Negev, 07 2021.

[38] G. Quaranta, "A short practical guide to non linear stability," 2013.

[39] D. Rainville and P. Bedient, *Elementary Differential Equations. 6th Edition.* Macmillan Company; London: Collier-Macmillan, 1969.

[40] W. Rugh, *Linear System Theory*, ser. Prentice-Hall information and system sciences series. Prentice Hall, 1996.

[41] S. Bittanti and P. Colaneri, *Periodic Systems: Filtering and Control*, ser. Communications and Control Engineering. Springer London, 2008.

[42] N. Wereley and S. Hall, "Frequency response of linear time periodic systems," pp. 3650–3655 vol.6, 1990.

[43] N. M. Wereley and S. R. Hall, "Linear time periodic systems: Transfer function, poles, transmission zeroes and directional properties," pp. 1179–1184, 1991.

[44] S. R. Hall and N. M. Wereley, "Generalized nyquist stability criterion for linear time periodic systems," pp. 1518–1525, 1990.

[45] W. Larimore, "Canonical variate analysis in identification, filtering, and adaptive control," pp. 596–604 vol.2, 1990.

[46] "Estimate state-space model using subspace method with time-domain or frequency-domain data," (Accessed on May, 19th 2022). [Online]. Available: https://www.mathworks.com/help/ident/ref/n4sid.html

[47] M. Verhaegen, "Identification of the deterministic part of mimo state space models given in innovations form from input-output data," *Automatica*, vol. 30, no. 1, pp. 61–74, 1994, special issue on statistical signal processing and control.

[48] R. Pintelon and J. Schoukens, *System Identification: A Frequency Domain Approach*. IEEE Press, The Institute of Electrical and Electronics Engineers, Inc. New York, 2001.

[49] E. K. Hidir, I. Uyanik, and O. Morgül, "Harmonic transfer functions based controllers for linear time-periodic systems," *Transactions of the Institute of Measurement and Control*, vol. 41, no. 8, pp. 2171–2184, 2019.

[50] "Solve nonstiff differential equations — medium order method," (Accessed on May, 19th 2022). [Online]. Available: https://www.mathworks.com/help/matlab/ref/ode45.html

[51] "Add white gaussian noise to signal," (Accessed on May, 19th 2022). [Online]. Available: https://www.mathworks.com/help/comm/ref/awgn.html

[52] "Find minimum of constrained nonlinear multivariable function," (Accessed on May, 22th 2022). [Online]. Available: https://www.mathworks.com/help/comm/ref/fmincon.html

[53] W. Johnson, *Helicopter Theory*, ser. Dover Books on Aeronautical Engineering Series. Dover Publications, 1994.

[54] A. Bramwell, G. Done, and D. Balmford, *Helicopter Dynamics*, second edition ed., A. Bramwell, G. Done, and D. Balmford, Eds. Oxford: Butterworth-Heinemann, 2000.